SURFACE ENGINEERING OF PROTEIN NANOCLUSTERS TO OVERCOME MUCUS BARRIERS

A Dissertation Presented to
The Academic Faculty

By

Thomas Pho

In Partial Fulfillment of the

Requirements for the Degree

Master in Bioengineering

Georgia Institute of Technology

December 2021

SURFACE ENGINEERING OF PROTEIN NANOCLUSTERS TO

OVERCOME MUCUS BARRIERS

Approved by:

Dr. Julie Champion, Advisor
School of Chemical & Biomolecular Engineering
Georgia Institute of Technology

Dr. Ravi Kane
School of Chemical & Biomolecular Engineering
Georgia Institute of Technology

Dr. Jennifer Curtis
School of Physics
Georgia Institute of Technology

ACKNOWLEDGEMENTS

I want to sincerely thank my thesis advisor, Prof. Dr. Julie Champion, for her endless support since the first day I've met you. I honestly can't thank you enough. Your optimism and motivation in science have helped me so much in the past two years, and I'm thankful that I still have so much time left with you. I want to thank the whole Champion lab, with whom I had such a great time working and being friends. I couldn't have asked for better past mentors than Alex, Adam, Sam, and Anshul. Thank you for being such a great team and friends to my current coworkers, Dylan, Yirui, Jaeyoung, Sydney, and Adaya.

To my cousins, Bianca and Elizabeth, thanks for calling me every single day. It's genuinely entertaining to see how crazy your lives are. Thank you to my family for always lets me bombard them with my facetime calls. Thank you to my dog, Casper, and my late dog, Dakota, for giving so much joy in my life. Finally, thank you to my girlfriend Nam; even though you're 900 miles away, you always manage to support me whenever I need someone to talk to and be there to make my life great.

TABLE OF CONTENTS

LIST OF SYMBOLS AND ABBREVIATIONS

2D	Two-Dimensional
AmB	Amphotericin B
APC	Antigen-Presenting Cells
AuNP	Gold Nanoparticles
BBB	Blood-Brain Barrier
BCA	Bicinchoninic Acid Assay
BDNF	Brain-Derived Neurotrophic
CD	Cluster Of Differentiation
CNP	Chitosan Nanoparticles
cOVA	Cationic Ovalbumin
cP	Centipoise
CpG ODN	Cpg Oligodeoxynucleotide
CTAB	Cetyltrimethylammonium Bromide
D_{eff}	Diffusion Coefficient
DLS	Dynamic Light Scattering
DTSSP	3,3'- Dithiobis(Sulfosuccinimidyl Propionate)
EDC	1-(3-Dimethylaminopropyl)-3-Ethylcarbodiimide Hydrochloride
ELS	Electrophoretic Light Scattering
f4M2e	Four Tandem Copies of The Ectodomain of Matrix Protein 2
FBS	Fetal Bovine Serum
FC	Fragment Crystallizable
FliC	Flagellin
FWF	Fine Welding Fume
GI	Gastrointestinal Tract
GLA	Glutaraldehyde
GM-CSF	Granulocyte-Macrophage Colony-Stimulating Factor
HA	Hemagglutinin
IONP	Iron Oxide Nanoparticle
LBL	Layer-By-Layer
LC-MS/MS	Liquid Chromatography–Mass Spectrometry2
LNP	Lipid Nanoparticles
LPS	Lipopolysaccharide
MES	(Morpholino)-Ethanesulfonic
MPT	Multiple Particle Tracking
MW	Molecular Weight
NALT	Nasal-Associated Lymphoid Tissue
NHS	N-Hydroxy succinimide

NTA	Nanoparticle Tracking Analysis
OVA	Ovalbumin
PAS	Periodic Acid-Schiff
PBS	Phosphate-Buffered Saline
PDI	Polydispersity Index
PEG	Polyethylene Glycol
PEG NP	Pegylated Nanoparticles
PLGA	Poly (Lactic-Co-Glycolic Acid
PNC	Protein Nanocluster
PRR	Pattern Recognition Receptors
PSM	Peptide Spectrum Match
PVA	Polyvinyl Alcohol
PVP	Oly(N-Vinylpyrrolidone)
SDS-PAGE	Sodium Dodecyl Sulfate Polyacrylamide Gel Electrophoresis
SLN	Solid Lipid Nanoparticles
TEM	Transmission Electron Microscopy
TLC	Thin-Layer Chromatography
TNF	Tumor Necrosis Factor
UFWF	Ultrafine Welding Fume
ZP	Zeta Potential
γ	Shear Rate
η	Viscosity

LIST OF TABLES

LIST OF FIGURES

SUMMARY

Protein nanoparticles are a novel class of biomaterial that has been designed for the delivery of proteins. This class of materials also allows for a high number of functional surface groups on the surface and nanoscale size that is applicable for many therapeutic applications. These properties allow protein nanoparticles to be a promising candidate for intranasal delivery, which is an attractive delivery method due to its unique benefits such as the production of mucosal immune response and stimulation, and as one of the main entrances to many pathogens. However, intranasal delivery consists of several barriers that remain challenging for the delivery of drugs and vaccines. Synthetic nanoparticles, such as gold and poly (lactic-co-glycolic acid) nanoparticles, have been used to evaluate their ability to be delivered through the nasal mucus and corresponding tissues. Despite the vast amount of work, there is still a significant limitation on the amount of therapeutic or antigen these nanoparticles can carry, and little is known on the transport of nanoparticles with heterogeneous surfaces. To address these issues and bridge the gaps of heterogeneous surfaces in mucosal transport, we developed protein nanoparticles with different properties such as different surface charges to evaluate their transportation in mucus and cellular uptake with both epithelial cells and dendritic cells. In addition, we measured the basal protein corona, which occurs when biomaterials enter the biological fluids in which biomolecules within the fluid are adsorbed onto the material, creating a layer of protein. This work was done on four engineered protein nanoparticles to examine the identity of the protein adsorbed during intranasal delivery of different surfaces and investigate their protein corona fingerprint during intranasal nanoparticle administration. This work highlights engineering coatings on nanoparticles to modify the behavior of nanoparticles during intranasal delivery and bridge the gap on protein corona from nasal fluids, which can enhance our understanding of nanoparticles during intranasal delivery and translation to *in vivo* study.

CHAPTER 1. INTRODUCTION

1.1 Composition and Function of Mucus

The unique feature of mucus is derived from its multitude of chemical interactions and physical traits. This barrier can significantly hinder the ability of pathogens to enter the body and limit the delivery of drugs and vaccines. However, mucus-based delivery systems are still popular due to their intrinsic behavior as a part of the innate immune system and because mucus surfaces are the entrance to the body for many pathogens. To improve the delivery of therapeutics, understanding the composition and behavior will allow tuning materials for better delivery of therapeutics. The mucosa or mucus membrane acts as the openings to the body and various organs such as the nasal cavity, mouth, and lungs. This barrier is an important layer that is one of the first hurdles to the body's internal organs. A layer of mucus resides above epithelial cells that provide protection to the external environment. This layer of mucus is secreted by cells adjacent to epithelial cells, and is classified as a biological barrier, a complex viscoelastic material that covers over the epithelial lining. This adherent secreted fluid is produced by highly specialized cells called mucous cells and goblet cells. These cells are surrounded by columnar or squamocolumnar epithelial cells attached to adjacent cells through tight junction structures. [1, 2] The collective activity and function of the epithelial cells allow for ciliation, absorption, and secretion. Moreover, it can be stimulated with foreign objects that cause a hyperreactivity response to overproduction of mucus to remove the object. [3] The mucus gel lining the mucosal tissues can be found in various systems in the body such as the gastrointestinal, respiratory, and reproductive tracts and the eyes and differs in composition, ionic strength, pH, viscoelasticity, and pore size. [6]

While the structure and composition of mucus may be different across the body, the composition tends to be high in water (90-98%), with mucins (0.2-5%), salts (0.5-1.0%), proteins (0.5%), and

trace level of cells and cellular debris, DNA, bacteria, and lipids. [1, 6, 7, 8, 9, 10] The characteristic of mucus is dictated by the mucins, which are high-molecular-weight glycoproteins that form the structure of the mucus gel and dictate its viscosity properties. Structurally, mucins have a central protein core with one or multiple domains that are heavily glycosylated. The glycosylated regions have a high level of serine and threonine that can form a linkage to O-glycans through a N-acetyl galactosamine sugar molecules [4] Other O-glycans in mucin can be formed linked using N-acetylglucosamine, galactose, fucose, sialic acid, and sulfate. [5] The heavy glycosylation results in a high density of negative charge and structure that resemble bottlebrushes, with branched oligosaccharide chains, or glycans, arranged radially from the protein core. Moreover, mucin has a high level of cysteine-rich regions at end terminuses that form disulfide bonds, creating small pore-like structures in mucus. [12,13, 14] Overall, mucins can interact with foreign species through electrostatic and hydrophobic interactions and hydrogen bonds. Additionally, physical entanglement can occur due to the mesh-like, viscoelastic gel structure of the mucus stabilized by disulfide bonds between mucin molecules, as illustrated in Figure 1.1.

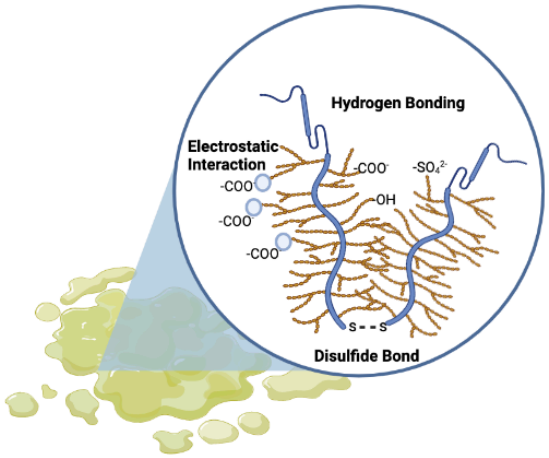

Figure 1.1. Diagram of molecular interaction with mucin highlighting disulfide bonding and various intermolecular interactions. Diagram created using BioRender (Toronto, ON).

Currently, there are 21 mucin-type glycoproteins identified within the mucin family. The different subgroups are divided into secreted mucin, tethered, and cell surface-associated mucin. The secreted mucin group is commonly known as gel-forming mucins. This group consists of MUC2, MUC5AC, MUC5B, MUC6, and MUC19, which are oligomers of mucin, while MUC7 and MUC8 are consider nonpolymeric glycoproteins. [15] This group of mucins can be seen in the outside of the epithelial layer and individual protein polymerized end-to-end by disulfide bonds to form even larger macromonomer chains that have linear, and branched, trimeric structures with other mucin proteins. [17,18] The cell tethered mucins are MUC1, MUC3A, MUC3B, MUC4, MUC12, MUC13, MUC15, MUC16, MUC17, MUC20, and MUC21. This group is known for short cytoplasmic domains that reside inside of the cell, as well as extensive extracellular domains.[19] Mucins are generated in and secreted from goblet cells, which are specialized cells in the surface epithelium, and from mucous cells in submucosal glands. Figure 1.2 outlines the mucin classifications and domains. [15, 20]

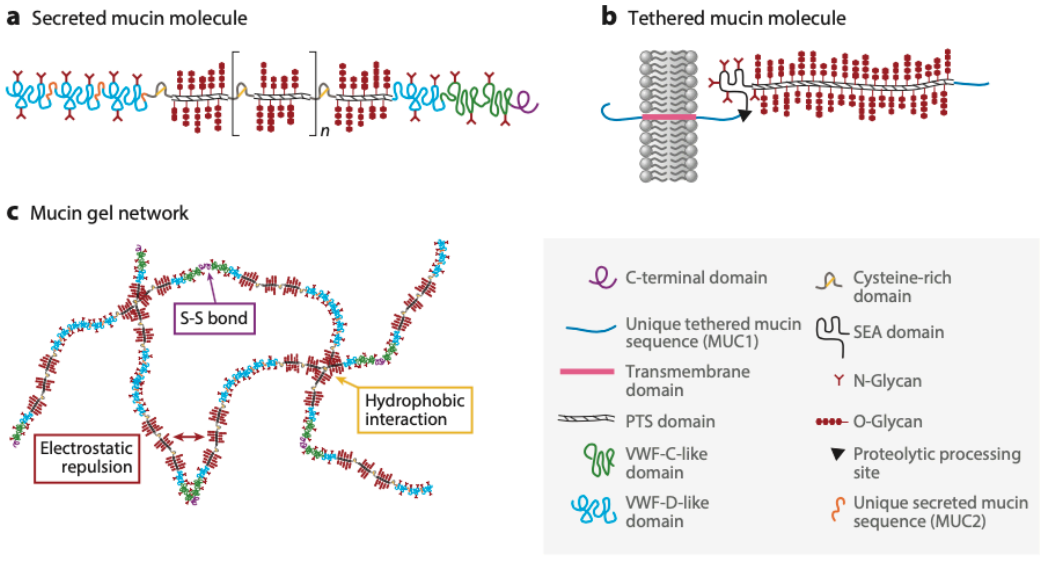

Figure 1.2 (a,b) Schematics of the general structure of (a) secreted and (b) tethered mucin molecules. (c) An illustration of the network established by the gel-forming, secreted mucins. Individual mucin subunits associate via end-to-end disulfide bonds to form even larger macromonomer chains. The network is formed from reversible associations such as hydrophobic interactions between the non-glycosylated, cysteine-rich regions of the molecules and is stabilized by electrostatic repulsion between the charged sugar side chains. Abbreviation: PTS domain, proline, threonine, and/or serine domain, VWF, von willebrand factor, SEA, sea urchin sperm protein enterokinase and agrin. Panels a and b adapted from Bansil & Turner (2006), Dekker et al. (2002), and McGuckin et al. (2011) with permission from Elsevier and Springer Nature. Panel c adapted with permission from Wagner et al. (2017). Reprinted from Wagner al et Copyright 2018, Annual Reviews.

The collective interactions of the high molecular-weight mucin and the other components of mucus are mediated by a complex series of reversible physical bonds, including hydrophobic interactions, and stabilized by electrostatic repulsion between the negatively charged polysaccharide side chains such as sialic acid. Mucus itself can significantly change its mechanical due to differences in pH and ionic strength and small molecules across different mucus systems in the body. [21] Mucus possesses different physical and biochemical properties based on their location and intended physiological function. For example, the mucus in the eye is thin and allows for hydration and lubrication. In the stomach, the mucus is stiffer and can protect the epithelial lining against acidic gastric fluids.[23] In the gastrointestinal tract, mucus can facilitate nutrient absorption while reducing inflammation of intestinal epithelial cells and acts as a protective barrier from acidic environments and commensal bacteria. [24] Overall, the function of mucus is widely diverse; it can serve a cleansing transport function where external particles trapped in the mucus layer can be eliminated from organ cavities by cilia facilitated expulsion of the mucus layer [24] and act as a selectively permeable gel layer for the diffusion, exchange, and absorption of gases as in the eye and lung.

1.2 Mucosal Delivery

Mucosal delivery is an attractive approach due to its high permeability of drugs in the body, large surface area, and potential mucosal response. [12, 23, 25, 26] Mucosal strategies have been used

in oral, buccal, ocular, nasal, and vaginal delivery, to avoid first-pass effect, targeting specific tissues, and improve bioavailability. [13, 23, 27-34] One of the most common methods used for mucosal delivery is oral delivery, which is characterized by relatively high permeability (i.e., 20-fold more permeable than skin). However, not all drugs can be used for oral transmucosal administration, such as most hydrophilic compounds and biologics. [35, 36] Several drugs have been evaluated for oral transmucosal delivery; however oral transmucosal delivery are limited to existing products, with slight modifications in the selection and development process for new drugs, candidates for oral transmucosal delivery are limited. [37]

The buccal mucosa is located between the lining of the cheeks and the back of the lips. This route allows drugs to avoid first-pass effects, a phenomenon in which a drug or material gets metabolized at a specific region in the body that results in a reduced concentration of the active drug upon reaching its site of action or the systemic circulation. [38] Often biopharmaceutical products such as proteins and oligonucleotides are used for extended drug delivery, classified as bioadhesive or mucoadhesive polymers to improve retention. These polymers are hydrophilic molecules containing hydrogen bonding groups such as poly((meth)acrylic acid), sodium carboxymethylcellulose, and hydroxypropyl cellulose and have been used as buccal mucoadhesive films with propranolol loaded nanoparticles to treat cardiovascular disorders such as angina pectoris. [33, 34, 38-41] Other and more recent mucoadhesive polymers have aimed to an enhanced attraction using site-specific ligands like lectins that have been seen to bind receptors found in the Caco-2 intestinal epithelial barrier cell line. [42]

Ophthalmic drug delivery is used for targeted delivery, as the eye is an isolated organ. However, eye mucus acts as a barrier and has fluid mechanisms that limit the entry of foreign substances into the eye. [43] Novel drugs and materials have been engineered to enable higher

bioavailability from conventional ophthalmic formations by using hydrogels, nanoparticles, and even a mixture of a hydrogel nanoparticle. This method incorporate nanoparticle either through entrapment, encapsulation, or attachment to the surface. Chitin nanogel has been shown to improve bioavailability for fluconazole in the treatment of corneal fungal infections because of the increase in slow release with increase stability. [44] Another ophthalmic delivery method has used poly (lactic-co-glycolic acid) (PLGA) and Polyethylene glycol (PEG) nano- and microparticles to carry loteprednol etabonate (LE), a corticosteroid designed explicitly for ophthalmic inflammatory indications to the eye and allow for rapid diffusion and slow release due to the PLGA nanoparticle mucus-penetrating ability from the PEG coating to overcome the mucus barrier. [45]

Nasal delivery is a method to deliver materials to the blood-brain barrier, or to activate the immune system for vaccines. The nasal cavity is covered with mucus under single-layer columnar epithelial cells in the turbinate portion, and the pseudostratified columnar epithelium covers the olfactory epithelium region for the target blood-brain barrier (BBB). [28,46-49]. The epithelial layer has tight junction molecules such as JAM-A, ZO-1, ZO-2, and claudin that are highly expressed in the human upper airway and nasal epithelial cells. [47-51] Blood-brain barrier penetration have been successful in delivering Brain-Derived Neurotrophic (BDNF) to the brain via nose using chitosan nanoparticles as barrier modulating agent for the treatment of Parkinson's disease by reducing tight junction gaps.[52] Nasal delivery is also used for stimulation of the mucosal immune system. This system has two main components: the inductive sites and the effector sites. The inductive site is composed of antigen-specific immune responses and assist germinal centers in development of IgA and IgB, B cell expansion and cytotoxic T cell generation. Moreover, these regions under the epithelium are rich with antigen-presenting cells (APC) such as residential as dendritic cells, macrophages, and antigen sampling M cells. [25, 26, 28, 37, 48, 49] The effector sites are in the

lamina propria and oversee antibody production and cell-mediated immune responses. Intranasal delivery has been used with mucoadhesive chitosan nanoparticles (CNPs) encapsulated with inactivated swine influenza virus vaccine, and it elicited strong cross-protective mucosal and systemic immune responses in pigs. This has also been done using subunit protein for influenza viruses' nanoparticles in mice models [53, 54]

Lastly, vaginal delivery is an administration route traditionally employed to deliver anti-infective drugs having a local effect in the vaginal region. Vaginal drug delivery is greatly influenced by vaginal fluid dynamics and biomechanical interactions that cause poor diffusion and site absorption to the epithelial lining. Methods to overcome this barrier have used mucoadhesive formulations, such as semi-solids and films. [55, 56] These materials are made from pectin, chitosan, carboxymethyl cellulose, and polyvinyl alcohol (PVA) to increase binding to the mucus and increase residence time. One study demonstrated an expansible thermal gelling aerosol foam with a mucoadhesive enhancer to extend amphotericin B (AmB) release for 4 hours to reduce microbial infection, with no tissue irritation. [57]

1.3 Nanoparticles for Mucosal Delivery

Nanoparticles have critical attributes that allows for their successful use in tissues with mucus barriers. Nanoparticles can contain advantages, such as improved bioavailability by enhancing aqueous solubility of encapsulated drugs and increased intracellular delivery of drugs due to endocytosis which is beneficial for mucosal delivery. Nanoparticles can increase drug residence time in the body and be targeted to specific cell types. While nanoparticles can be directly administered to many mucosal tissues, the penetration of nanocarriers into the tissues is considerably hindered by interactions between the particles and the mucus layer. [7, 8, 10, 29, 45, 58-64] Nanoparticle diffusion

is limited by electrostatic and hydrophobic attractive forces with mucus. [64, 66, 70] The porous structure of mucus filters larger-sized particles and prevents their penetration relative to smaller nanoparticles that do not have attraction interactions with mucus. [71, 72] Various nanoparticles have been used for mucus penetration and delivery in different applications, as summarized in Figure 1.3.

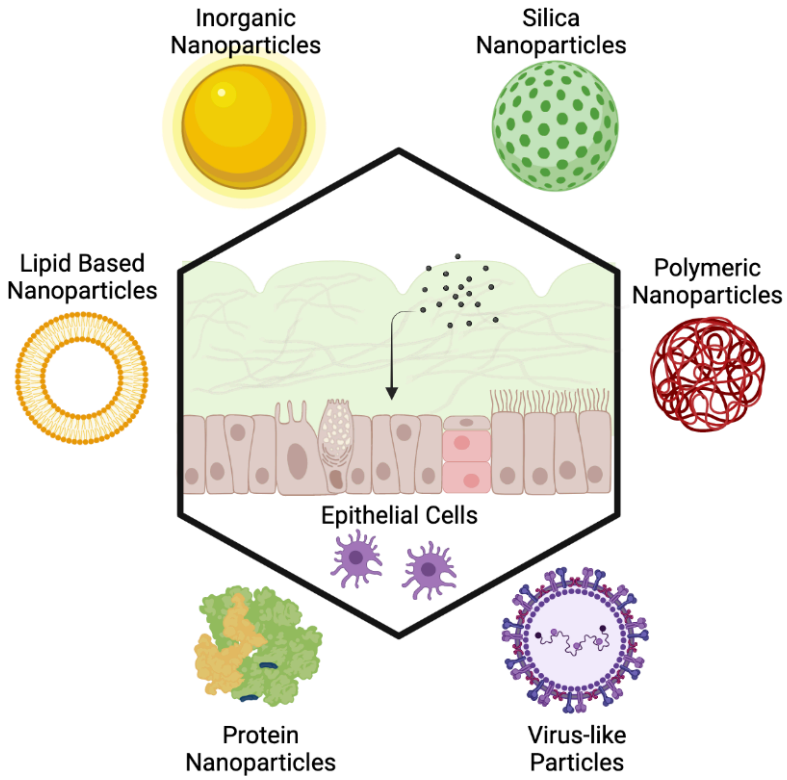

Figure 1.3. Schematics of the diverse nanoparticles used for mucosal delivery.

1.3.1 Inorganic Nanoparticle

Several studies have used inorganic nanoparticles complexes as potential applications for mucosal-controlled delivery. Inorganic nanoparticles are made from elemental metals, metal oxides, and metal salts have been used for bioimaging, drug delivery and vaccination delivery carriers. Thiolate silica nanoparticles functionalized with polyethylene glycol (PEG), poly-2-ethyl-2-

oxazoline, poly-2-methyl-2-oxazoline, poly-2-n-propyl-2-oxazoline, and hydroxyethyl cellulose have been applied to mucus to improve penetration.[73] These coatings mask the mucoadhesive behavior of free thiol groups on silica nanoparticles. When administered to bovine eyes it was shown that the unmodified nanoparticle could not penetrate the deepithelialized cornea because of the interactions of their thiol groups with the cysteine domains of the corneal stroma. However PEGylated (with 5000 Da PEG) silica nanoparticles were able to penetrate the deepithelialized cornea, which could be due to better coverage of silica particles with a stealth layer to decrease the nanoparticles–cysteine interactions.[74] These particles also demonstrated enhanced diffusion in porcine gastric mucin dispersions and penetration into the porcine gastric mucosa as measured by nanoparticle tracking analysis (NTA). [75] When comparing silica nanoparticles that have been modified with chitosan it was shown to improve adhesion to the mucus barrier and improved cellular attachment on HT29-MTX cells, a mature goblet cells from human colon tissues from compared to the uncoated silica nanoparticles. [76]

1.3.2 Gold Nanoparticle

Gold Nanoparticles have been used in various medical applications, from biosensors to vaccine delivery. [49, 77] Gold nanoparticles are fabricated from a gold seed source and a reducing/capping agent such as cetyltrimethylammonium bromide (CTAB). The surface of gold nanoparticles is rich with thiol groups, which promotes thiol and mucin interactions. [78] This is caused by the thiol groups from mucus interacting with the gold core to form gold-sulfur bonds, immobilizing the nanoparticle in the mucus matrix.

1.3.3 Lipid Nanoparticles (LNPs)

Lipid-based nanoparticles are made from lipids consists of amphiphilic fatty acids that assemble into nanoscale liposomes (LNP) or solid lipid nanoparticles (SLN) depending on the exact

formulation and processing conditions. [79] These nanoparticles have been used to encapsulate small molecules, proteins, and nucleic acids for delivery to many tissues, including mucosal tissues. [80-83] Solid lipid nanoparticles (SLN) modified with different surface chemistries have been used to understand the filtering mechanisms and adsorption behaviors of mucus using a Langmuir trough. [84] These studies indicated that surface charge was a more dominant parameter than particle size for adsorption and interaction with the mucin layer. As the dominant mechanisms behind the poor penetration abilities of the particles are the size and interaction filtering of the mucus gel, these filtering mechanisms employed by the mucus should be understood well when developing mucus-penetrating particles.[85] A study from the Bernkop-Schnürch's group has demonstrated charge shifting SLN triggered by alkaline phosphatase for site-specific mucosal drug delivery. [86] This SLN with hydrophilic exterior and loaded with phosphate ester surfactant and the fatty amine octadecylamine demonstrated penetration through mucus gel and forms aggregates above cell layer surface of Caco-2 cells, immortalized cell line of human colorectal adenocarcinoma cells by the presences of alkaline phosphatase. The phosphate ester surfactant provided a negatively charged phosphate-decorated shell to foster mucus permeation. [86] The cell environment provides alkaline phosphatase that removes the outer shell revealing the positively charged octadecyl amine residues. This results in a decrease of interparticle repulsion and an increase of interparticle electrostatic interactions leading to the aggregation of SLN for better retention in the mucus.[86]

1.3.4 Polymeric Nanoparticles

Polystyrene nanoparticles are often used as model particles to probe the impact of various surface interactions with biological mucus matrix. Specifically, polystyrene nanoparticles have been heavy studies within the past decade to probe mucus interfacial interactions due to their ability to easily modify their surface and tune their size. The Hanes group have studied diffusion of polystyrene

of different size nanoparticle in a transwell diffusion chamber with porcine gastric mucin gel, which identified a decrease in translocation permeability when particle size approached 300 nm. [87]. Similarly, the Hane lab have suggested low percentage of carboxylate polystyrene nanoparticles movement across 220 μm-thick cystic fibrosis sputum layers after a duration of 150 mins, and the largest nanoparticles at ~560 nm are blocked by the sputum. [63] Polystyrene nanoparticles were also coated with hydrophilic DNA, which demonstrated high transport rate and increased diffusion by 10-fold in pig gastric mucus compared to similar-sized hydrophobic nanoparticles. [63, 88] Polystyrene nanoparticles have been coated with low molecular weight (2 kDa) PEG at a high surface density to shield the hydrophobic polystyrene core, reducing particle interactions with mucus. [89, 90]

1.3.5 Virus-Like Particle

Virus-like particles are particles that mimic the structure of viruses. These are non-infectious carriers that carry no viral genetic materials but often drugs that is encapsulated. These particles are synthesized and fabricated through the individual expression of viral structural proteins, which will self-assemble into the virus-like structure. Wang et al. found that the surface makeup of different VLPs presenting neuraminidase, a sialic acid cleaving enzyme commonly found in influenza viruses, had no significant impact on diffusion in the mucus. [91] However, VLPs modified with 2 kDa polyethylene glycol had 10-fold higher diffusion 10-fold higher compared to the VLPs with neuraminidase. This result highlights strategic modifications to improve diffusion through the mucus and demonstrate how coatings can be used on different nanoparticles systems as mentioned in previously.

1.3.6 Protein Nanoparticles

Protein Nanoparticles are a unique blend of nanoparticles that allows for the drug or protein used to potentially be the carrier. The versatility of protein and their polymeric behavior allows for

unique fabrication methods. One examples can been seen with gliadin nanoparticles, which are proteins that are suitable for targeted drug delivery for their high affinity to the upper gastrointestinal tract; therefore, gliadin nanoparticles have been previously made using the desolvation method, and the size ranging from 285 ± 44 nm to 392 ± 20 nm. [92] It is believed that the lipophilic amino acids residues in gliadin interact with the mucus through hydrophobic interactions, explaining their increased affinity. [93] These gliadin nanoparticles were loaded with amoxicillin to reduce Helicobacter pylori in the upper gastrointestinal (GI) tract. The gliadin successfully increased the retention time in the GI tract and demonstrated better efficacy than soluble amoxicillin. [94] Deng et al. have shown the usage of desolvation to produce nanoparticles with flagellin carrier fused to influenza conserved epitopes to provide full protection against influenza A virus challenge using Intranasal immunization. They designed fusion proteins for flagellin (FliC) with four tandem copies of the ectodomain of matrix protein 2 (f4M2e), HA1, HA2 domain (fHApr8) and H3 HA2 domain (fHAaichi) and upon nasal vaccination saw successful antigen-specific humoral immune responses. [95]

1.4 Motivation and Objectives

The development and engineering of nanoparticles for mucus delivery is greatly impacted by nanoparticles' surface chemistry and resulting interactions with the mucus. This has led to the development of surface-modified nanoparticles of many different types to achieve better transport through the mucus mesh.[88] However, modifications designed to overcome the first biological barrier, the mucus, may lead to poor performance at subsequential barriers such as the epithelial lining beneath the mucus, and deeper tissues beyond such as the common PEGylation methods that allows for improved mucus delivery but poor intracellular uptake. Research has heavily focused on

improving the bioavailability of nanoparticles to move pass the mucus. However, much fewer work designs for both mucus and cellular barriers.

There is a significant gap in engineering nanoparticles to improve both mucus delivery and improvement in cellular uptake. The mucus is one of multiple barriers nanoparticles that will need to be overcome to reach the desired target of reaching the mucosal immune regions. The main objectives of this thesis are (1) engineer protein nanoparticles with different surface chemistry to evaluate their mucus transport. Protein nanoparticle has unique properties such as high carrier to drug ratio, surface for bioconjugations and applications for vaccines and protein therapeutics. (2) dentify the protein corona (protein adsorbed) found when engineered nanoparticles in the nasal secretion, and (3) evaluate the cellular uptake and response when exposed to nasal fluids.

1.5 Thesis Overview

This thesis aims to engineer protein nanoparticles with different surface properties, achieved via covalent and non-covalent methods, to modulate their diffusion in mucus, identify protein association to nanoparticles in nasal fluids, and interaction with mucus as well as cellular interactions. To accomplish these objectives, Chapter 2 describes the design of protein nanoparticles with different surface modifications, the characterization of nanoparticle diffusion in porcine mucus using multiple analytical techniques, and the evaluation of the combination of diffusion and uptake by dendritic cells. Using these nanoparticles, Chapter 3 describes identification the protein corona that is adsorbed from human mucus onto the nanoparticles and epithelial cell internalization of nanoparticles with corona. Finally, Chapter 4 summarizes the work presented in this thesis and provides an outlook on future aspects of this work.

CHAPTER 2. ENGINEERING PROTEIN NANOPARTICLES FOR MUCOSAL TRANSPORT

2.1 Introduction

Intranasal delivery has unique benefits, such as access to the blood-brain barrier and nasal-associated lymphoid tissue (NALT), which can stimulate an immune response. However, the mucus barrier of the nasal cavity is a significant challenge to overcome due to its intrinsic physical mesh nature and attractive chemical interactions.

One solution to overcome this is with nanoparticles, many types of engineered nanoparticles are developed and used for drug delivery and biomedical applications. Nanoparticles have unique attributes such as high surface to volume ratio, the ability for endocytosis, and high amount of material taken up after cellular uptake. [49,94] Moreover, the literature has shown that various nanoparticles such as inorganic nanoparticles, polymeric nanoparticles, lipid-based nanoparticles, protein nanoparticles such as virus-like particles have been used for intranasal delivery by surface modification. [10, 45, 61, 94-97] These modifications often change the behavior of nanoparticles in mucus and enhance their delivery through the mucosa. For example, it has been shown that carboxylate polystyrene nanoparticles have poor penetration and diffusion due to the interacting with much and size filtering phenomena that promote strong adsorption to the mucus mesh. [98] However, coating a short, highly dense brush of 2 kDa Polyethylene Glycol (PEG) on polystyrene nanoparticles reduced the mucus interaction significantly. [87, 99, 100] In order to change the surface chemistry of nanoparticles, bioconjugation has been explored as a chemical strategy to form stable covalent bonds between a nanoparticle and coating agent or molecule of interest. Famously, gold nanoparticles (AuNP) have used bioconjugation as a pivotal technique for nanoparticle surface modification. [77, 101] The surface of gold nanoparticles is rich with cysteine or amine groups while maintaining

different molecular interactions such as electrostatic and hydrophobic interactions. One frequency method used on AuNP is carbodiimide crosslinkers using 1-(3-dimethylaminopropyl)-3-ethylcarbodiimide hydrochloride N-hydroxysuccinimide (EDC/NHS). This reaction allows for the formation of a covalent bond between a carboxylic acid and a primary amine. In which EDC couples NHS to the carboxyls, forming an NHS ester while allowing for efficient conjugation to primary amines at physiologic pH. This have been employed for the conjugation of molecules such as antibodies on AuNP. [101] Another method commonly used is forming stabilize coats using thiol conjugation from the surface of gold nanoparticles to chitosan that contains thiol group to form stabilize disulfide bonds. [101] To probe different surface chemistry of nanoparticles in mucus, we have modified antigen proteins nanoparticles and evaluate their ability for intranasal vaccination. Protein antigens can be used as subunit vaccines, which have advantages over traditional vaccines such as improved safety profile and greater control over the host's immune response. [102] Protein nanoparticles have significant potential to be used as intranasal vaccines but their modifications for mucosal delivery due to their high antigen load and incorporation of different surface modifications. The use of vaccines to invoke an immune response in mucosal environments is essential due to the high number of viral and bacterial pathogens that are transmitted via mucosal tissues especially respiratory and genital tracts. Mucosal vaccination, such as intranasal, can result in local antibody production and immune cell activation in the tissue, in addition to a systemic immune response. Mucosal antibodies can interact with pathogens before they enter systemic circulation, where serum antibodies are, providing first line protection as demonstrated by Deng al et. [95] The challenge with intranasal delivery is the multitude of barriers and low access to the NALT. [104, 105]

In addition to antigens, nanoparticles can also be manipulated to carry adjuvants, which stimulate the body's immune response, either by encapsulation or by surface conjugation or coating.

Examples of adjuvants are aluminum hydroxide, aluminum phosphate, potassium aluminum sulfate (Alum), chitosan and CpG oligodeoxynucleotide (CpG ODN). [106, 107] For example, CpG ODNs improve the function of professional antigen-presenting cells and boost the generation of humoral and cellular vaccine-specific immune responses. [107] Chitosan is a sugar obtained from the hard outer skeleton of shellfish and enhances both humoral and cell-mediated immune responses by promoting a balanced Th1/Th2 immune response. [108, 109]

Aside from adjuvants, other materials can also be included in nanoparticles to assist in delivery rather than immune response. For example, iron oxide can be incorporated for directed magnetic delivery of nanoparticles. Si et al. have delivery of superparamagnetic microspheres directed with a series of magnets on the nose for brain penetration. This strategy improved the delivery efficiency to the olfactory region, which is the layer that covers the brain from the nasal route, which improved to 45% locations compared to less than <1% without magnetic delivery. [111]

In this chapter, we engineer 5 different modifications of protein nanoparticles made from model protein antigen ovalbumin (OVA). The nanoparticles are fabricated by desolvation where a desolvant, such as ethanol, is added to solvent (water) dispersed protein. This induces protein clustering due to hydrophobic interaction and the clusters are then stabilized using covalent crosslinkers. Desolvation has produced functional protein nanoparticles for both vaccination and therapeutic applications [113,114]. The desolvated OVA protein nanoclusters (PNC) were then modified by covalent or non-covalent methods to alter their transport properties in mucus. We evaluated the diffusion of nanoparticles in porcine mucus using both bulk and multiple particle tracking analyzes. We also evaluated the uptake of nanoparticles in mucus by an antigen presenting dendritic cell line. This study demonstrated the impact of protein nanoparticle surface modification in the opposing processes of mucus diffusion and cell uptake and identified formulations with potential for improved *in vivo*

performance. These results and methods presented here may also be applied to other classes of nanoparticles used mucosal delivery.

2.2 Methods

2.2.1 Fabrication of Chicken Egg Albumin Protein Nanoparticles (OVA-PNC)

The synthesis of OVA-PNC was performed according to desolvation process. The desolvent phase containing pure ethanol was added dropwise to 0.1 mL protein solvent phase that contained 6.2 mg/mL chicken egg albumin in phosphate-buffered saline (PBS, pH 7.4) under constant mixing at 700 rpm. The protein NPs were then collected using centrifugation at 14,000 xg for 10 mins and resuspended by sonication in 0.5 mL PBS. Next, 3,3'- dithiobis(sulfosuccinimidyl propionate), DTSSP (Thermo Fisher) was added at a ratio of 2.2 lysines to one molecule DTSSP and the nanoparticle suspension was mixed at 600 rpm at room temperature for one hour. The solution was centrifuged for 32 mins 16,000 x g at 4˚C. The supernatant was removed, and the pellet was resuspended in 500 μL of PBS. The nanoparticles were sonicated on ice for 1 minute, for 1 second on and 3 seconds off at 50% amplitude. The nanoparticles were then centrifuged for 5 minutes at 500 x g and the supernatant was collected and the pellet was discarded.

2.2.2 PEGylated (PEG) OVA Protein Nanoparticles

A 1.0 mL suspension of OVA NPs in PBS (10 mg/mL) was combined with 0.1 mL sodium bicarbonate solution (1 M, pH 9.0) and 0.4 mg O-[(N-Succinimidyl) succinyl-aminoethyl]-O′-methylpolyethylene glycol (average M_n 750). The mixture was reacted at room temperature as it inverted for 1 hour on a Rocking Platform Shaker (VWR) at a 10˚ tilt angle. The PEGylated OVA NPs were collected using centrifugal filtration (Amicon, 10 kDa).

2.2.3 Cationic OVA Protein Nanoparticles

Cationic PNC were prepared using a modified method [114]. 1.0 mL of protein OVA PNCa were centrifuged at 18000 xg for 10 mins. The PNC pellets were resuspended in 1 mL of 0.1 M 2-(N-Morpholino)-ethanesulfonic acid buffer (MES, 4.7 pH) and sonicated on ice 2s on and 2 s off at 30% amplitude for 1 min. Approximately 40 mg of 1-ethyl 3-(3-dimethylaminopropyl)carbodiimide hydrochloride (EDC) in 0.5 mL of MES buffer (pH = 4.7) was added to the to the nanoparticle solution and reacted on ice for 1 hr. A 1:1 ratio of ethylenediamine solution to MES buffer was prepared and pH was adjusted to 4.7 on ice to cool heat released from reaction. The cold ethylenediamine solution was added to nanoparticle solution for 30 mins and centrifuged at 18,000 xg and resuspended in PBS.

2.2.4 Layer by Layer OVA PNC Fabrication

To adjust for size, the core OVA PNC used for layer-by-layer OVA PNC were prepared using a modified desolvation method from above. 20 mg/mL OVA in 0.1 mL PBSs desolvated under constant stirring at 700 rpm with 0.4 mL ethanol added dropwise. The resuspension was collected using centrifugation and resuspended by sonication in 0.5 mL PBS. DTSSP (Thermo Fisher) was added to stabilize the protein nanoparticles and stirred at 600 rpm for 1 hour at room temperature. The protein NP were centrifuged at 18,000 xg and the supernatant was collected to be the cores of the Layer-by-Layer OVA PNC. The layers were developed through dip coating in chitosan and short oligonucleotide for the cationic and anionic layers, respectively. The chitosan coating adheres to the surface of the nanoparticle due to electrostatic interaction, followed by subsequent anionic and cationic layers. A 0.6% w/v solution of deacetylated chitosan was prepared in 10% v/v aqueous acetic acid. The pH was then adjusted to 6.0 using 1 M NaOH, and protein nanoparticles were incubated in the chitosan solution for 30 mins at 30˚C. The suspension was then centrifuged at 18,000 xg at 4˚C

and washed with Milli-Q water (18.2 MΩ·cm) and centrifuged to remove excess chitosan twice. The particles were then added to a solution of 22.1 nM CpG oligonucleotide and incubated for 30 mins at 30˚C, centrifuged at 18,000 xg at 4˚C and washed with Milli-Q water (18.2 MΩ·cm). An additional coating of chitosan was added following the same procedure as the first layer.

2.2.5 Magnetic Protein Nanoparticles

OVA protein NPs loaded with Iron Oxide Nanoparticle (IONP) were prepared following a similar desolvation method. Methyl-functionalized IONPs (10 nm, Cytodiagnostics) were sonicated, and 10 µl of 5 mg/ml IONP was added to 0.1 ml of 22 mg/ml OVA and stirred briefly. The ethanol desolvation and glutaraldehyde crosslinking were performed exactly as described above for the undoped OVA NPs. IONP-protein NPs were collected by centrifugation at 18,000×g, resuspended in 0.5 ml PBS, and separated using a neodymium magnet (Applied Magnets, Plano, TX).

2.2.6 Nanoparticle Characterization

Protein nanoparticle size distribution and zeta potential were assessed by dynamic light scattering (DLS) and electrophoretic light scattering (ELS) respectively with a Malvern Zetasizer Nano ZS (Malvern Instruments, Westborough, MA). Protein concentration in the nanoparticle solution was assessed with a BCA assay according to the manufacturer's instructions (Thermo Scientific, Waltham, MA). Protein nanoparticles (0.5 mg/ml in 0.1X PBS for zeta potential) were measured using dynamic light scattering (DLS; Malvern Zetasizer, Nano-Z; Malvern Instruments, Worcestershire, England). Measurements were carried out in triplicate with three distinct samples. Each measurement consisted of 12–30 runs. Electrophoretic mobility was converted to zeta potential using the Smoluchowski approximation.

To determine the release of chitosan and DNA layers from the LBL nanoparticles, LBL particles were made from chitosan labeled using labeled using Alexa Fluor™ 647 NHS Ester

(Succinimidyl Ester) from molecular probes. Due to poor solubility at high pH, 2 µL Alexa Fluor 647 was added dropwise to a solution of deacetylated chitosan (0.6% w/v solution in 10% v/v aqueous acetic acid), which was adjusted to pH 8.3 using 0.1 M sodium hydroxide dropwise with 10 mins between each drop. Once at pH 8.3 the sample was incubated for 1 h at room temperature, followed by adjustment to pH 4 and removal of excess dye using filtered centrifugation (Amicon, 10 kDa). To confirm removal of all excess dye, thin-layer chromatography (TLC) silica gel with methanol and water (8:2 v/v) mobile phase was used. The TLC plate was visualized using Chemidoc MP imaging system (Bio-Rad Laboratories) under the Alexa Fluor 647 filter. LBL nanoparticles was incubated in dilute mucus for 30 mins and spun down at 16,000 xg for 10 mins. The supernatant was measured at 650(ex)/665(em) nm to determine chitosan release.

TEM for iron oxide protein NPs was carried out on a CX-100 (JEOL) TEM. PNC images were obtained at 100 kV with × 80K magnification. All samples were prepared by drop casting on 400-mesh copper grids (Electron Microscopy Sciences) and dried at room temperature. Protein NPs were stained with 5 µl of 1% sodium phosphotungstate (Thermo Fisher) solution and washed twice with Milli-Q water.

2.2.7 Mucus Isolation from Porcine Nasal Cavity

Freshly isolated pig's nasal turbinate tissues and overlying mucosa from the nasal cavity was obtained from a local abattoir (Holifield Farms). Mucus from the cavity were isolated and the nasal turbinate tissues was rinsed with cold phosphate buffered saline. Additional mucus was harvested from the adherent mucus layer using gentle scraping and all samples were stored at -20˚C.

2.2.8 Rheological Studies on Mucus

The rheological viscosity was measured by ratio of shear stress to shear rate using Brookfield DV2T Rotational Viscometer with CP-51 cone and DV2TLV spindle. Extracted mucus samples were measured following manufacturer's instructions at various shear rates (0.1, 0.6, 1, 5, and 10). All measurements were conducted at room temperature. After the samples were loaded into the rheometer, they were equilibrated for 10 mins. The shear stress to shear rate of three samples were plotted using graphPad Prism 9.01 (GraphPad Software).

2.2.9 Alexa Fluor-647 Fluorescent Nanoparticles

Alexa Fluor 647 succinimidyl esters-labeled albumin (OVA) was prepared by incubation of 2.5 μg of AF647 from molecular probes to 0.4 mg of OVA in 1 M sodium bicarbonate solution (pH=8.3) for 1 hr. Excess dye was removed using filtered centrifugation (amicon, 10 KD)and buffered exchanged to PBS. Degree of labeling and the final protein concentration was measured using the fluorescent dye labeling settings on a NanoDrop 2000. 7% soluble OVA conjugated with Alexa Fluor 647 was supplemented into the OVA solution. The nanoparticle desolvation and characterization procedures described above were used to fabricate fluorescent protein nanoparticles.

2.2.10 2D Bulk Channel Diffusion

Bulk diffusion was measured using a custom-made borosilicate glass channel 1.2 mm thick entrance. The channel was filled with 3 mL of extracted nasal pig mucus and 0.1 mL of 1.0 mg/mL of Alexa Fluor 647 labeled albumin protein nanoparticles (OVA NP) on the entrance of the channel. Diffusion was measured as a function of time using Chemidoc MP imaging system (BioRad) under the Alexa Fluor 647 filter. The glass slide was stationed horizontally to reduce the impact of gravity as the nanoparticles moved across the mucus. Images of the channel were taken at the same exposure and gain, and the image was then analyzed using ImageJ surface plot function. For the iron oxide

protein nanoparticles, a neodymium magnet was placed on end of the glass side for directed magnetic delivery through the mucus.

2D bulk diffusion images were analyzed using ImageJ surface plot analysis. The luminance of the channel image from the labeled nanoparticles is interpreted as height for the surface plot on a length axis. A threshold of the mucus was used to determine to removed background fluorescence and an average surface plot (n=3) was graphed using graphPad Prism 9.01 (GraphPad Software). A summary of 2D bulk diffusion values were normalized as a binary value for nanoparticle occupancy of the length slice using the mucus' threshold value and summed as nanoparticle penetration for each quartile of the glass channel (n=3).

2.2.11 Multiple Particle Tracking (MPT) in Mucus

NP diffusion through nasal mucus was assessed using MPT technique using described mathematical methods to determine a diffusion coefficient (D_{eff}) in diluted mucus. Around 25 ug of Alexa Fluor-647 nanoparticles were resuspended in 10-fold diluted mucus and incubated for 30 mins in a well plate with glass bottom (MatTek). Video capture involved 2-dimensional imaging on a PerkinElmer UltraVIEW VoX spinning disk confocal microscope with Hamamatsu C9100-23b back-thinned EM-CCD with 640 nm red laser (x63 magnification oil immersion lens) running at 10 frames s^{-1} with 500 frames for each video. Multiple particle tracking analysis was performed using Fiji ImageJ software with MOSAICsuite [2D particle analysis] plugin. [115-117] Videos were exported and converted into the position of each nanoparticle across the duration of the videos. Particles were filtered with a 4-radius pixel count and a cutoff of 2 pixels under Brownian in motion dynamics. The mean square displacement value for each particle as a function of time using X-Y trajectories was calculated as in Equation 1. Particles with mean square displacement that was out of the X-Y frame

under 30 frames were filtered out. The analysis follows a similar approach found in literature. [115-117]

$$\mathrm{MSD}_{\mathrm{NP}} = (\mathrm{X}_{\Delta t})^2 + \mathrm{Y})^2 \qquad \text{Equation 1}$$

In each nanoparticle type, roughly 500 individual NP trajectories were assessed. The effective diffusion coefficient (D_{eff}) for each NP type was then calculated under 2D random walk approximation shown in Equation 2. MATLAB code provided in Appendix Code.

$$\mathrm{D}_{\mathrm{eff}} = \frac{<\mathrm{MSD}>}{4\Delta t} \qquad \text{Equation 2}$$

Each particle diffusion profile was plotted using GraphPad Prism 9.01. The profiles were modeled using Gaussian curve fit. Layer-by-layer nanoparticles displayed a binomial distribution and were separated into a high and low diffusion coefficient group for Gaussian fitting.

2.2.12 Periodic Acid-Schiff (PAS) Mucus Assay

Periodic acid-Schiff is a method for the detection of polysaccharides, which are components of mucin. Periodic acid-Schiff colorimetric assay has been previously used to determine the mucin adsorption on chitosan particles. [115,116] Schiff reagent contained 1% basic fuchsin in 1 M hydrochloric acid. 0.1 g sodium metabisulphite (Sigma) was added to 6 mL fuchsin solution and heated at 37˚C until solution was clear. The periodic acid solution was prepared adding 10 µL of 50% aqueous periodic acidto 7 mL of 7% aqueous acetic acid. Calibration curves were made using the extracted porcine mucus, diluted by adding 0.2 mL periodic acid to 2 mL of mucus sample followed by incubation at 37˚C for 2 h. Finally, 0.2 mL of the Schiff solution was added to the solution. After a 30 min incubation at room temperature, the sample absorbance was recorded at 555 nm on a Biotek Synergy HT Microplate Reader. To determine the adsorption of mucus on nanoparticles, they were incubated in 10-fold diluted mucus for 30 mins. The samples were then centrifuged at 16,000 xg for

5 mins, and the pellet and supernatant were collected for polysaccharide detection to determine mucus adsorption. A blank of mucus suspension was used at 16,000 xg for 5 mins to determine the amount of mucus being spun down from the centrifugation of the samples as a background and particles were used to determine background in detection (n=3).

2.2.13 JAWSII Cell Culture

JAWS II immature dendritic cell line was obtained from the American Type Culture Collection (Manassas, VA) and cultured in MEM-alpha (Corning, Manassas, VA) supplemented to 4 mM glutamine and 5 ng/mL GM-CSF (Peprotech, Rocky Hill, NJ), 20% fetal bovine serum (FBS), and 1% penicillin/streptomycin (Amresco, Solon, OH). Cells were cultured in T-75 flasks with 10 ml media/flask until ~70% confluency was reached. All cells were incubated under humidified conditions at 37 °C, 5% CO_2. For all experiments, cells were plated at a density of 10^5 cells/mL and incubated for 24 hours prior to incubation with particles unless indicated otherwise. Cells with less than 10 passages were used for all experiments.

2.2.14 Flow Cytometry

Nanoparticle uptake was assessed by flow cytometry. Fluorescent nanoparticles were fabricated as previously described with 10 wt% AlexaFluor 488-conjugated OVA (Life Technologies, Grand Island, NY). JAWS II dendritic cells were plated in 96 well plates at 3 x 10^5 cells per well in triplicate and incubated with 0.2 ng NP/cell fluorescent OVA nanoparticles or soluble OVA. Each particle concentration was confirmed using BCA assay and fluorescent intensity measured at 488 nm excitation and emission 525 nm using a Biotek Synergy 2 Microplate plate reader. Particles were incubated with high- and low- concentrated mucus for 30 mins, then exposure to JAWS II cells. Cells were washed once with PBS, briefly trypsinized, then filtered with 40 μm cell Strainers (VWR) and resuspended in chilled trypan blue to quench external green fluorescence. Cell

fluorescence was measured after 1- and 4-hours incubation with particles using a Beckman Coulter CytoFLEX. Gating was established using cells without exposure to nanoparticles, and all conditions were run with triplicates.

To measure CD86 maturations, 1.5 $X10^5$ cell/well of JAWS II dendritic cells were plated in a 48-well plate for 24 hours. Nanoparticles and soluble OVA was added with mucus for a 24-hour incubation with media. Cells were washed with PBS, and well were blocked using a 1% Bovine Serum Albumin Fraction V (Sigma-Aldrich) for 5 minutes. TruStain FcX receptor blocking solution (BioLegend) was used to block the FC region and non-specific blocking, and Anti-CD86-PE (BioLegend) was then added to each well. Finally, 3.7% paraformaldehyde was added on ice to each well and cells were scraped and strained through strainer for flow cytometry.

2.2.15 <u>Confocal Microscopy</u>

JAWS II dendritic cells were seeded at a density of $1x10^4$ cells per well in a 6-well chamber No. 1.5 coverslip glass bottoms (Mattek) with growth medium. After 24 hours, cells were incubated with medium without Fetal bovine serum (FBS) with 0.2 ng/cell of particles that been incubated for 30 mins in dilute mucus. Cells were washed three times with ice cold PBS and fixed with 3.7% paraformaldehyde for 10 minutes at room temperature. Cells were incubated with 0.0528 μM rhodamine phalloidin (Biotium) in blocking buffer for 15 minutes at room temperature to stain for actin, and cell nuclei were stained with 0.02 μM Hoechst 33342 for 20 minutes at room temperature. Cells were washed three times after each stain with PBS and imaged with a Perkin Elmer UltraVIEW VoX spinning disk confocal.

2.2.16 Statistical analysis

Statistical significance was determined using two-tailed Student's t-test in comparing two different conditions. Two-way ANOVA was used to analyze the significant difference among 3 or more groups. P-values less than 0.05 were significant (*, $p < 0.05$; **, $p < 0.005$; ***, $p < 0.001$). The analysis was performed with GraphPad Prism (version 9.01) software (GraphPad Software, San Diego, CA)

2.3 Results and Discussion

2.3.1 Nanoparticle Fabrication and Characterization

Nanoparticle surface charge is one of the most important physiochemical properties that influence the interaction between mucus and nanoparticle, and the overall net charge of nanoparticles on moderately homogenous surfaces can greatly impact the outcome of surface attachment of mucus on inorganic nanoparticles. [10, 29, 45, 63, 77] Therefore, tuning protein nanoparticle surface charge properties may allow for unique mucus interactions compare to one another. Moreover, protein nanoparticle is a heterogenous surface that reflects the net charge of OVA bare (unmodified) nanoparticle. Therefore, modifying the surface of these nanoparticles will potentially allow for overall net changes to their surface. For example, the EDC/EDA modification provides the addition of primary amines on the surface of these protein nanoparticles. This modification will allow for a net positive charge which will mimic the impact of electrostatic interaction previously seen with carboxyl polystyrene nanoparticles in mucus. Using a short Polyethylene Glycol (PEG) coating, we can shield the heterogenous surface to provide a uniform protein nanoparticle with a net neutral charge. Lastly, we explored a noncovalent fabrication method using a layer-by-layer approach, which allowed for alternating charged coatings which could allowed for shedding in the mucus. The protein

nanoparticles were fabricated using OVA, a model antigen protein using desolvation and crosslinked with DTSSP. To remove the impact of size, fabrication conditions were tuned to maintain similar size distribution among all particle types. Dynamic light scattering was used to determine the size and polydispersity index (PDI) of each nanoparticle (Table 2.1, Figure 2.1). All particle diameters fell in the range of 315 to 326 nm with PDI of 0.23 or less and this consistency indicates that differences in mucus interactions are due to surface properties and not particle size.

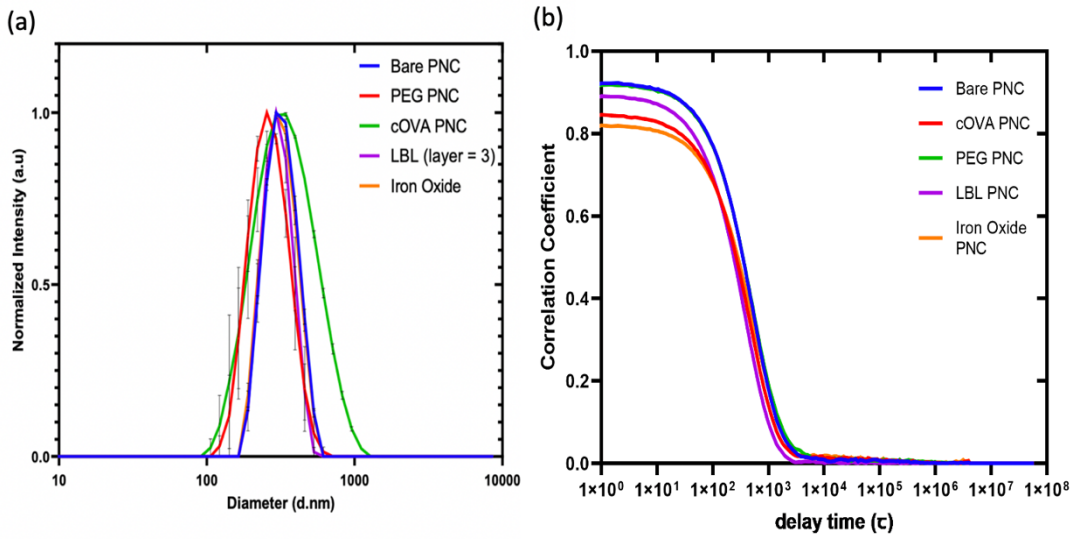

Figure 2.1: A) Size distribution overlay of Bare PNC, cOVA, PEG PNC, LBL PNC, and Iron Oxide PNC using dynamic light scattering) (n = 3 independent batches of nanoparticles). B) DLS correlogram overlay of Bare PNC, cOVA, PEG PNC, LBL PNC, and Iron Oxide PNC confirming the similar size of all three nanoparticles (n = 3 independent batches of nanoparticles). The overlapping length of exponential decay indicates similar size distributions for each nanoparticle.

The surface charge is the physicochemical parameter of interest in this study that will impact the diffusion of nanoparticles in mucus and interaction with cells. To probe the impact of the charge, we reacted OVA nanoparticles with dimethyl aminopropyl) carbodiimide hydrochloride) (EDC) and ethylenediamine, the primary amine, to produce cationic OVA nanoparticles (cOVA NPs). The zeta potential for the cOVA was +19.43 ±1.47 mV, compared to the unmodified OVA PNC nanoparticle with a zeta potential of -23.73 ±1.25 mV. In order to "cover" all the charged amino acids in OVA and

form a neutral nanoparticle, we conjugated methyl polyethylene glycol (average Mn 750) functionalized with a succinimidyl ester group to primary amines on OVA PNC The zeta potential was -10.36 ±0.83 mV, which is in the range considered to be neutral (-10 to +10 mV). We developed a non-covalent layer-by-layer approach using two charged adjuvants, mucoadhesive chitosan and single-stranded DNA to produce particles with dynamic surface charge in comparison to the other, static nanoparticle surfaces. We made the core OVA nanoparticles smaller to compensate for the additional size each layer added: chitosan, DNA, chitosan. The goal was to allow for a unique ability to shed layers in the mucus environment and enable both mucoadhesion (positive chitosan layers exposed) and mucorepulsion (negative DNA layer exposed) to occur. Zeta potential alternated with each layer, with the outermost layer being +21.1± 1.6 mV.

Table 2.1: Summary of Bare OVA PNC, cOVA, PEG PNC, LBL PNC, and Iron Oxide PNC using dynamic light scattering (d.nm) and zeta potential (mV) using Smoluchowski approximation.

Sample[a]	Size (d.nm)[b]	PDI[c]	ZP (mV)[d]
Bare OVA PNC	326.36 ± 4.2	0.21 ± 0.05	-23.73 ± 1.3
cOVA PNC	315.8 ± 5.6	0.23 ± 0.09	19.43 ± 1.5
PEG PNC	321.43 ± 1.3	0.19 ± 0.06	-10.36 ± 0.8
LBL PNC			
Core	161.3 ± 6.3	0.23 ± 0.08	-22.5 ± 1.8
1	220.1 ± 12.2	0.26 ± 0.07	18.3±1.4
2	255.4± 6.3	0.23 ± 0.07	-20.8±1.6
3	324.2 ± 7.2	0.22 ± 0.05	21.1 ± 1.6
Iron Oxide PNC	324.43 ± 5.3	0.21 ± 0.07	-22.52 ± 1.5

[a] n=3 independent batches of nanoparticles; [b] hydrodynamic diameter; [c] polydispersity index, and [d] zeta potential (mV)

While varying surface charge and chemistry alters the diffusion of particles in mucus, we also identified a modification to enable active transport by encapsulation of iron oxide nanoparticles during fabrication of protein nanoclusters. Iron oxide nanoparticles are a superparamagnetic material that is highly reactive to the attractive force from magnets. We isolated only OVA nanoparticles containing iron oxide using a neodymium magnet. Both size and surface charge were indistinguishable from non-magnetic OVA particles. The 10 nm iron oxide nanoparticles encapsulated in OVA nanoparticle were detectable using TEM, as shown in Figure 2.2.

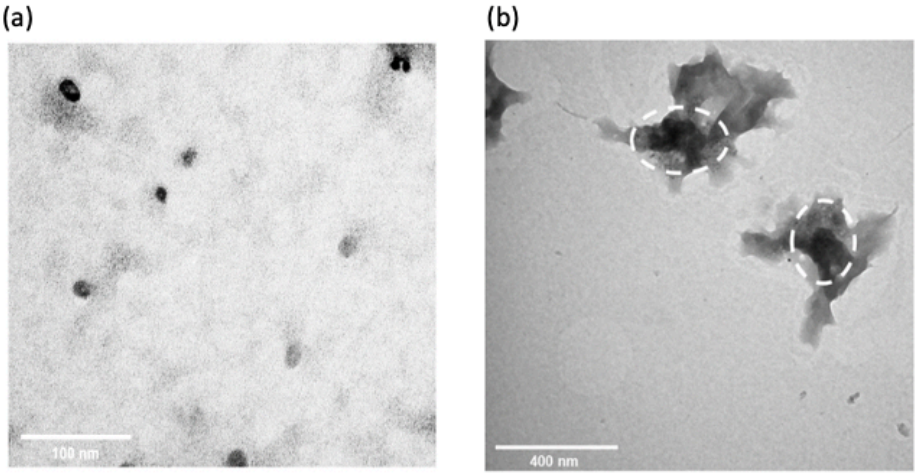

Figure 2.2: a) Transmission electron microscopy water soluble iron oxide nanoparticle ~10.0 nm, scale bar, 100 nm. b) Transmission electron microscopy of protein nanoparticle with iron oxide nanoparticle, circles indicate dense iron oxide nanoparticles embedded in the protein nanoparticle, scale bar, 400 nm.

2.3.2 Mucus Characterization

We extracted fresh mucus from a pig's nasal cavity to study the impact of protein nanoparticle modifications on mucus interactions. Judge et al. reported that the physical properties of mucus derived from porcine respiratory system show physical and chemical similarly to human mucus, which allows it to serve as a model for translational research. The extracted mucus was analyzed using a viscometer to confirm its shear thinning behavior. The shear rate (sec^{-1}), γ, was altered to measure apparent viscosity, η (centipoise, cP), as a function of shear rate (sec^{-1}) (Figure 5). This confirms the extracted porcine mucus has the expected properties that make it an appropriate model to mimic human mucus, moreover it has been reported a viscosity of 1.6 ± 1.5 Pa/s or 1600 ± 1500 cP at 1 Hz or 1 sec for shear rate, this range fits our value of 1931.4 cP at the shear rate of 1 sec. [24]

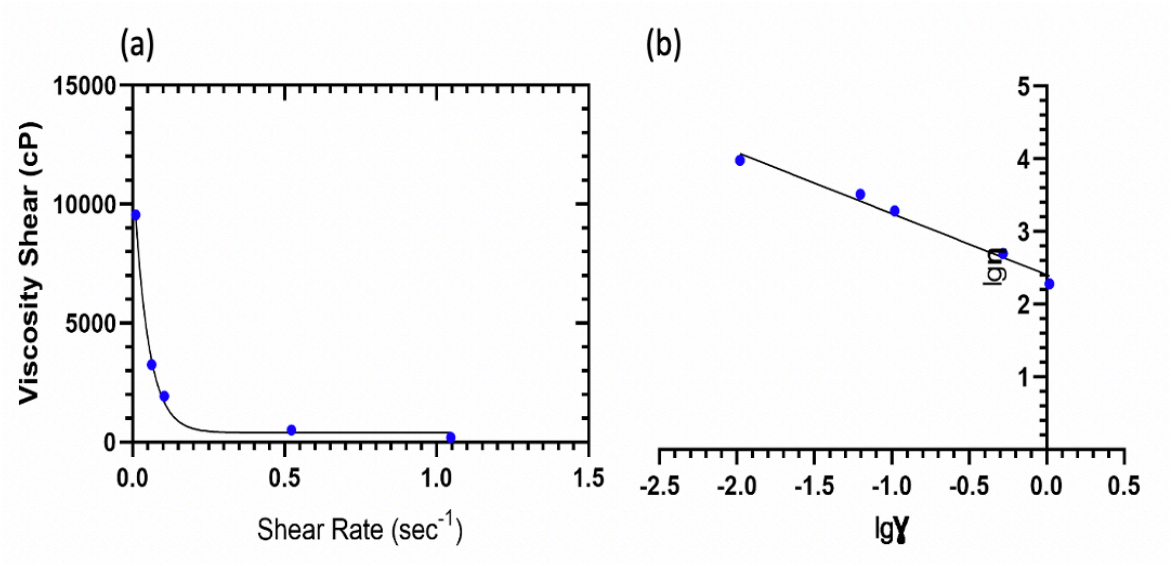

Figure 2.3: a) shear rate vs viscosity shear (cP) from viscometer of raw pig mucus b) log of the shear rate vs viscosity shear to show linear decrease of log apparently viscosity and log shear rate for shear thinning property.

2.3.3 Bulk Diffusion Results

A customized glass channel, coated with poly-l-lysine was constructed to measure the bulk diffusion, in which fluorescent nanoparticles could be visualized as they diffused across the mucus filled channel (Figure 2.4). Using the surface plot analysis, the intensity of the nanoparticles was shown as a function of intensity over relative position of the channel (Figure 2.5).

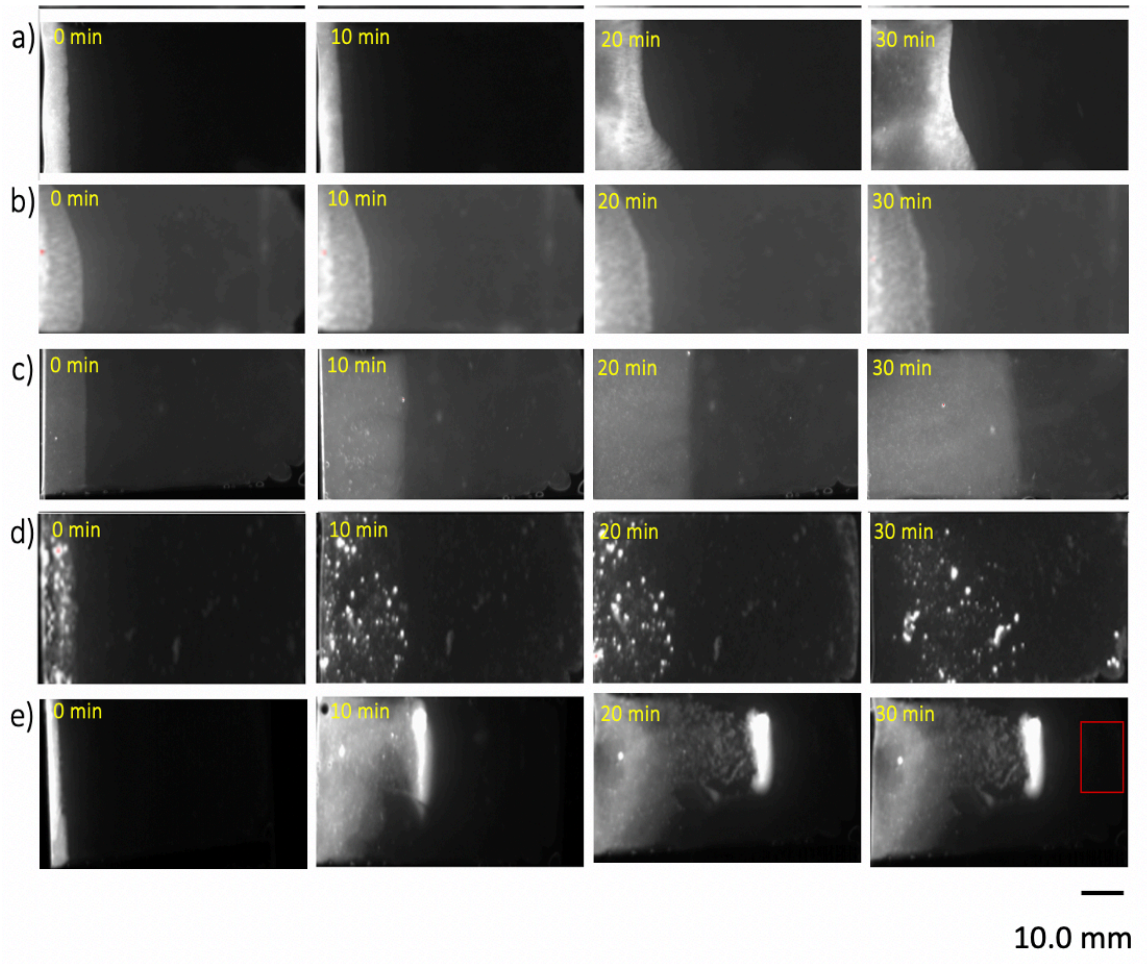

Figure 2.4: a) Mucus bulk diffusion in slide of bare protein nanoparticle, b) cOVA, c) PEG protein Nanoparticle, d) layer-by-layer, and e) Iron oxide protein nanoparticle with the red box as the magnet location.

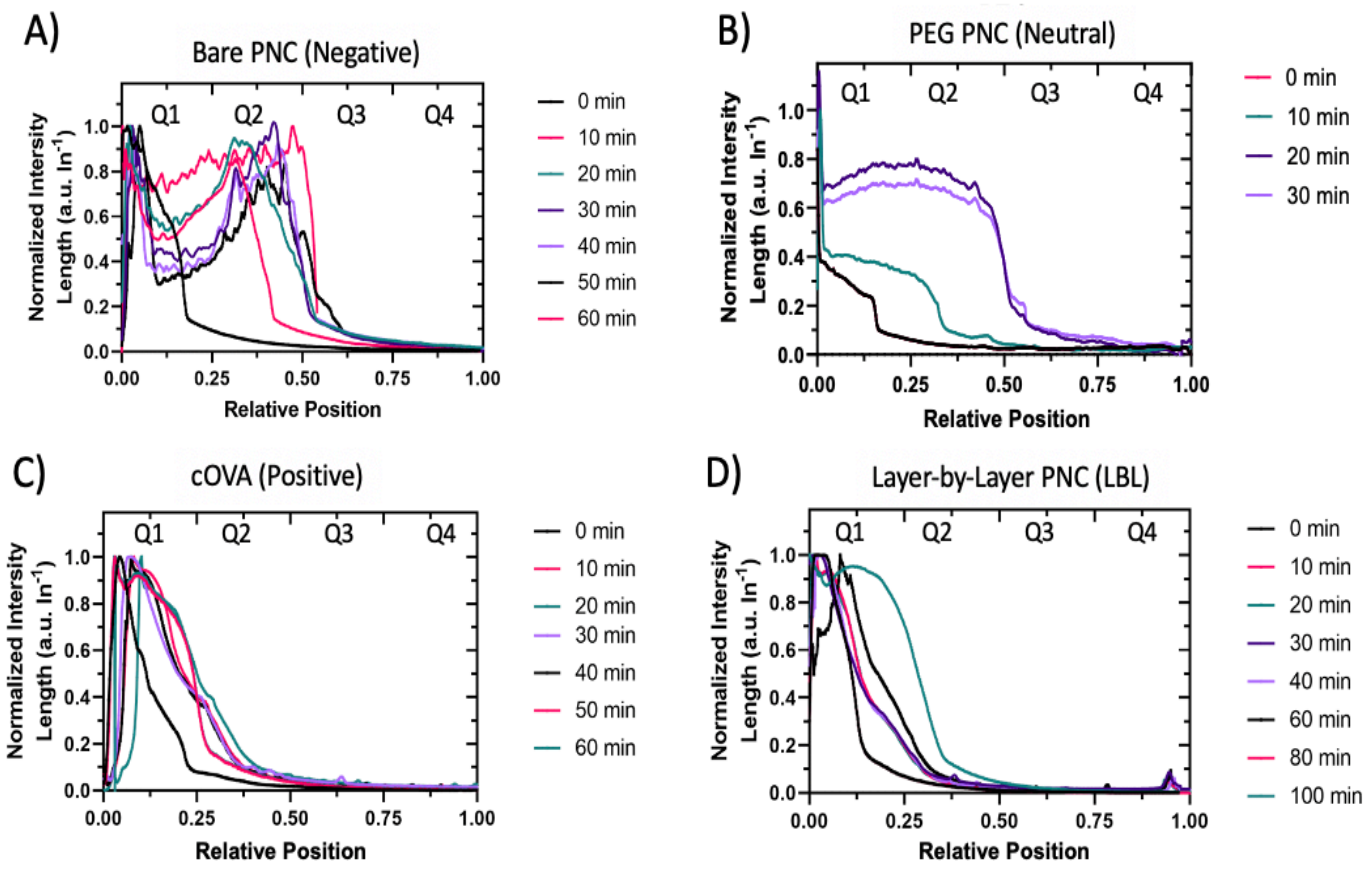

Figure 2.5: Summary of bulk analysis from surface plot analysis. a) Bare PNC, b) PEG PNC, c) cOVA, and d) Layer-by-layer.

The surface plots indicate significant diffusion across the channel for the PEGylated protein nanoparticles as a function of time, in which particles were able to penetrate across half of the channel within 30 mins. Conversely, cOVA particles were unable to demonstrate significant movement. This is consistent with literature reporting highly cationic nanoparticles immobilized by mucins. The positive surface charge on cOVA nanoparticles will interact with oligosaccharides in the mucus, which allows for interaction between primary amines to sialic acids groups on mucin. [28, 109]

PEG nanoparticle was able to freely diffuse, demonstrating antifouling interaction between the charge mucin group to the neutral charge from the PEG protein nanoparticle. [87,88] Interestingly, the negative charged PNC nanoparticles contained a fraction of the population which was at first quartile of the channel. This could be due to repulsion of the mucus to the nanoparticle in the first encounter. The LBL PNC exhibited similar features of the cOVA, such as the high population in the first quarter of the channel. However, a small population of nanoparticles was able to pass to the fourth quartile. This phenomenon could be a function of the shedding ability of the LBL protein nanoparticle. The LBL nanoparticle appears to have a synergistic impact that is different from both a negative and positive nanoparticle, allowing for a small population to diffusion. It is important to note that the LBL nanoparticles will aggregation together potentially due to their interaction with DNA and chitosan, making the nanoparticle appear larger. The iron oxide protein nanoparticles also had a bimodal distribution, though in this case a large fraction of the population was directed into the mucus using a neodymium magnet. Iron oxide protein nanoparticle was directed by the magnetic, which is shown as a high intensity shown in Figure 2.6. The surface interaction of the iron oxide protein nanoparticle is expected to behave similarly to bare PNC and the population of particles at the beginning of the gel may indicate that efficiency of iron oxide incorporation varies. To better summarized the data, the surface plots for each particle were divided into quartiles and examined at the 30 min mark (Figure 2.7).

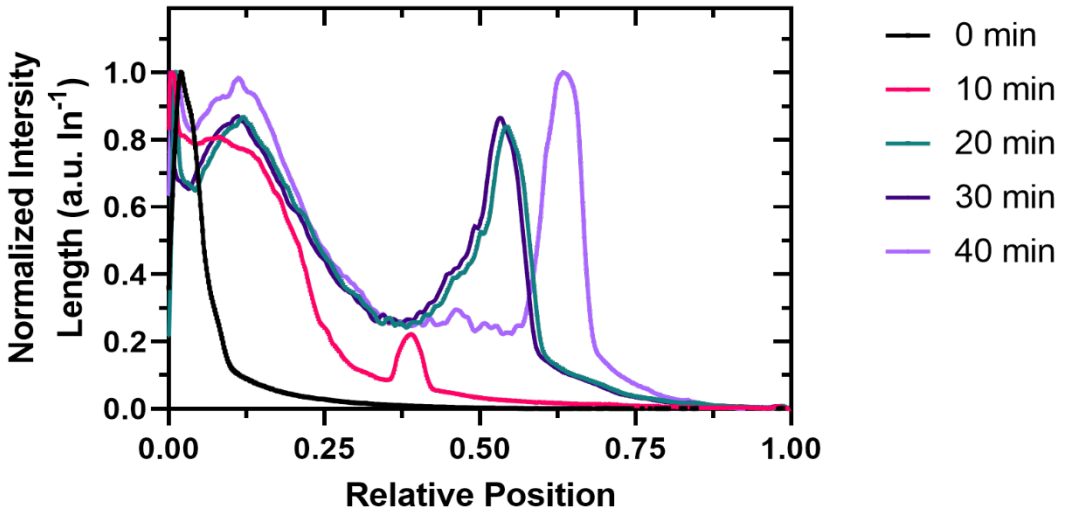

Figure 2.6: Summary of bulk analysis from surface plot analysis for iron oxide protein nanoparticle.

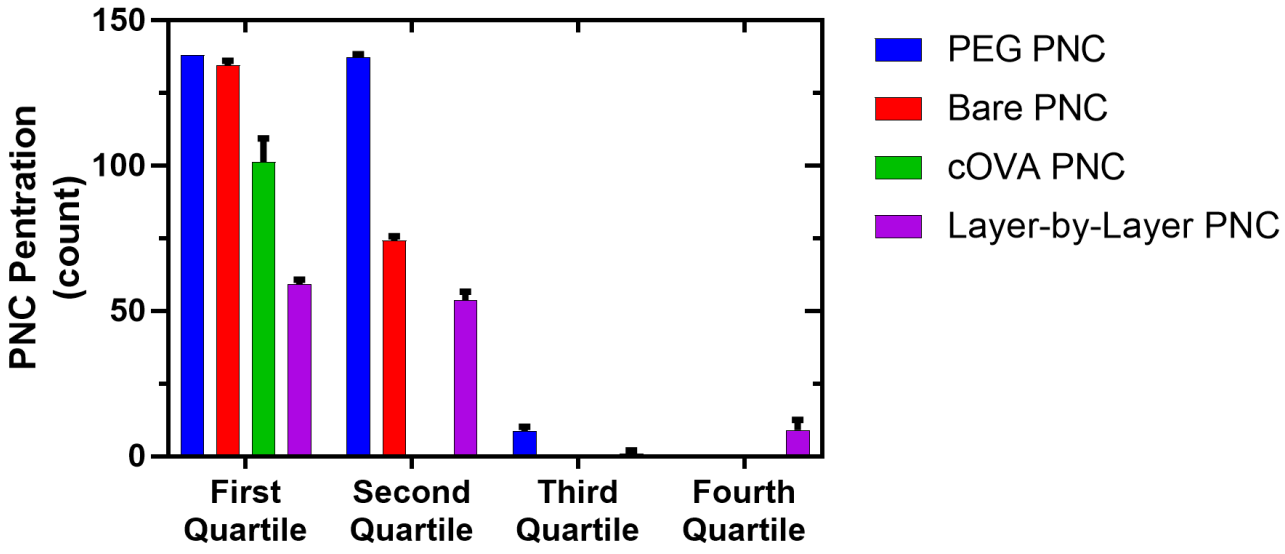

Figure 2.7: Summary of bulk analysis from surface plot analysis at 30 minute timepoint blue = PEG PNC, red = Bare PNC, green = cOVA PNC, and purple = Layer-by-layer nanoparticle. Protein nanocluster count for each quartile based on pixels of the image.

At the 30 min mark, LBL nanoparticles resembled bare PNC much more than cOVA but the small population of highly diffusing particles is unique. While PEG PNC had broad and uniform diffusion,

they did not reach the 4th quartile. To better understand the dynamic change better mucus and the layer-by-layer shedding, a coating release study was done. LBL PNC was fabricated using labeled chitosan for the positive coating, to ensure no free dye was available, thin layer chromatography using 80:20 (MeOH:Water) was used as the mobile phase and was then visualized for free Alexa Fluor 647 in the chitosan sample using a fluorescent imager, shown in Figure 2.8. The TLC result demonstrated no free dye in the mobile phase. The incubation of LBL nanoparticles was done in diluted amount of mucus. Samples were incubated for a timepoint of no incubation and incubation for 30 minutes at room temperature. The mucus and nanoparticles were centrifuged to remove the excess mucus and nanoparticles. The fluorescent reading indicted the amount of chitosan that could not be spun down, demonstrating a release of layered chitosan material to the mucus solution. The residual amount is the soluble chitosan found in the supernatant. Figure 2.8 illustrates that less than 20% of chitosan is lost in the mucus solution for 30 minutes, while less than ~10% of chitosan is in the residual or supernatant at the 0-minute timepoint. This data suggests the potential for shedding in a mucus-like environment where the electrostatic interaction is disrupted or potentially pulled apart due to interaction with the bulk mucus. This potentially could be the reason why the LBL nanoparticle is shown to have a binomial distribution.

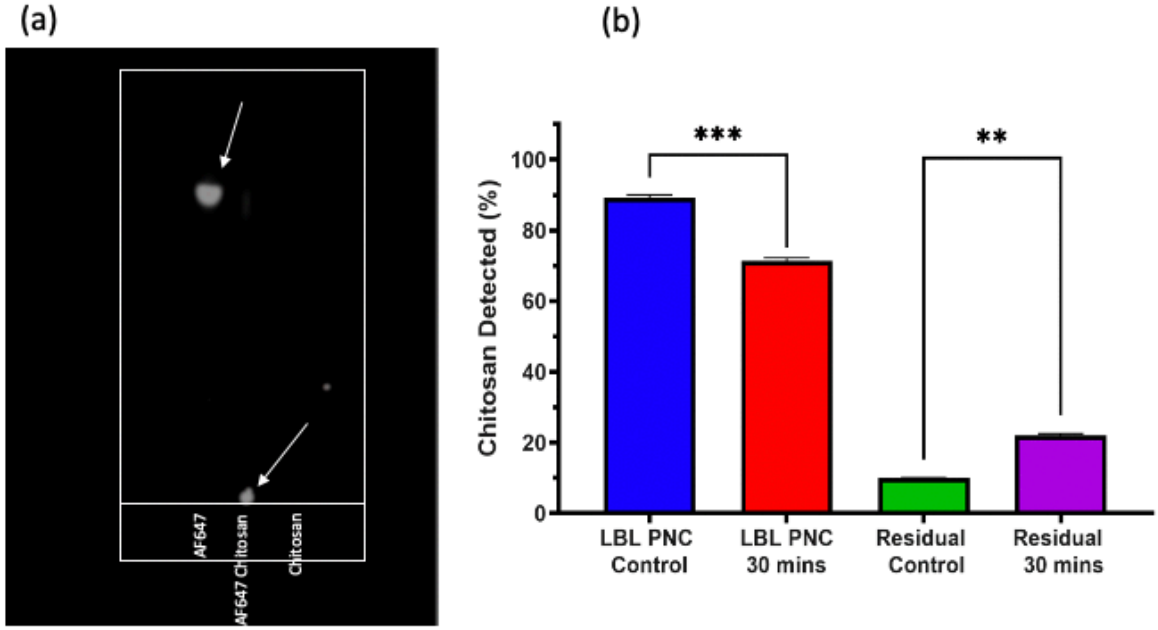

Figure 2.8: a) TLC plate under florescent imager for AF647 NHS ester free dye, AF647 conjugated to chitosan, and chitosan (left to right). b) Measured AF647 signal of LBL PNC incubated in mucus for the particle and residual chitosan in the supernatant. Comparison for each subgroup used student's t-test ** $P \leq 0.01$, *** $P \leq 0.001$.

2.3.4 Multiple Particle Tracking Results

Multiple particle tracking (MPT) was used to visualize the diffusion of individual nanoparticles in diluted mucus and calculate diffusion coefficient (Figure 2.9). The bulk diffusion driving force is a concentration gradient, but MPT quantifies random diffusion. Diffusion coefficients for each particle modification are reported in Figure 2.10. The iron oxide nanoparticle could not be used due to magnetic sensitivity of the microscope. However, the LBL nanoparticle distribution interesting demonstrated a binomial split, in which the curve was separated into a high- and low-diffusion coefficient histogram shown in Figure 2.10. The diffusion coefficient was then plotted into a histogram using over 500 nanoparticles as shown in Figure 2.10. The curves were modeled using graphPad Prism 9.01 (GraphPad Software) Gaussian distribution function.

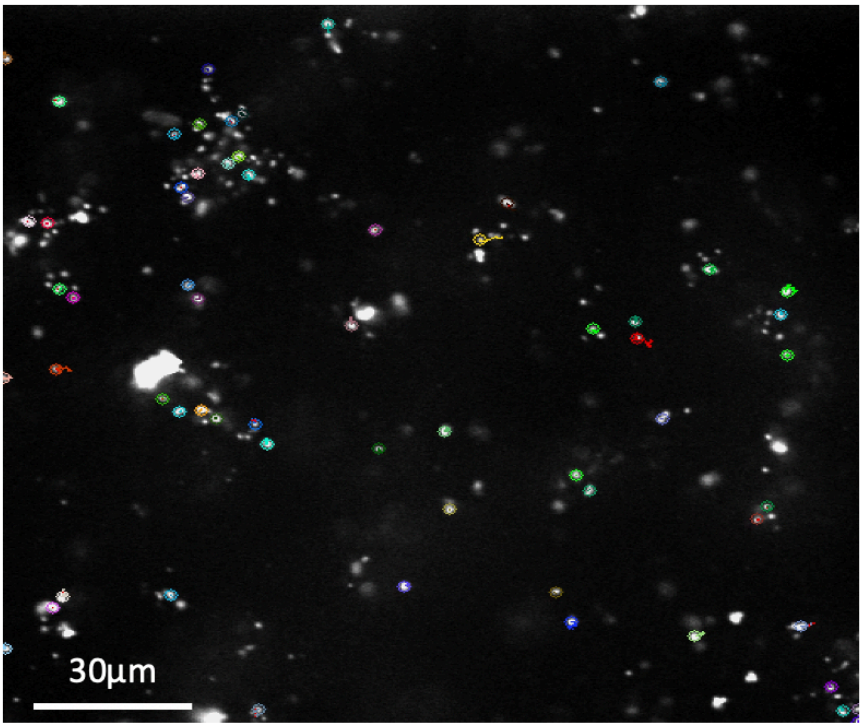

Figure 2.9: MOSAICsuite tracking software for protein nanoparticles in mucus, scale bar = 30 um)

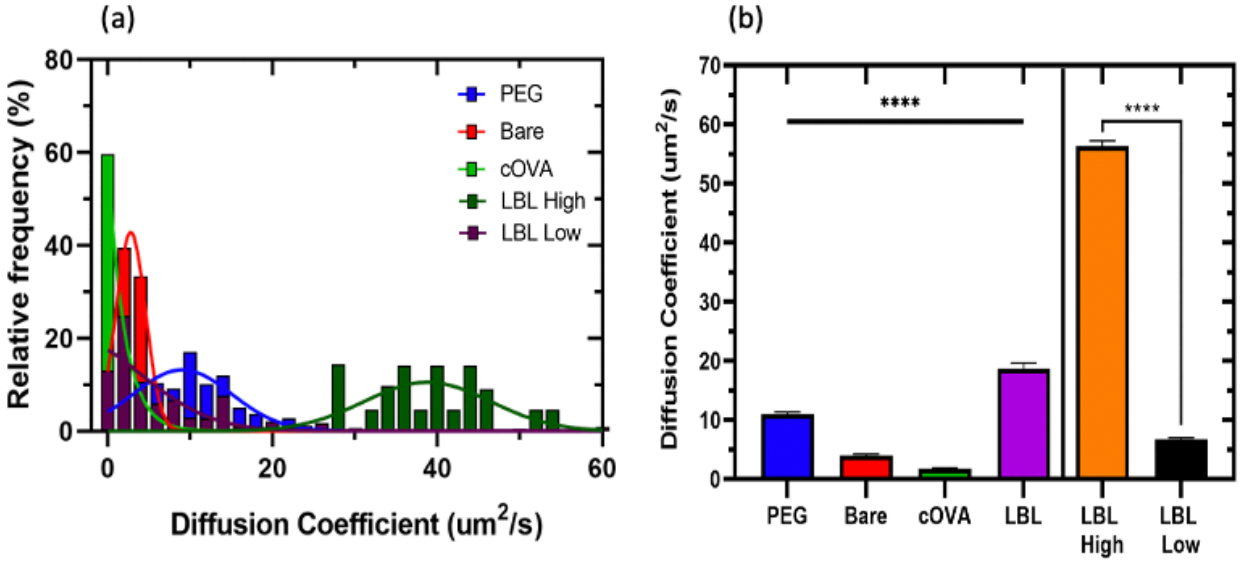

Figure 2.10: a) Histogram of diffusion coefficient (um^2/s) of each nanoparticle group with gaussian model curve. B) summary of diffusion coefficient (um^2/s) comparison for each subgroup were indicated using wwo-way ANOVA was used to analyze the significant difference among 3 or more groups. P-values less than 0.05 were significant (*, $p < 0.05$; **, $p < 0.005$; ***, $p < 0.001$). T-student test **** $P \leq 0.0001$ was used for the LBL condition comparing high and low diffusion coefficient.

The impact of using diluted mucus is to compare the diffusion of nanoparticle among these set of groups. Because of this, the nanoparticle may appear faster in comparison to the bulk analysis. The diffusion coefficients are consistent with the trends found in the literature and in the bulk, diffusion results, with PEG particles diffusing more than bare, which diffused more than cationic particles. [83, 109, 115] These particles had relatively uniform diffusion coefficients across the population. However, as expected from the bulk diffusion results, layer-by-layer nanoparticles had a bimodal distribution of diffusion coefficients, one population that is high and one that is low. The fraction of highly diffusing particles seemed to be greater than in the bulk diffusion measurement.

When separated into high and low, the histograms for the LBL could be modeled using a Gaussian distribution frequency model (Figure 2.10a). While the average diffusion for the slowly diffusion LBL population was lower than PEG particles, the combined average was higher due to the large contribution from the fast-diffusing population, which had an average diffusion coefficient ~5x higher than PEG particles. It has been shown that coating with hydrophilic, negatively charged DNA improved the average nanoparticle transport rates by 10-fold in reconstituted pig gastric mucus compared to slightly smaller, hydrophobic polystyrene particles. [62] This could potentially be the reason why there are two distributions for the LBL nanoparticle, where the LBL can shed the chitosan layer during the 30 minutes of incubation in mucus.

2.3.4 Mucus Adsorption Results

To understand how mucus adsorption phenomenon was affected by nanoparticle modifications, we evaluated the mucus adsorption using a periodic acid-schiff reaction to detect polysaccharides. [115, 116] The results from 30-minute incubation with dilute porcine mucus are shown in Figure 2.11. The pellet contained the nanoparticles, while the residual sample contained the excess mucus. As expected, cOVA particles demonstrated the highest adsorption of mucus, while the pegylated nanoparticles demonstrated the lowest and bare PNC in between. This demonstrates a higher association to the mucus for cOVA which is a similar trend shown with cationic nanoparticle. [29, 115] Layer-by-layer protein nanoparticles was not used for this assay due to heterogenous combination of DNA or Chitosan layer that could form aggregate or skew the results due to the heterogenous mixture of coatings in each layer.

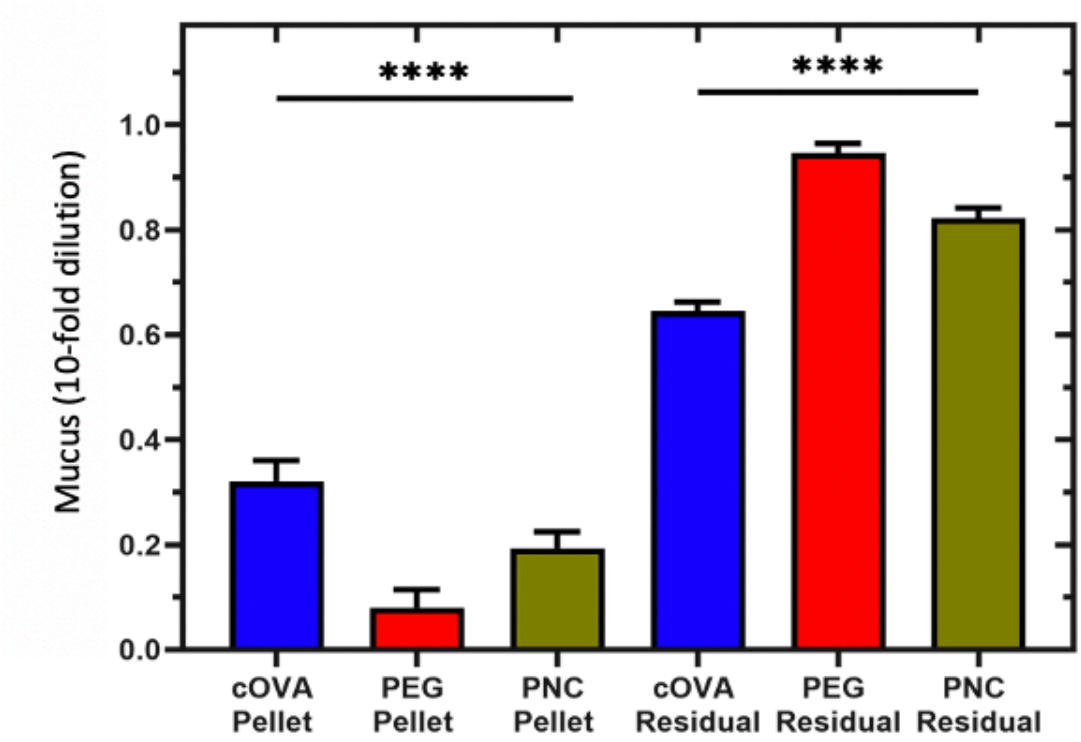

Figure 2.11: Summary of periodic acid–schiff assay measuring mucus of PNC charge group from each group and the supernatant of each respective group, comparison for each subgroup were indicated using Two-way ANOVA was used to analyze the significant difference among 3 or more groups. P-values less than 0.05 were significant ($p < 0.005$; ***, $p < 0.001$).

2.3.5 Cellular Uptake

Given the differences in the mucus diffusion for each nanoparticle group, we aimed to understand better the combination of mucus and nanoparticles for cellular uptake and interaction. Specifically, modifications like PEG to reduce molecular interactions with mucus may also reduce desired interactions that promote cell uptake. Additionally, adsorption of mucus to nanoparticles alters the surface that interacts with cells and may have a positive or negative affect compared to pristine nanoparticles. We used JAWSII cells, immortalized C57BL/6 murine bone marrow derived DCs.[119] As antigen presenting cells, DCs need to internalize antigen nanoparticles, process the antigen, and undergo maturation, then present antigen to T cells. In this work, we measured the

cellular uptake and maturation marker CD-86. [122, 123] There has been extensive work on demonstrating low nanoparticle cytotoxicity using protein nanoparticles and the formulation of the other modifications such as DNA, Chitosan, and Polyethylene glycol (PEG). [88, 89] A 0.2 ng NP/cell dosage has been demonstrated to be non-toxic for cationic (cOVA) and bare ova nanoparticles. [120] In this work, both raw mucus and dilute mucus from the pig nasal cavity were incubated with nanoparticles for 30 minutes prior to cell exposure and both the nanoparticle and mucus was given to the cells. PBS and soluble fluorescent OVA protein were used as controls. Cellular uptake of nanoparticles with both high and low mucus is shown in Figure 2.12.

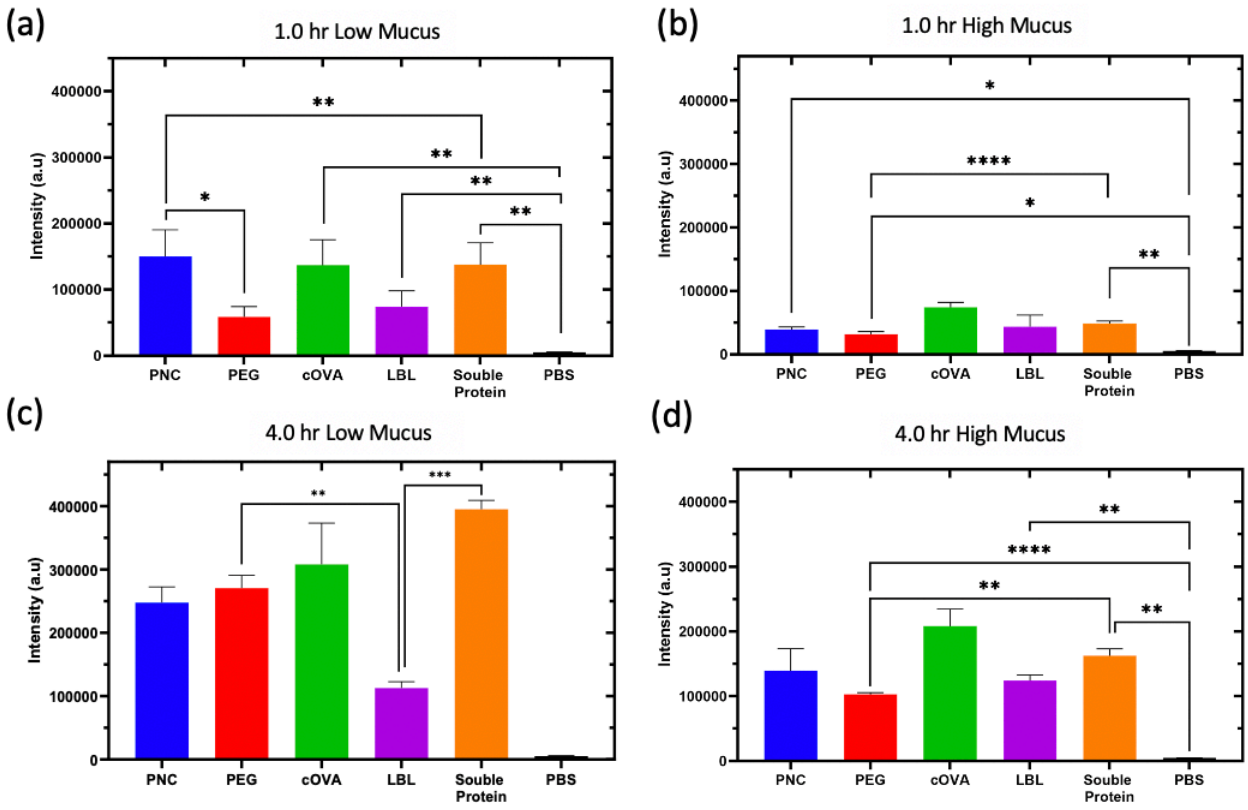

Figure 2.12: Summary of cellular uptake for JAWSII cells under high- and low- mucus concentration incubation. a) 1.0-hour low mucus incubation, b) 1.0-hour high mucus incubation, c) 4.0 hour low mucus incubation, d) 4.0 hour high mucus incubation comparison for each subgroup were indicated using Two-way ANOVA was used to analyze the significant difference among 3 or more groups. P-values less than 0.05 were significant (*, $p < 0.05$; **, $p < 0.005$; ***, $p < 0.001$).

The cellular uptake of JAWSII observed from high and low concentration of mucus indicated the impact of the surface charge of the nanoparticle as well as the diffusion limitation. We witnessed a decrease in nanoparticle uptake and soluble OVA with high- vs low- mucus concentration, as shown with the decrease in signal comparing the high and low concentration of mucus. While the cOVA nanoparticle demonstrated poor diffusion, the positive charge allowed for greater cellular uptake. This is aligned with previous literature showing improve uptake due to the association between the negative cellular membrane to the positive surface of the nanoparticle. [82, 101] Moreover, the adhesion of positively charged NPs to the cell membrane can promote membrane-wrapping phenomena. The results confirmed the dominant role of electrostatic interactions; specifically, the positively charged NPs maximized adhesion and increased uptake and the dilemma in which properties that promote mucus diffusion and cell uptake conflict. We observe the lowest cellular uptake in the nanoparticle group with the PEGylated nanoparticle and LBL nanoparticle in all cases except the low mucus at 4 hrs where LBL was the lowest. The LBL nanoparticle is shown to have low cellular uptake, this could be due to maturation or due to improved shielding of certain OVA from certain receptors. OVA can be internalized using receptors such as glycoprotein 18 and glycoprotein 30 which are scavenger receptors or be internalized through clathrin-mediated endocytosis via the [191, 230] mannose receptor. It has been hypothesized that the bare OVA nanoparticle can trigger pattern recognition receptors (PRRs). This could lead to more coatings to reduce the cellular uptake of nanoparticles. This could be confirmed evaluating high soluble OVA uptake in all conditions, in which no mucus diffusion limitation can occur, and OVA can engage certain recognition receptors with less limitations on coating modifications. To confirm uptake of JAWSII, we observed cellular uptake on confocal on JAWSII cells as shown in Figure 1.13.

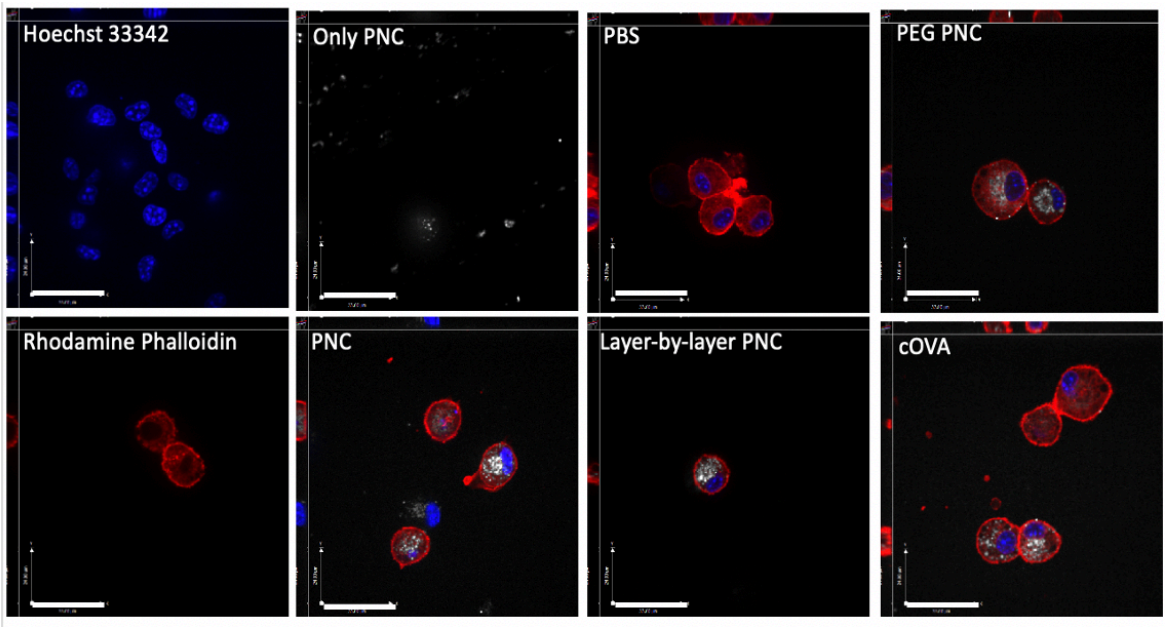

Figure 2.13: Confocal microscopy of internalized Bare OVA, cOVA PNC, PEG PNC and LBL PNC with an adsorbed protein corona. Fluorescent protein nanoparticles (0.1 ng/cell), fabricated by conjugating OVA protein with Alexa Fluor 488 prior to desolvation, were incubated with JAWSII cells for 4 hours at 37°C. Center slice images were obtained after nanoparticle incubation using a Perkin Elmer UltraVIEW VoX spinning disk confocal. (Scale bar – 33 μm; nanoparticles – green or white, JAWSII actin cytoskeleton – red, nuclei - blue)

To understand the impact of coatings for the immune response, we measured CD86 expression as preliminary data, to provide insight on DC costimulatory signals necessary for T cell activation and survival. This will enable understanding of the impact of dendritic cell's processing and immune responsive activation. To evaluate the response, we used an anti-cd86 antibody to target the activation marker CD86 on the surface of JAWS II cells. Correct gating was needed to reflect the in JAWS II morphological changes once maturation occur as shown by Vilekar al et. [119] In Figure 2.14a, there is a new population of JAWS cells in the presences of mucus. Due to the heterogeneous nature of mucus, we hypothesize that mucus can mature the JAWS cell which will shift the morphology of the cell to gate. We then used the shift in the histogram to determine the CD86 responsive from flow cytometry data shown in Figure 2.14e. Figure 2.14 shows the level of fluorescent labeling of CD86,

with PBS as the negative control and lipopolysaccharide (LPS) as a positive control for upregulation of CD86.

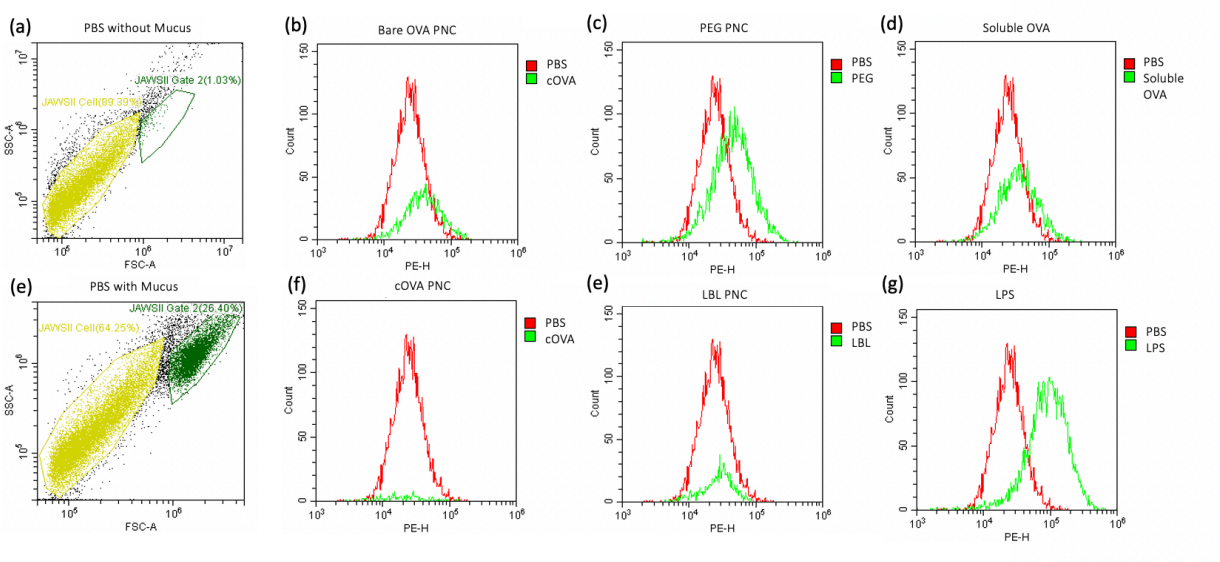

Figure 2.14: Histogram shift for positive CD86 signal using PBS control as comparison. a) gating with no mucus, b) bare OVA PNC, c) PEG PNC, d) Soluble OVA, e) gating for JAWS activation, f) cOVA PNC, e) LBL PNC, and f) LPS.

The histograms for CD86 have demonstrated small shifts in CD86 expression for the soluble OVA and bare OVA PNC. The PEG PNC group showed a greater increase in CD86, though less than that for LPS. However, there is poor signal for the cOVA and LBL. The positive charge from the cOVA and LBL seem to have a reduce population of mature JAWS cells with slight activation of CD86. Surprisingly, we see that the PEG PNC contained high levels of activation of CD86. This could be due to long duration of incubation that allows for PEG to freely diffuse in the mucus and reach the JAWS cells to uptake more particles. However further testing is need longer cellular uptake and to understand the impact of CpG ODN and chitosan, we need to examine cells that express TLR9+ which is not present in JAWSII. [108, 109]

2.4 Conclusion

Intranasal delivery has several barriers that can significantly hinder the ability of nanoparticles containing drugs and vaccines to be processed. There have been several studies on producing nanoparticles to improve diffusion in the mucus barrier, [73, 83, 86] however often few particles are able to diffuse across these barriers which can reduce the amount of therapeutic drug or vaccine to the desired location. We have engineered five different protein nanoparticles models using ovalbumin as an antigen to address this issue. We have demonstrated that improving the diffusion using coatings such as Polyethylene glycol (PEG) may improve the transport phenomena in mucus but can significantly hinder the cellular uptake, and shockingly produced high CD86+ level on JAWSII dendritic cells. One hypothesizes could be that the PEG nanoparticle allowed for more assess to nanoparticle during the 24 hours incubation to the dendric cells. Therefore, CD86 maturation study does not reflect the current challenges that intranasal delivery hold, as the residence time before nanoparticles are cleared are in the order of 20-30 mins with PEG and longer with a mucoadhesive coating before it is cleared from by cilia. [87, 88] In order to test this, longer uptake studies must be done to see the amount of nanoparticle taken up during a 24-hour exposure to nanoparticles. Layer-by-layer adjuvant coatings on nanoparticle can improve diffusion and potentially assist other immune response that is not evaluated in CD86+ signal. Unmodified PNC allowed for great cellular uptake while exhibiting CD86+ signal, demonstrating the ability of specific OVA receptors such as scavenger receptors to improve *in vitro* assessment. Lastly, cOVA enables high cellular uptake, but low diffusion based on the diffusion results. Cationic particles are known to be a mucoadhesive due to their positive nature, which can prevent them from reaching their cellular target, the long duration of 24 hours for CD86 maturation mark may highlight the impact of longer retention time from the mucus with poor access to nanoparticle due to electrostatic interaction which allows DC cells to be

activated through consumption of mucus to reduce phagocytosis. These results highlights the differences between coatings on protein nanoparticles in the mucus environment and reveals the challenges associated with mucus delivery of nanoparticles into cells. Based on these findings, future studies may develop similar strategies of coatings to tune mucus delivery for better control in navigating through the mucosa.

CHAPTER 3. NASAL PROTEIN CORONA ON ENGINEERED PROTEIN NANOPARTICLES

3.1 Introduction

The development of nanotechnology for drug delivery has demonstrated promising results to overcome barriers, improve retention in the body, and target specific cell markers. [7, 8, 10, 29, 52, 61, 68, 85, 94, 114] A common strategy for engineering drug delivery nanoparticles is to modify their surface for specific ligand binding or to control physico-chemical properties, such as surface charge, to improve desired versus undesired interactions with barriers, cells, or molecules. [123-125] However, one challenge of nanoparticles within a biological fluid such as blood, saliva, or mucus is the adsorption of biomolecules onto the surface of nanoparticles. This can significantly change the surface of nanoparticles and obscure surface ligands or modifications. This specific layer is called a protein corona and changes the biological fingerprint of the nanoparticle and its interactions and lifetime in the body. [126, 127] The protein corona consists of the soft and hard corona. The hard corona is defined as the analytically accessible proteins that are firmly attached to the nanoparticle, where the soft corona consists of loosely associated that are weakly associated, rapidly exchange, and are usually inaccessible to analyses. [124, 128, 129] The protein corona is impacted by the properties of the nanoparticle including surface charge and hydrophobicity, size, and morphology. [114] Extensive study has been done to understand the formation of nanoparticle coronas in the bloodstream. Examples of protein corona interactions can be seen with opsonins, such as antibodies, complement proteins and other immune proteins that increase nanoparticle clearance by the immune system through the process of opsonization. [128, 130, 131, 132] There has been extensive work on antifouling coatings such as Poly(N-vinylpyrrolidone) (PVP), Poly (ethylene glycol) (PEG), and glycocalyx. [10, 66, 88] These materials are often utilized to reduce hydrophobic and electrostatic

interactions due to their zwitterionic property or hydrophilic shielding. Given these properties, antifouling coatings are often used to reduce biological interactions and have been used by many nanoparticle systems to control protein corona formation in blood. [126, 129, 132] One of the most dominant physiochemical properties of nanoparticle corona formation is the charge on the surface that often recruits proteins through electrostatic interaction. Because most native proteins at physiological conditions (7.4 = pH) are deprotonated, they tend to carry a net negative surface. Therefore, nanoparticles with positive surface charge tend to adsorb more protein. [115, 116]

There is extensive literature on understanding the protein corona fingerprint for several classes of materials such as quantum dots, silica nanoparticle, polymer nanoparticles, liposomes, virus-like particles, and protein nanoparticles in blood. [134, 135] However, little is known about the protein corona developed in mucus, specifically in the nasal fluid located in the nasal cavity. [134, 135, 136] In the past 20 years, there have been few literature reports on the nasal secretion associated protein corona on nanoparticles. The most relevant report determined the protein corona for nanosized welding particles: Magnetite Fe3O4, Fe2O3, stainless steel chamber ultrafine welding fume (UFWF) particles < 0.1 μm in diameter and fine welding fume (FWF) particles ranging from 0.1 μm to 2.5 μm in diameter. [137] This work sought to understand nanotoxicity in welders and found abundances of proteins that cause an immune response such as inflammation However, there are several knowledge gaps on the impact of different charged protein nanoparticles on the formation of corona in mucus and there is no work on nanoparticles relevant to human vaccines or therapeutics. This work give insight on vaccine and drug delivery directed in the nasal cavity using protein carriers.

In this chapter, we characterized the hard protein corona on 4 different surface engineered protein nanoparticles to understand the impact of charge and surface chemistry for nanoparticles in human nasal fluids. This analysis is important to understand and design protein nanoparticles as

intranasal vaccines or other drug delivery applications that utilize the nasal route. The hard protein corona mass and identity was determined using SDS-PAGE and liquid chromatography with tandem mass spectrometry. Cellular internalization was determined with A549, adenocarcinomic human alveolar basal epithelial cells, to model the epithelial barrier in the presence of human nasal fluid. [136] The protein corona fingerprint was used to map out the protein cascade using ontology pathway analysis to predict potential trends during in vivo administration of nanoparticles intranasally. [137,138]. This work highlights the protein corona of on protein nanoparticle which will assist understanding the impact during intranasal delivery.

3.2 Methods

3.2.1 Fabrication of Chicken Egg Albumin Protein Nanoparticles (OVA-NP)

The synthesis of OVA-PNC was performed according to desolvation process. The desolvent phase containing pure ethanol was added dropwise to 0.1 mL protein solvent phase that contained 6.2 mg/mL chicken egg albumin in phosphate-buffered saline (PBS, pH 7.4) under constant mixing at 700 rpm. The protein NPs were then collected using centrifugation at 18,000 xg for 10 mins and resuspended by sonication in 0.475 mL PBS; 32.5 µl of a 50-fold dilution of glutaraldehyde was added and the nanoparticle suspension was mixed at 600 rpm at room temperature for one hour. The solution was centrifuged for 32 mins 16,000 x g at 4˚C. The supernatant was removed, and the pellet was resuspended in 500 µL of PBS. The nanoparticles were sonicated on ice for 1 minute, for 1 second on and 3 seconds off at 50% amplitude. The nanoparticles were then centrifuged for 5 minutes at 500 x g and the supernatant was collected and the pellet was discarded.

3.2.2 PEGylated (PEG) OVA Protein NP Bioconjugation

A 1.0 mL suspension of OVA NPs in PBS (10 mg/mL) was combined with 0.1 mL sodium bicarbonate solution (1 M, pH 9.0) and 0.4 mg O-[(N-Succinimidyl)succinyl-aminoethyl]-O′-methylpolyethylene glycol (average M_n 750). The mixture was reacted at room temperature as it inverted for 1 hour on a Rocking Platform Shaker (VWR) at a 10˚ tilt angle. The PEGylated OVA NPs were collected using centrifugal filtration (Amicon, 10 kDa).

3.2.3 Cationic EDA/EDC Protein Nanoparticle Fabrication

Cationic PNC were prepared using a modified method [114]. 1.0 mL of protein OVA PNCa were centrifuged at 18000 xg for 10 mins. The PNC pellets were resuspended in 1 mL of 0.1 M 2-(N-Morpholino)-ethanesulfonic acid buffer (MES, 4.7 pH) and sonicated on ice 2 s on and 2 s off at 30% amplitude for 1 min. Approximately 40 mg of 1-ethyl 3-(3-dimethylaminopropyl)carbodiimide hydrochloride (EDC) in 0.5 mL of MES buffer (pH = 4.7) was added to the to the nanoparticle solution and reacted on ice for 1 hr. A 1:1 ratio of ethylenediamine solution to MES buffer was prepared and pH was adjusted to 4.7 on ice to cool heat released from reaction. The cold ethylenediamine solution was added to nanoparticle solution for 30 mins and centrifuged at 18,000 xg and resuspended in PBS.

3.2.4 Layer by Layer OVA PNC Fabrication

To adjust for size, the core OVA PNC used for layer-by-layer OVA PNC were prepared using a modified desolvation method from above. 20 mg/mL OVA in 0.1 mL PBSs desolvated under constant stirring at 700 rpm with 0.4 mL ethanol added dropwise. 32.5 µl of a 50-fold dilution of glutaraldehyde was added to stabilize the protein NPS and stirred with constant stirring at 600 rpm for 1 hours at room temperature. The protein NP were centrifuged at 18,000 xg and the supernatant

was collected to be the cores of the layer-by-layer OVA PNC. The layers were developed through dip coating in chitosan and short oligonucleotide for the cationic and anionic layers, respectively. The chitosan coating adheres to the surface of the nanoparticle due to electrostatic interaction, followed by subsequent anionic and cationic layers. A 0.6% w/v solution of deacetylated chitosan was prepared in 10% v/v aqueous acetic acid. The pH was then adjusted to 6.0 using 1 M NaOH, and protein nanoparticles were incubated in the chitosan solution for 30 mins at 30˚C. The suspension were then centrifuged at 18,000 xg at 4˚C and washed with Milli-Q water (18.2 MΩ·cm) and centrifuged to remove excess chitosan twice. The particles were then added to a solution of 22.1 nM CpG oligonucleotide and incubated for 30 mins at 30˚C, centrifuged at 18,000 xg at 4˚C and washed with Milli-Q water (18.2 MΩ·cm). An additional coating of chitosan was added following the same procedure as the first layer.

3.2.5 Nanoparticle Characterization

Protein nanoparticle size distribution and zeta potential were assessed by dynamic light scattering (DLS) and electrophoretic light scattering (ELS) respectively with a Malvern Zetasizer Nano ZS (Malvern Instruments, Westborough, MA). Protein concentration in the nanoparticle solution was assessed with a BCA assay according to the manufacturer's instructions (Thermo Scientific, Waltham, MA). Protein nanoparticles (0.5 mg/ml in 0.1X PBS for zeta potential) were measured using dynamic light scattering (DLS; Malvern Zetasizer, Nano-Z; Malvern Instruments, Worcestershire, England). Measurements were carried out in triplicate with three distinct samples. Each measurement consisted of 12–30 runs. Average and standard deviation are reported for all measurements Table 3.1. Electrophoretic mobility was converted to a zeta potential using the Smoluchowski approximation.

3.2.6 Nasal Lavage Sample

Nasal lavage samples, collected by flushing the nasal cavity, from were purchased from Lee Biosolutions from. Samples were pooled from 5 donors and concentrated using an Amicon Ultra-15mL centrifugal filters (3 kDa cut-off) (Millipore, Carrigtohill, Ireland) at 4,000 xg for 10 min and washed with Milli-Q water (18.2 MΩ·cm). The total protein content was determined with a bicinchoninic acid (BCA) protein assay kit (Pierce, Rockford, IL). The concentrated pooled nasal lavage solutions were then used for all experiments.

3.2.7 Nasal Lavage Corona Adsorption on Nanoparticles

Each type of particle concentrated at 0.5 mg was added to 1.5 mg of nasal lavage protein in solution. The samples were incubated for 30 min and 4 hours at 30°C to mimic nasal temperature and a retention time of 30 min and a long duration. All incubations were performed in triplicate. Unbound proteins were separated from the particles by centrifugation for 30 min at 16,000 x g. The nanoparticles were washed three times with milliQ water followed by a second and third centrifugation at 20,000 xg for 10 min each. Each supernatant wash was collected for SDS-PAGE (sodium dodecyl sulfate polyacrylamide gel electrophoresis) analysis using 4-20% mini-PROTEAN TGX Precast protein gel (BioRad) at 150 V for 40 min. BCA assay (bicinchoninic acid assay) to determine amount of protein that the final wash was clean, and all unbound or weakly bound proteins were removed from the nanoparticles.

3.2.8 Protein Corona Characterization

Nanoparticles with protein corona were incubated with 10 µL Laemlli Buffer for 10 min and sonicated to completely remove adsorbed corona proteins. Each sample was centrifuged at 21,000 x g for 10 min at 4˚C and the supernatants collected. The nasal proteins in each sample were reduced, alkylated and digested with trypsin according to the FASP protocol.[139] The peptides were analyzed

by nano-LC-MS/MS (Liquid chromatography–mass spectrometry Q Exactive™ Plus Hybrid Quadrupole-Orbitrap with Thermo UltiMate 3000 HPLC System), and peptide identification was performed as previously described [139] with the following modifications. Reverse phase chromatography was performed using an in-house packed column (40 cm long X 75 µm ID X 360 OD, Dr. Maisch GmbH ReproSil-Pur 120 C18-AQ 1.9 µm beads) and a 120 min. gradient. The raw files were searched using the Mascot algorithm (ver. 2.5.1) against a protein database constructed by combining the sequences of the Uniprot human reference database (downloaded 5-22-19, 20,303 entries) and a contaminant database (cRAP, downloaded 11-21-16 from http://www.thegpm.org) via Proteome Discoverer 2.1. Only peptide spectral matches with expectation value of less than 0.01 ("High Confidence") were used. Relative protein abundance was determined by the [140] UNIPROT to obtain protein molecular weight (MW). The spectral count of each identified protein was normalized by MW to determine the relative quantitative concentrations of each protein in the protein corona of each NP. The protein's identity (SpC) of each protein identity was normalized to the protein mass and expressed as the relative protein quantity by applying Equation 3.

$$\mathrm{NpSpC_k} = \frac{(\mathrm{SpC}/(\mathrm{MW})_\mathrm{K}}{\sum_{t=1}^{n}(\mathrm{SpC}/(\mathrm{MW})_t} \qquad \text{Equation 3}$$

NpSpCk is the normalized percentage of the peptide spectra count for each protein k, SpC is the peptide spectra count identified using nano- LC-MS/MS, and MW is the molecular weight (Da) of protein k. A heatmap was generated using GraphPad Prism 9.01 (GraphPad Software).

3.2.9 Protein Corona Analysis

PANTHER (protein analysis through evolutionary relationships) classification system is a comprehensive platform that can group proteins to their molecular function. [141-145] The data was

used to cross list proteins with 10 or more peptide spectral matches. The data was then converted into pie charts to illustrate biological functions from each grouping using GraphPad Prism 9.01 (GraphPad Software).

To generate a function linkage network, we used GO term enrichment analysis (scanning for GO categories overrepresented in the input list) to form this network. The GOnet database was used for ontology mapping. This application visualizes biological interactions of proteins to their downstream molecular function. [145] Proteins with 10 or more peptide spectral matches (PSM) were cross referenced to the GOnet database for function mapping.

To understand the number of proteins that are overlapping in each sample, we constructed Venn diagrams with greater than 5 PSM for higher sensitivity to see common proteins adsorbed on the surface.

In order to measure the fold changes of each protein, we used Equation 4 to demonstrate the log fold change based on the NpSpCk of each particle type relative to the bare OVA nanoparticle for either the 30 min or 4 hours timepoint.

$$\text{fold change } \Delta = \log_2 \frac{\mathrm{NpSpC_k}_{\text{PNC type}}}{\mathrm{NpSpC_k}_{\text{OVA control}}} \qquad \text{Equation 4}$$

The fold changes were then separated to understand the regulation of proteins. [146] The proteins were evaluated using g:Profiler for functional enrichment analysis and graphed using GraphPad Prism 9.01 (GraphPad Software). [147-150]

3.2.10 A549 Cell Culture

A549 cells were cultured in complete media consisting of Ham's F-12 (Kaighn's medium), 10% fetal bovine serum (FBS), and 1% penicillin/streptomycin (Amresco, Solon, OH). Cells were

cultured in T-75 flasks with 10 ml media/flask until ~70% confluency was reached, and the cells were grown as adherent cells. Passages 5-12 were used for all experiments.

3.2.11 Alexa Fluor-488 Fluorescent Nanoparticles

Alexa Fluor 488 Succinimidyl Esters-labeled albumin (OVA) from molecular probes was prepared according to the manufacturer manual with incubation of 2.5 μg of AF488 to 0.4 mg of OVA in 1M sodium bicarbonate solution (pH=8.3) for 1 hr. Excess dye was removed using filtered centrifugation (amicon, 10 KD and buffered exchanged to phosphate-buffered saline (PBS, pH 7.4). Degree of labeling and the final protein concentration was measured using the fluorescent dye labeling settings on a NanoDrop 2000. Below 10% soluble OVA conjugated with Alexa Fluor 488 was supplemented into the OVA solution. The nanoparticle fabrication and characterization procedures described above were used to fabricate fluorescent protein nanoparticles (n=3).

3.2.12 Flow Cytometry

Nanoparticle uptake was assessed by flow cytometry. Fluorescent nanoparticles were fabricated as previously described with OVA containing 10 wt% AlexaFluor 488-conjugated OVA. A549 Cells were plated in 96 well plates at 2 x 10^5 cells per well in triplicate and stimulated with 0.2 ng NP/cell fluorescent OVA nanoparticles or fluorescent soluble OVA previously incubated with nasal fluid for 30 mins to cells. BCA assay and fluorescence intensity measurements were used to confirm particle concentration. Cells were washed once with PBS, briefly trypsinized, filtered with cell strainer (VWR) and resuspended in chilled trypan blue to quench external green fluorescence. Cell fluorescence was measured after 1 and 4 hours of incubation with a Beckman Coulter CytoFLEX. Cells where gated using PBS A549 Cells without nanoparticles.

3.2.13 Confocal Microscopy

A549 cells were seeded at a density of $1x10^4$ cells per well in a 6-well chamber No. 1.5 coverslip glass bottoms (Mattek) with growth medium. After 24 hours, cells were incubated with medium without FBS with 0.2 ng/cell of particles that been incubated for 30 mins in dilute mucus. Cells were washed three times with ice cold PBS and fixed with 3.7% paraformaldehyde for 10 minutes at room temperature. Cells were incubated with 0.0528 μM rhodamine phalloidin (Biotium) in blocking buffer for 15 minutes at room temperature to stain for actin, and cell nuclei were stained with 0.02 μM Hoechst 33342 for 20 minutes at room temperature. Cells were washed three times after each stain with PBS and imaged with a Perkin Elmer UltraVIEW VoX spinning disk confocal.

3.2.14 Statistical analysis

Statistical analysis Statistical significance was determined using two-tailed Student's t-test in comparing two different conditions. Two-way ANOVA was used to analyze the significant difference among 3 or more groups. P-values less than 0.05 was significant (*, $p < 0.05$; **, $p < 0.005$; ***, $p < 0.001$). The analysis was performed with GraphPad Prism (version 9.01) software (GraphPad Software, San Diego, CA)

3.3 Results and Discussion

3.3.1 Protein Nanoparticle Fabrication and Characterization

Nanoparticle physiochemical properties influence the protein corona formation significantly, which has been extensively studied many different nanoparticles [149]. However, protein nanoparticles contain unique properties such as surface charge that is not perfectly uniform and folded domains that specifically engage receptors or soluble proteins. While the corona formed from serum proteins on protein nanoparticles has been the subject of a few studies [150], nasal secretion corona

has not been investigated on any organic nanoparticles, including protein particles. Therefore, this study aims to specifically examine the nasal secretion protein corona on protein nanoparticles modified with different surface charges formed through covalent and non-covalent layer-by-layer methods. The protein nanoparticles were fabricated using desolvation. As previously mentioned in Chapter 2, desolvant is added to aqueous solvent containing soluble ovalbumin (OVA) to produce protein clusters. These nanoclusters were stabilized using glutaraldehyde, which reacts with proteins through alkylation of available amines, forming stable secondary amine linkages through condenses amines via mannich reactions and reductive amination. [151] Glutaraldehyde is used in corona studies instead of DTSSP to minimize OVA contamination when the corona is removed from the particles for characterization. Each type of nanoparticle was tuned to have similar size distributions, with average diameters ranging from 300 to 314 nm, as conformed using dynamic light scattering (DLS). The summary of size and distribution in Table 3.1 and Figure 3.1 confirms overlapping size. This removes any impact of surface area, curvature or size on protein adsorption and corona composition. Zeta potential is shown in Table 3.1, which highlights the net charge among each group.

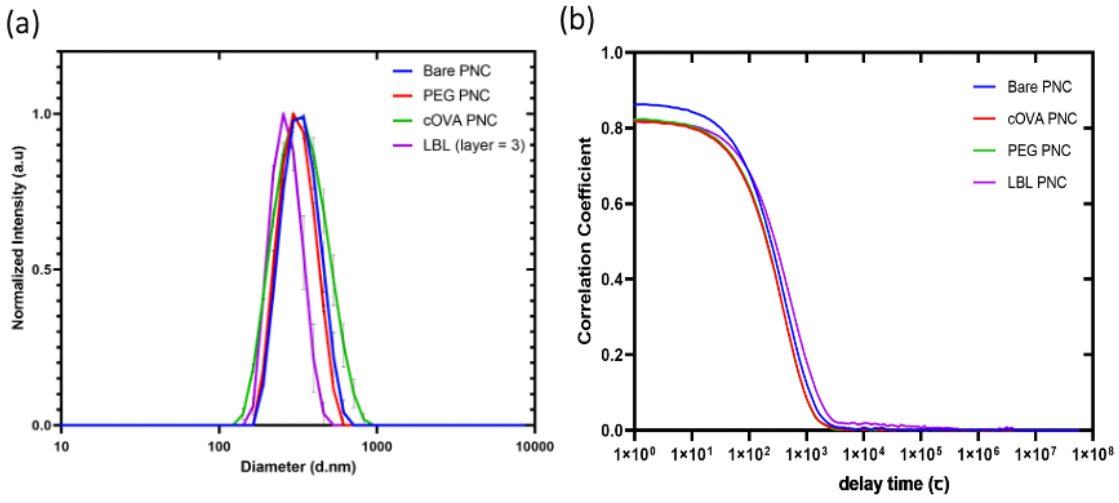

Figure 3.1: A) Size distribution overlay of Bare PNC, cOVA, PEG PNC, and LBL PNC using dynamic light scattering) (n = 3 independent batches of nanoparticles). B) DLS correlogram overlay of Bare PNC, cOVA, PEG PNC, and LBL PNC confirming the similar size of all four

nanoparticles (n = 3 independent batches of nanoparticles). The overlapping length of exponential decay indicates similar size distributions for each nanoparticle.

Table 3.1 Nanoparticle characterization summary using dynamic light scattering (DLS) and Zeta Potential measurements.

Sample[a]	Size (d.nm)[b]	PDI [c]	ZP (mV) [d]
Bare OVA PNC	300.36 ±3.2	0.19 ±0.08	-23.43 ±1.1
cOVA PNC	305.5 ±9.1	0.24 ±0.04	20.63 ± 1.9
PEG PNC	310.73 ±8.8	0.20 ±0.04	-9.51 ±1.5
LBL PNC			
Core	152.5 ±9.9	0.20 ±0.07	-22.5 ±1.8
1	205.1 ±8.1	0.24 ±0.09	21.3±2.1
2	261.4±5.2	0.23 ±0.09	-22.8±1.8
3	314.2 ±9.2	0.21 ±0.05	23.3 ± 1.7

[a] n=3 independent batches of nanoparticles; [b] hydrodynamic diameter; [c] polydispersity index, and [d] zeta potential (mV)

3.3.2 Protein Corona Anaysis

To remove the soft corona, multiple washes with PBS were used to the weakly attached proteins on the nanoparticles until the detection of protein in the wash was under 0.01 mg/mL of protein confirmed using BCA assay (Figure 3.2A, B) [114]. The hard corona on the protein nanoparticles was removed using Laemmli buffer, which contains denaturing agents such as sodium dodecyl sulfate . Using SDS-PAGE analysis, we can visualize a particle nanoparticle band in the sample well and the hard corona in the separating gel. We then analyzed the hard corona, where little amount of particle were detected in the stacking gel with a trace amount of bands detected. This allowed to confirm that a bulk of the particles had been removed from the sample. However, the resolution of the corona composition is low and allowed to the identification of the protein.

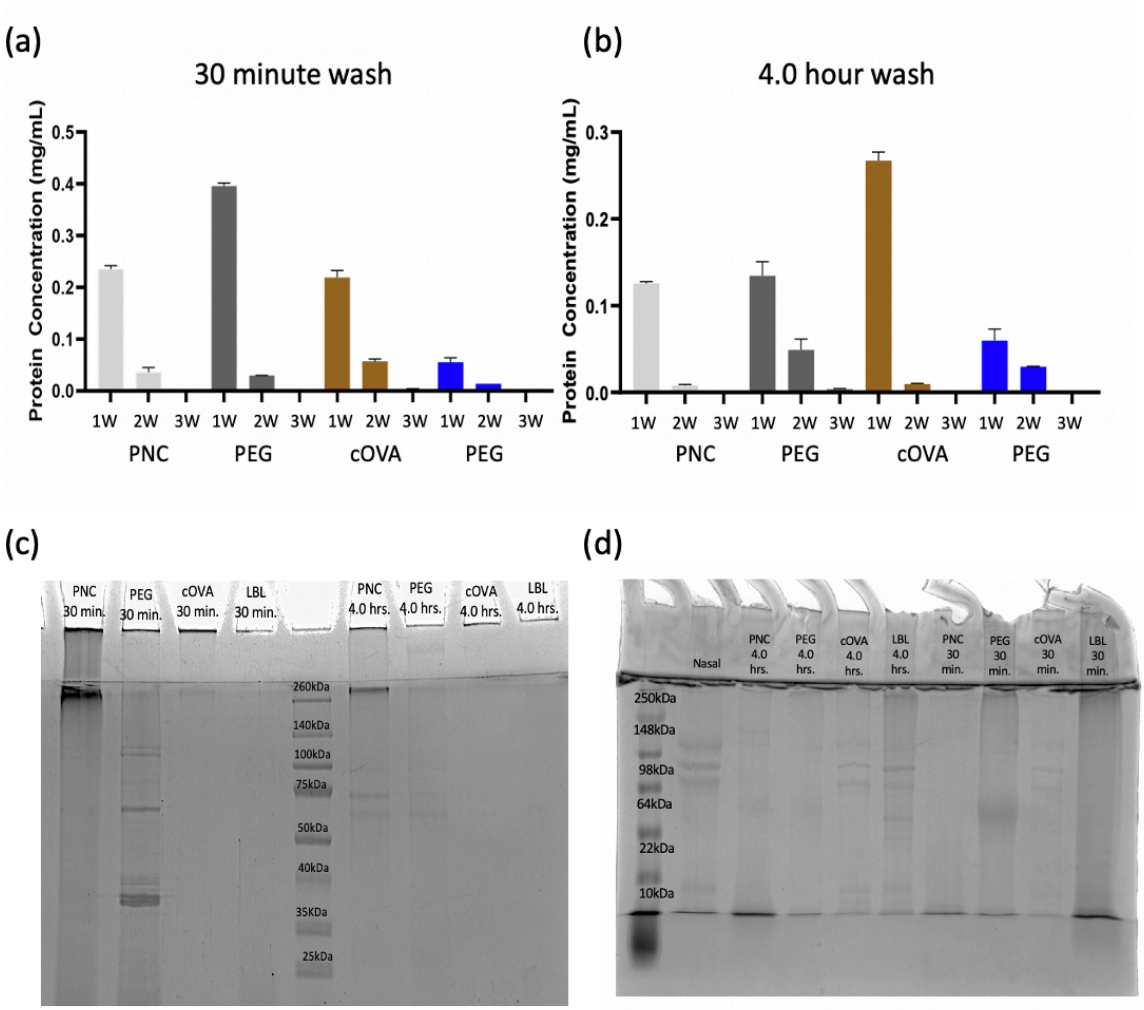

Figure 3.2: a) 30-minute incubation wash protein content confirmed with BCA (Bicinchoninic Acid) protein assay for each nanoparticle. B) 4 hours incubation wash protein content confirmed with BCA (Bicinchoninic Acid) protein assay for each nanoparticle. c) SDS-PAGE gel with small band on the stacking well and hard corona on the separating gel. d) SDS-PAGE gel of the hard corona.

Shotgun proteomics, using liquid chromatography-tandem mass spectroscopy (LC-MS/MS), was used to identify the composition of each protein corona. The shotgun approached identified over 300 unique proteins in the protein coronas of th different particles. A complete list of all identified proteins is shown in the Appendix, Tables B.1-B.8. The corona formation is based on the interactions such as non-specific binding through hydrophobic and electrostatic interactions between the surface of nanoparticle and proteins in the nasal fluid, which can be impacted by the relative abundance of proteins present within the nasal fluid. The top 20 proteins found on each nanoparticle type are listed

based on the normalized peptide spectrum in Table 3.2 - 3.5. These tables highlights the diversity of protein assoication on these nanoparticles.

Table 3.2. Top 20 identified proteins in each protein corona determined using molecular weight normalization for Bare OVA PNC.

Bare OVA PNC				
	30 min		4 hours	
#	Protein	NpSpC	Protein	NpSpC
1	Lysozyme C	13.492	Isoform Deltalf Lactotransferrin	15.437
2	Isoform Deltalf Of Lactotransferrin	9.259	Lysozyme C	12.926
3	Protein S100-A8	8.362	Protein S100-A9	12.793
4	Protein S100-A9	7.883	Protein S100-A8	11.111
5	Immunoglobulin Kappa Constant	6.177	Keratin, Type I Cytoskeletal 10	7.825
6	Keratin, Type I Cytoskeletal 14	6.093	Keratin, Type Ii Cytoskeletal 1	7.132
7	Keratin, Type I Cytoskeletal 10	5.214	Isoform 2 Of Bpi Fold-Containing Family A Member 1	7.049
8	Immunoglobulin J Chain	4.954	Immunoglobulin Kappa Constant	5.456
9	Keratin, Type Ii Cytoskeletal 1	4.886	Antileukoproteinase	5.281
10	Immunoglobulin Heavy Constant Alpha 1	4.306	Zymogen Granule Protein 16 Homolog B	5.086
11	Antileukoproteinase	4.285	Bpi Fold-Containing Family B Member 1	4.410
12	Keratin, Type I Cytoskeletal 9	4.108	Keratin, Type I Cytoskeletal 9	4.122
13	Keratin, Type Ii Cytoskeletal 2 Epidermal	3.154	Keratin, Type Ii Cytoskeletal 2 Epidermal	3.805
14	Neutrophil Defensin 1	3.111	Prolactin-Inducible Protein	3.746

Continued...

15	Histone H4	3.078	Neutrophil Defensin 1	3.705
16	Bpi Fold-Containing Family B Member 1	3.050	Immunoglobulin Heavy Constant Alpha 1	3.365
17	Keratin, Type Ii Cytoskeletal 6B	2.664	Immunoglobulin J Chain	3.191
18	Keratin, Type I Cytoskeletal 16	2.267	T Cell Receptor Alpha Joining 56 (Fragment)	3.016
19	Keratin, Type Ii Cytoskeletal 5	2.197	Keratin, Type I Cytoskeletal 14	2.586
20	Prolactin-Inducible Protein	2.078	Isoform 5 Of Deleted In Malignant Brain Tumors 1 Protein	2.302

Table 3.3. Top 20 identified proteins in each protein corona determined using molecular weight normalization for PEG PNC.

PEG PNC				
	30.0 min		4 hours	
#	Protein	NpSpC	Protein	NpSpC
1	Lysozyme C	7.832	Lysozyme C	9.985
2	Keratin, Type I Cytoskeletal 10	5.206	Isoform Deltalf Of Lactotransferrin	7.548
3	Isoform Deltalf Of Lactotransferrin	5.197	Keratin, Type I Cytoskeletal 10	6.993
4	Keratin, Type Ii Cytoskeletal 1	3.968	Keratin, Type Ii Cytoskeletal 1	5.274
5	Protein S100-A8	3.779	Keratin, Type I Cytoskeletal 9	4.932
6	Isoform 3 Of Tripartite Motif-Containing Protein 46	3.375	Immunoglobulin Kappa Constant	4.402
7	Immunoglobulin Kappa Constant	3.272	Keratin, Type I Cytoskeletal 14	4.092
8	Keratin, Type I Cytoskeletal 14	3.001	Keratin, Type Ii Cytoskeletal 2 Epidermal	4.062

Continued...

9	Keratin, Type I Cytoskeletal 9	2.568	Antileukoproteinase	4.015
10	Neutrophil Defensin 1	2.166	Protein S100-A8	3.458
11	Keratin, Type Ii Cytoskeletal 2 Epidermal	2.128	T Cell Receptor Alpha Joining 56 (Fragment)	3.018
12	Antileukoproteinase	2.087	Neutrophil Defensin 1	2.489
13	Protein S100-A9	2.084	Keratin, Type Ii Cytoskeletal 6B	1.84
14	T Cell Receptor Alpha Joining 56 (Fragment)	2.008	Immunoglobulin J Chain	1.827
15	Immunoglobulin Heavy Constant Alpha 1	1.909	Actin, Cytoplasmic 1 (Fragment)	1.776
16	Lysozyme C	1.844	Mammaglobin-B	1.745
17	Actin, Cytoplasmic 1 (Fragment)	1.634	Lysozyme C	1.64
18	Prolactin-Inducible Protein	1.398	Keratin, Type Ii Cytoskeletal 5	1.4
19	Bpi Fold-Containing Family B Member 1	1.329	Bpi Fold-Containing Family B Member 1	1.386
20	Immunoglobulin J Chain	1.280	Prolactin-Inducible Protein	1.262

Table 3.4. Top 20 identified proteins in each protein corona determined using molecular weight normalization for cOVA PNC.

cOVA PNC				
	30.0 min		4 hours	
#	Protein	NpSpC	Protein	NpSpC
1	Immunoglobulin Kappa Constant	9.895	Immunoglobulin Kappa Constant	8.613
2	T Cell Receptor Alpha Joining 56 (Fragment)	8.378	Isoform Deltalf Of Lactotransferrin	6.655

Continued...

3	Isoform Deltalf Of Lactotransferrin	6.523	Protein S100-A8	6.071
4	Protein S100-A8	6.044	Bpi Fold-Containing Family B Member 1	5.857
5	Immunoglobulin J Chain	5.451	T Cell Receptor Alpha Joining 56 (Fragment)	5.535
6	Serum Albumin	4.697	Isoform 2 Of Bpi Fold-Containing Family A Member 1	5.296
7	Immunoglobulin Heavy Constant Alpha 1	4.67	Immunoglobulin J Chain	4.861
8	Keratin, Type I Cytoskeletal 10	4.646	Immunoglobulin Heavy Constant Alpha 1	4.538
9	Keratin, Type Ii Cytoskeletal 1	4.192	Serum Albumin	4.225
10	Bpi Fold-Containing Family B Member 1	4.047	Protein S100-A9	3.525
11	Keratin, Type I Cytoskeletal 9	3.942	Actin, Cytoplasmic 1 (Fragment)	3.500
12	Actin, Cytoplasmic 1 (Fragment)	3.869	Fibrinogen Gamma Chain (Fragment)	2.690
13	Isoform 2 Of Bpi Fold-Containing Family A Member 1	3.346	Polymeric Immunoglobulin Receptor	2.656
14	Protein S100-A9	3.286	Keratin, Type I Cytoskeletal 9	2.554
15	Keratin, Type Ii Cytoskeletal 2 Epidermal	3.116	Lipocalin-1	2.544
16	Keratin, Type I Cytoskeletal 14	2.962	Lysozyme C	2.489

Continued...

17	Polymeric Immunoglobulin Receptor	2.833	Keratin, Type Ii Cytoskeletal 1	2.355
18	Immunoglobulin Lambda-Like Polypeptide 5	2.451	Zinc-Alpha-2-Glycoprotein	2.332
19	Lipocalin-1	2.222	Immunoglobulin Lambda-Like Polypeptide 5	2.244
20	Fibrinogen Gamma Chain (Fragment)	2.188	Hemoglobin Subunit Alpha	2.188

Table 3.5. Top 20 identified proteins in each protein corona determined using molecular weight normalization for LBL PNC.

LBL PNC				
	30.0 min		4.0 hours	
#	Protein	NpSpC	Protein	NpSpC
1	Immunoglobulin Kappa Constant	9.65	Immunoglobulin Kappa Constant	8.721
2	Prolactin-Inducible Protein	8.703	Serum Albumin	7.777
3	Serum Albumin	7.491	Protein S100-A8	7.133
4	Immunoglobulin Heavy Constant Alpha 1	7.297	Isoform Deltalf Lactotransferrin	6.793
5	Immunoglobulin J Chain	7.235	Protein S100-A9	5.878
6	Protein S100-A9	6.438	Immunoglobulin J Chain	5.506
7	Protein S100-A8	5.992	Immunoglobulin Heavy Constant Alpha 1	5.201
8	Isoform Deltalf Of Lactotransferrin	5.877	Keratin, Type I Cytoskeletal 10	4.637
9	Keratin, Type I Cytoskeletal 10	4.548	Prolactin-Inducible Protein	4.513
10	Lipocalin-1	3.857	Keratin, Type Ii Cytoskeletal 2 Epidermal	3.515
11	Keratin, Type Ii Cytoskeletal 1	3.261	Keratin, Type Ii Cytoskeletal 1	3.495
12	Bpi Fold-Containing Family B Member 1	3.111	Lipocalin-1	3.477

Continued...

13	Isoform 3 Of Wap Four-Disulfide Core Domain Protein 2	3.081	T Cell Receptor Alpha Joining 56 (Fragment)	2.949
14	Keratin, Type I Cytoskeletal 14	2.679	Bpi Fold-Containing Family B Member 1	2.693
15	Polymeric Immunoglobulin Receptor	2.549	Polymeric Immunoglobulin Receptor	2.584
16	Neutrophil Defensin 1	2.292	Immunoglobulin Lambda Constant 2	2.482
17	Keratin, Type I Cytoskeletal 9	2.238	Zinc-Alpha-2-Glycoprotein	2.46
18	Lysozyme C	2.173	Actin, Cytoplasmic 1 (Fragment)	2.202
19	Immunoglobulin Lambda Constant 2	2.142	Keratin, Type I Cytoskeletal 14	2.196
20	Isoform 5 Of Deleted In Malignant Brain Tumors 1 Protein	1.975	Immunoglobulin Lambda-Like Polypeptide 5	2.122

The proteomic characterization demonstrated that the 30 min and 4-hour time points contained several overlapping unique proteins not found in any other groups of nanoparticles. We used PANTHER analysis to produce pie charts based on the grouping of the associated hard corona to distinct biological functions in Figure 3.3 using only proteins with higher than ten peptide spectrum mapping (PSM). The trends shown on the PANTHER analysis demonstrate the unique principles of enrichment allowing significant biological changes in biological fingerprint between groups in which the dominant functions are popped out of the pie chart, the biological fingerprint as a function of time remained similar for the PEG and cOVA group during their transition from 30 mins to 4 hours. This could be due to PEG's antifouling coating that enables small number of associations to occur on their surface, as highlighted based on the 47 proteins associated with PEG nanoparticles during the 30-

minute timepoint and 57 proteins during their 4-hour timepoint. [152, 153] The positive cOVA nanoparticle potentially demonstrated less fluctuation in their hard corona identity based on the biological process analysis, with 40 proteins maintain similar function. To visualize the amount of overlap, we lowered the threshold value to 5 PSM to observed trace amount of protein found within the samples. To represent the data, we constructed a Venn diagram of proteins in Figure 3.4 that shows the number of unique proteins that overlap with one or more groups or are found only in that sample. It is important to note that many of the proteins that are shared among each group within the 30-min samples are high abundance proteins found in the nasal fluid, such as Isoform DeltaLf Lactotransferrin Serum albumin, Mucin-5B, Haptoglobin, and Polymeric immunoglobulin receptors. However, there is a gradual decrease of universally adsorbed proteins comparing the 30 min and 4-hour timepoint. While analyzing the 4-hour timepoint, the presence of tumor necrosis factor alpha (TNF alpha) was missing for the 4.0 hours bare OVA PNC group and present in each other groups, which is a multifunctional cytokine that plays essential roles in diverse cellular events such as inflammation, cell survival, proliferation, differentiation, and death. [154, 155] As a pro-inflammatory cytokine, TNF alpha can be secreted by inflammatory cells, and has the potential to be a potent inducer of the inflammatory response, a key regulator of innate immunity and plays an important role in the regulation of Th1 immune responses against intracellular bacteria and certain viral infections. [156] There is also a loss in complement c3 in bare PNC, which functions as part of the complement system and contributes to innate immunity. Conversely, bare PNC gained unique proteins such as Isoform Short of Protocadherin alpha-C2, which is a calcium-dependent cell-adhesion protein, believed to be used as establishment and maintenance of specific neuronal connections in the brain, potentially useful for brain association. [156-159]

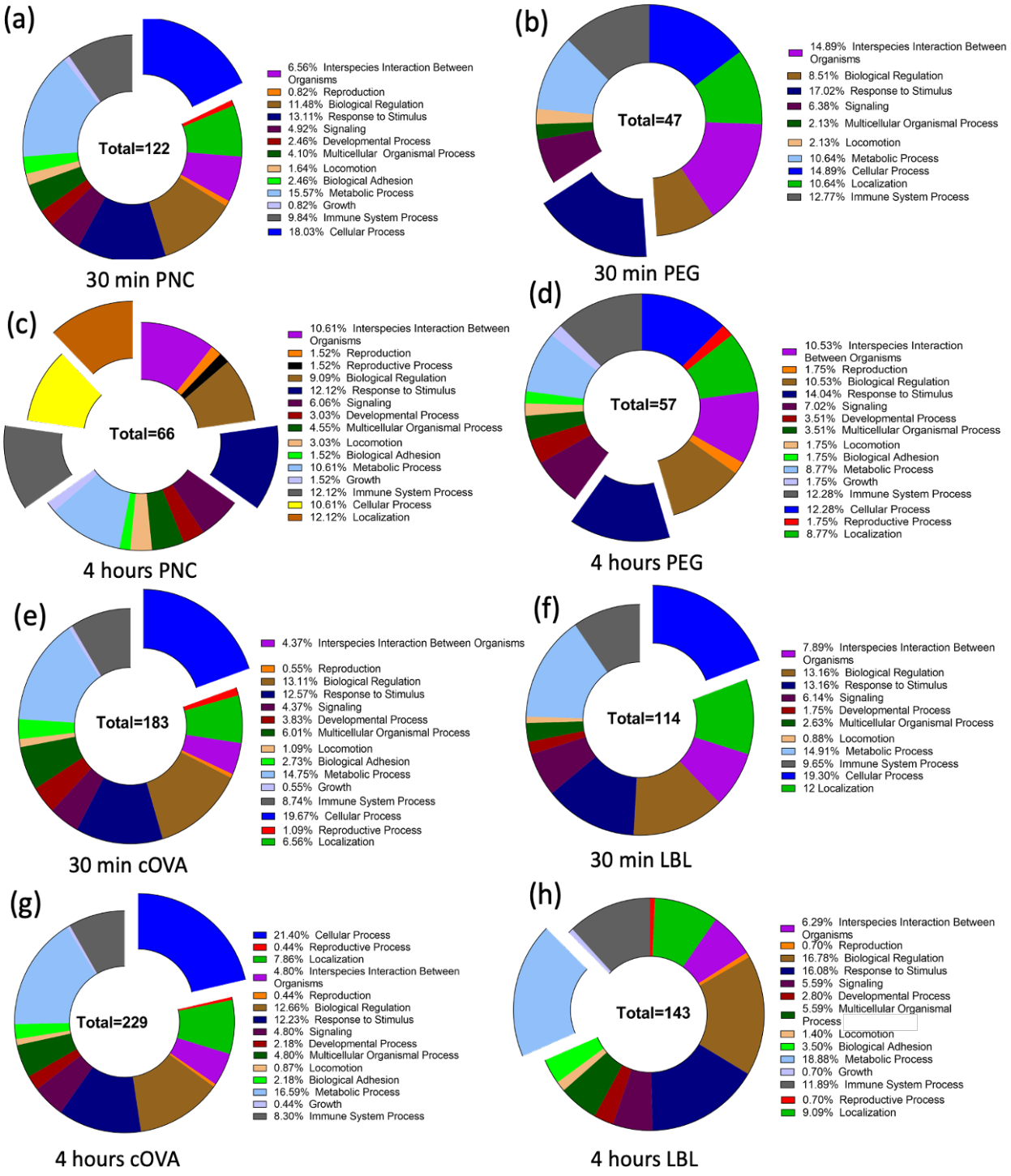
(a)
Total=122
6.56% Interspecies Interaction Between Organisms
0.82% Reproduction
11.48% Biological Regulation
13.11% Response to Stimulus
4.92% Signaling
2.46% Developmental Process
4.10% Multicellular Organismal Process
1.64% Locomotion
2.46% Biological Adhesion
15.57% Metabolic Process
0.82% Growth
9.84% Immune System Process
18.03% Cellular Process
30 min PNC
(b)
Total=47
14.89% Interspecies Interaction Between Organisms
8.51% Biological Regulation
17.02% Response to Stimulus
6.38% Signaling
2.13% Multicellular Organismal Process
2.13% Locomotion
10.64% Metabolic Process
14.89% Cellular Process
10.64% Localization
12.77% Immune System Process
30 min PEG
(c)
Total=66
10.61% Interspecies Interaction Between Organisms
1.52% Reproduction
1.52% Reproductive Process
9.09% Biological Regulation
12.12% Response to Stimulus
6.06% Signaling
3.03% Developmental Process
4.55% Multicellular Organismal Process
3.03% Locomotion
1.52% Biological Adhesion
10.61% Metabolic Process
1.52% Growth
12.12% Immune System Process
10.61% Cellular Process
12.12% Localization
4 hours PNC
(d)
Total=57
10.53% Interspecies Interaction Between Organisms
1.75% Reproduction
10.53% Biological Regulation
14.04% Response to Stimulus
7.02% Signaling
3.51% Developmental Process
3.51% Multicellular Organismal Process
1.75% Locomotion
1.75% Biological Adhesion
8.77% Metabolic Process
1.75% Growth
12.28% Immune System Process
12.28% Cellular Process
1.75% Reproductive Process
8.77% Localization
4 hours PEG
(e)
Total=183
4.37% Interspecies Interaction Between Organisms
0.55% Reproduction
13.11% Biological Regulation
12.57% Response to Stimulus
4.37% Signaling
3.83% Developmental Process
6.01% Multicellular Organismal Process
1.09% Locomotion
2.73% Biological Adhesion
14.75% Metabolic Process
0.55% Growth
8.74% Immune System Process
19.67% Cellular Process
1.09% Reproductive Process
6.56% Localization
30 min cOVA
(f)
Total=114
7.89% Interspecies Interaction Between Organisms
13.16% Biological Regulation
13.16% Response to Stimulus
6.14% Signaling
1.75% Developmental Process
2.63% Multicellular Organismal Process
0.88% Locomotion
14.91% Metabolic Process
9.65% Immune System Process
19.30% Cellular Process
12 Localization
30 min LBL
(g)
Total=229
21.40% Cellular Process
0.44% Reproductive Process
7.86% Localization
4.80% Interspecies Interaction Between Organisms
0.44% Reproduction
12.66% Biological Regulation
12.23% Response to Stimulus
4.80% Signaling
2.18% Developmental Process
4.80% Multicellular Organismal Process
0.87% Locomotion
2.18% Biological Adhesion
16.59% Metabolic Process
0.44% Growth
8.30% Immune System Process
4 hours cOVA
(h)
Total=143
6.29% Interspecies Interaction Between Organisms
0.70% Reproduction
16.78% Biological Regulation
16.08% Response to Stimulus
5.59% Signaling
2.80% Developmental Process
5.59% Multicellular Organismal Process
1.40% Locomotion
3.50% Biological Adhesion
18.88% Metabolic Process
0.70% Growth
11.89% Immune System Process
0.70% Reproductive Process
9.09% Localization
4 hours LBL

Figure 3.3: Summary pie charts with biological function process for each group from PANTHER a) 30-minute bare PNC, b) 30 minute PEG, c) 4.0 hours Bare PNC, d) 4.0 hour PEG, e) 30 minutes cOVA PNC, f) 30 minute LBL PNC, g) 4.0 hours cOVA, and h) 4.0 hours LBL.

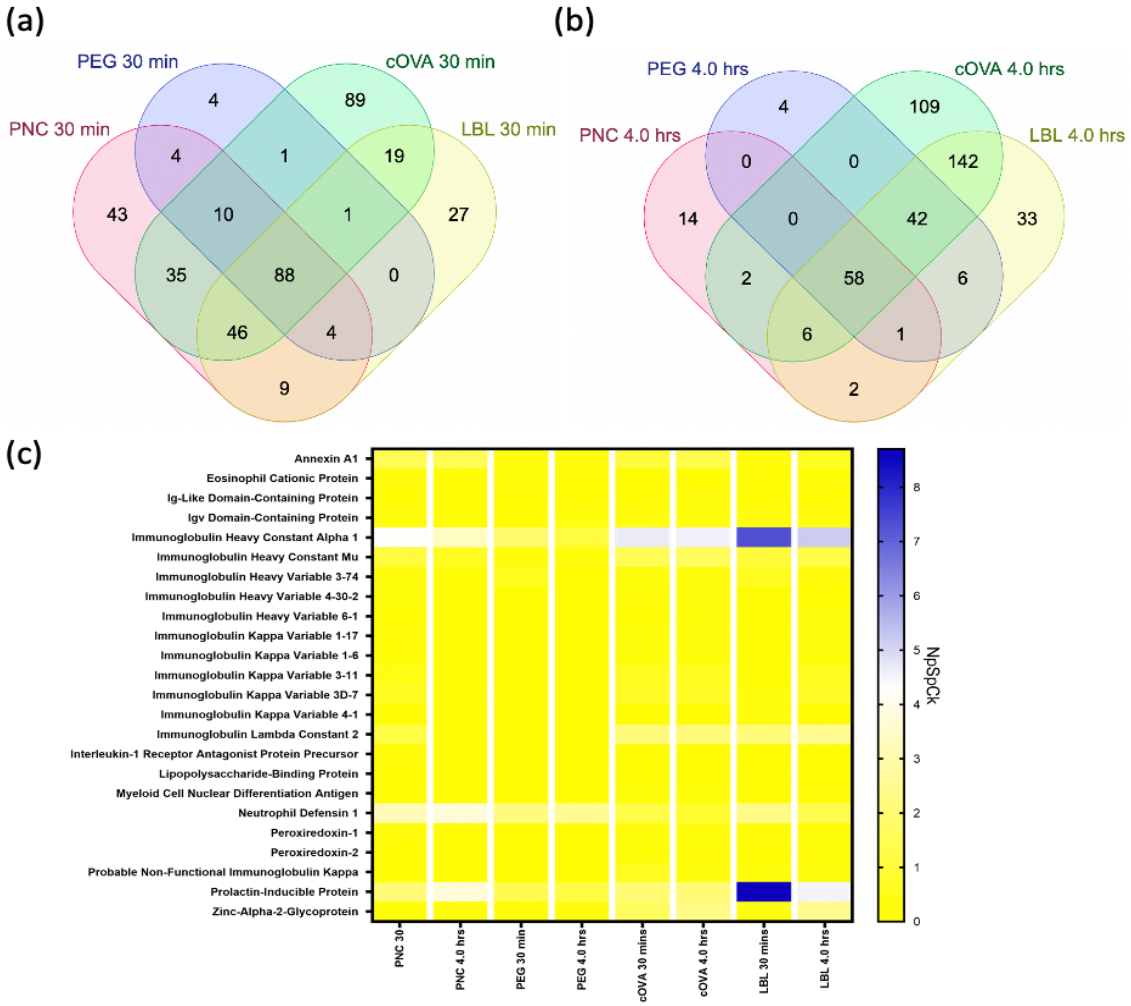

Figure 3.4: a) Venn Diagram showing the overlapping identified proteins in each protein nanoparticle group for 30 min incubation, b) Venn Diagram showing the overlapping identified proteins in each protein nanoparticle group for 4-hour incubation, c) heatmap of immune system proteins for each particle type and timepoint.

The associated protein in the hard corona change based on the coating and surface modification, the immunity profile from protein association also changes, as shown in Figure 3.4C

from the immunity heatmap. To further analyze the impact of the hard protein corona, we constructed a network mapping to outline the interaction and function of the corona Appendix (B.9-B.16). While this allowed to see a different cascade of interaction by grouping the presence of proteins found in the protein corona with a threshold of 10 or more PSM, we aim to highlight the impact of coatings by analyzing the fold change of each particle compared to the bare OVA PNC. We used Equation 4 to obtain the fold change of protein abundances compared to the bare PNC for each timepoint. We highlighted the top 25 up-and-down -fold changes in presence in the hard protein corona in appendix B.17-B.22 for PEG, cOVA, and LBL PNC. To measure the biological fold impact, we used g:Profiler, a tool for functional enrichment analysis gene ontology. For this analysis, the fold changes greater than Log2 up-or down-regulated were grouped for the enrichment analysis and a summary is shown in Table 3.6-3.10. 30-minute analysis of PEG PNC indicates a reduction in antigen binding and immunoglobulin receptor binding, with an increase in serine hydrolase, activity neutrophil-mediated immunity, and neutrophil activation. It has been shown that PEG coatings on polymer nanoparticles will significantly reduce the number of antigen-binding and immunoglobulin receptor binding, with an increase in neutrophil activity. [160] This same trend is also seen for the 4-hour PEG PNC nanoparticle during the fold analysis with the protein corona consisting of Leukotriene A-4 hydrolase and Desmoplakin, which have the biological process of neutrophil degranulation. [161, 162] While the analysis of cOVA at a 30-minute timepoint showed highly diverse biological regulation, some proteins for biological impact such as immune effector processes, neutrophil granulation, and leukocyte mediated immunity are found in the up-and down-regulated biological process, albeit with different proteins within those biological functions perhaps canceling out in net. However, we can see the presence of exocytosis regulation proteins, which are involved in receptor-mediated stimulation of granule mobilization and fusion with the plasma membrane for cOVA. [163] One

example is tetraspanins, which are molecular scaffolds that distribute proteins into highly organized microdomains consisting of adhesion, signaling, and adaptor proteins. [164] For cOVA 4 hour, we see the presence of proteins such as Pyruvate kinase PKM2, matrix metalloproteinase 9, and C3/C5 convertase, which all function in the immune system. As mentioned, fluid could contain lysed cells that could include intracellular proteins are present in the mixture. For example, transcriptional coactivator of STAT1 responsible for the induction of the protein PDL-1 expression and MMP-9 control the access of monocytes and T cells to the vascular wall. [165, 166, 167]. Lastly, we saw upregulation of immune effector process and regulated exocytosis with the LBL PNC for both time points, decreasing humoral immune response and vesicle-mediated transport.

Table 3.6. Biological Process for PEG 30 minute up- and down- regulation.

PEG 30 minute			
Upregulated	GO Identification	Downregulated	GO Identification
Leukocyte Activation Involved in Immune Response	GO:0002366	Antigen Binding	GO:0003823
Cell Activation Involved in Immune Response	GO:0002263	Immunoglobulin Receptor Binding	GO:0034987
Cornification	GO:0070268	Humoral Immune Response	GO:0006959
Immune Effector Process	GO:0002252	Immune Effector Process	GO:0002252
Immune Response	GO:0006955	Immune Response	GO:0006955
Keratinization	GO:0031424	Immune System Process	GO:0002376
Neutrophil Degranulation	GO:0043312	Defense Response to Bacterium	GO:0042742
Neutrophil Activation Involved in Immune Response	GO:0002283	Complement Activation, Classical Pathway	GO:0006958
Neutrophil Mediated Immunity	GO:0002446	Humoral Immune Response Mediated by Circulating Immunoglobulin	GO:0002455
Neutrophil Activation	GO:0042119	Complement Activation	GO:0006956
Granulocyte Activation	GO:0036230	Biological Process Involved in Interspecies Interaction Between Organisms	GO:0044419
Leukocyte Degranulation	GO:0043299	Phagocytosis, Recognition	GO:0006910
Leukocyte Mediated Immunity	GO:0002443	Regulated Exocytosis	GO:0045055
Leukocyte Activation	GO:0045321	Defense Response	GO:0006952

Table 3.7. Biological Process for PEG 4 hour up- and down- regulation.

PEG 4 Hour			
Upregulation	GO Identification	Downregulation	GO Identification
Immune Effector Process	GO:0002252	Antigen Binding	GO:0003823
Immune Response	GO:0006955	Cysteine-Type Endopeptidase Inhibitor Activity	GO:0004869
Leukocyte Mediated Immunity	GO:0002443	Immunoglobulin Binding	GO:0019865
Regulated Exocytosis	GO:0045055	Enzyme Inhibitor Activity	GO:0004857
Neutrophil Degranulation	GO:0043312	Immunoglobulin Receptor Binding	GO:0034987
Neutrophil Activation Involved in Immune Response	GO:0002283	Endopeptidase Inhibitor Activity	GO:0004866
Neutrophil Mediated Immunity	GO:0002446	Peptidase Inhibitor Activity	GO:0030414
Exocytosis	GO:0006887	Endopeptidase Regulator Activity	GO:0061135
Neutrophil Activation	GO:0042119	Humoral Immune Response	GO:0006959
Granulocyte Activation	GO:0036230	Vesicle-Mediated Transport	GO:0016192
Leukocyte Degranulation	GO:0043299	Leukocyte Mediated Immunity	GO:0002443
Myeloid Cell Activation Involved in Immune Response	GO:0002275	Phagocytosis, Recognition	GO:0006910

Table 3.8. Biological Process for cOVA 30.0 minute up- and down- regulation.

cOVA 30.0 minute			
Upregulation	GO Identification	Downregulation	GO Identification
Cell Adhesion Molecule Binding	GO:0061134	Endopeptidase Inhibitor Activity	GO:0004866
Endopeptidase Inhibitor Activity	GO:0004866	Peptidase Inhibitor Activity	GO:0030414
Peptidase Inhibitor Activity	GO:0030414	Leukocyte Mediated Immunity	GO:0002443
Endopeptidase Regulator Activity	GO:0061135	Immune Effector Process	GO:0002252

Continued...

Cadherin Binding	GO:0045296	Immune Response	GO:0006955
Serine-Type Endopeptidase Inhibitor Activity	GO:0004867	Neutrophil Degranulation	GO:0043312
Calcium-Dependent Protein Binding	GO:0048306	Immune System Process	GO:0002376
Identical Protein Binding	GO:0042802	Neutrophil Activation Involved in Immune Response	GO:0002283
Enzyme Regulator Activity	GO:0030234	Neutrophil Mediated Immunity	GO:0002446
Lipid Binding	GO:0008289	Neutrophil Activation	GO:0042119
Molecular Function Regulator	GO:0098772	Granulocyte Activation	GO:0036230
Oxidoreductase Activity, Acting on Peroxide as Acceptor	GO:0016684	Leukocyte Degranulation	GO:0043299
Immune Effector Process	GO:0002252	Myeloid Cell Activation Involved in Immune Response	GO:0002275
Immune Response	GO:0006955	Myeloid Leukocyte Mediated Immunity	GO:0002444
Leukocyte Mediated Immunity	GO:0002443	Peptide Cross-Linking	GO:0018149
Regulated Exocytosis	GO:0045055	Humoral Immune Response	GO:0006959
Neutrophil Degranulation	GO:0043312	Leukocyte Activation	GO:0045321
Neutrophil Activation Involved In Immune Response	GO:0002283	Leukocyte Activation Involved in Immune Response	GO:0002366
Neutrophil Mediated Immunity	GO:0002446	Cell Activation Involved in Immune Response	GO:0002263
Exocytosis	GO:0006887	Myeloid Leukocyte Activation	GO:0002274

Table 3.9. Biological Process for cOVA 4 hour up- and down- regulation.

cOVA 4 hours			
Upregulation	GO Identification	Downregulation	GO Identification
Cell Adhesion Molecule Binding	GO:0050839	Calcium Ion Binding	GO:0005509
Immunoglobulin Receptor Binding	GO:0034987	Humoral Immune Response	GO:0006959
Antigen Binding	GO:0003823	Extracellular Exosome	GO:0070062

Continued...

Calcium-Dependent Protein Binding	GO:0048306	Extracellular Vesicle	GO:1903561
Structural Constituent of Cytoskeleton	GO:0005200	Extracellular Organelle	GO:0043230
Lipid Binding	GO:0008289		
Identical Protein Binding	GO:0042802		
Complement Binding	GO:0001848		
Protein-Containing Complex Binding	GO:0044877		
Enzyme Binding	GO:0019899		
Phospholipase A2 Inhibitor Activity	GO:0019834		
Lipoprotein Particle Receptor Binding	GO:0070325		
Integrin Binding	GO:0005178		
Opsonin Binding	GO:0001846		
Phosphatidylcholine-Sterol O-Acyltransferase Activator Activity	GO:0060228		
Lipase Inhibitor Activity	GO:0055102		
MHC Class II Protein Complex Binding	GO:0023026		
Protein Binding	GO:0005515		

Table 3.10. Biological Process for LBL 30.0 minute up- and down- regulation.

LBL 30 minutes			
Upregulation	GO Identification	Downregulation	GO Identification
MHC Class I Protein Binding	GO:0042288	Neutrophil Activation Involved in Immune Response	GO:0002283
Angiostatin Binding	GO:0043532	Neutrophil Mediated Immunity	GO:0002446
Regulated Exocytosis	GO:0045055	Neutrophil Activation	GO:0042119
Leukocyte Mediated Immunity	GO:0002443	Humoral Immune Response	GO:0006959

Continued...

Immune Effector Process	GO:0002252	Leukocyte Activation	GO:0045321
Exocytosis	GO:0006887	Leukocyte Activation Involved In Immune Response	GO:0002366
Neutrophil Degranulation	GO:0043312	Cell Activation Involved in Immune Response	GO:0002263
Neutrophil Activation Involved In Immune Response	GO:0002283	Myeloid Leukocyte Activation	GO:0002274
Neutrophil Mediated Immunity	GO:0002446	Regulated Exocytosis	GO:0045055
Neutrophil Activation	GO:0042119	Phagocytosis, Recognition	GO:0006910
Granulocyte Activation	GO:0036230	Cell Activation	GO:0001775
Leukocyte Degranulation	GO:0043299	Response To External Stimulus	GO:0009605
Myeloid Cell Activation Involved in Immune Response	GO:0002275	Complement Activation, Classical Pathway	GO:0006958
Myeloid Leukocyte Mediated Immunity	GO:0002444	Vesicle-Mediated Transport	GO:0016192
Secretion By Cell	GO:0032940	Humoral Immune Response Mediated by Circulating Immunoglobulin	GO:0002455
Myeloid Leukocyte Activation	GO:0002274	Defense Response to Bacterium	GO:0042742
Export From Cell	GO:0140352	Exocytosis	GO:0006887
Cell Activation	GO:0001775	Defense Response	GO:0006952
Humoral Immune Response	GO:0006959	Complement Activation	GO:0006956

Table 3.11. Biological Process for LBL 4 hour up- and down- regulation.

LBL 4 hours			
Upregulation	GO Identification	Downregulation	GO Identification
Endopeptidase Inhibitor Activity	GO:0004866	Antigen Binding	GO:0003823
Peptidase Inhibitor Activity	GO:0030414	Humoral Immune Response	GO:0006959

Continued...

Endopeptidase Regulator Activity	GO:0061135	Antimicrobial Humoral Response	GO:0019730
Peptidase Regulator Activity	GO:0061134	Defense Response to Bacterium	GO:0042742
Enzyme Inhibitor Activity	GO:0004857	Vesicle-Mediated Transport	GO:0016192
Structural Molecule Activity	GO:0005198	Immune System Process	GO:0002376
Signaling Receptor Binding	GO:0005102	Humoral Immune Response Mediated by Circulating Immunoglobulin	GO:0002455
Cell Adhesion Molecule Binding	GO:0050839	Leukocyte Mediated Immunity	GO:0002443
Immunoglobulin Receptor Binding	GO:0034987	Extracellular Exosome	GO:0070062
Antigen Binding	GO:0003823	Extracellular Vesicle	GO:1903561
Calcium-Dependent Protein Binding	GO:0048306	Extracellular Membrane-Bounded Organelle	GO:0065010
Structural Constituent of Cytoskeleton	GO:0005200	Extracellular Organelle	GO:0043230
Lipid Binding	GO:0008289	Extracellular Space	GO:0005615
Identical Protein Binding	GO:0042802	Extracellular Region	GO:0005576
Serine-Type Endopeptidase Inhibitor Activity	GO:0004867	Blood Microparticle	GO:0072562
Enzyme Regulator Activity	GO:0030234	Collagen-Containing Extracellular Matrix	GO:0062023
Antioxidant Activity	GO:0016209	Secretory Granule	GO:0030141
Glycosaminoglycan Binding	GO:0005539	Extracellular Matrix	GO:0031012
Molecular Function Regulator	GO:0098772	External Encapsulating Structure	GO:0030312
Cadherin Binding	GO:0045296	Secretory Vesicle	GO:0099503
Protease Binding	GO:0002020	Platelet Alpha Granule Lumen	GO:0031093
Fatty Acid Binding	GO:0005504	Immunoglobulin Complex, Circulating	GO:0042571
Heparin Binding	GO:0008201	Monomeric IgA Immunoglobulin Complex	GO:0071748

Continued...

Sulfur Compound Binding	GO:1901681		
Complement Binding	GO:0001848		
Calcium Ion Binding	GO:0005509		
Protein-Containing Complex Binding	GO:0044877		
Integrin Binding	GO:0005178		
Opsonin Binding	GO:0001846		
Lipase Inhibitor Activity	GO:0055102		
MHC Class II Protein Complex Binding	GO:0023026		
Protein Binding	GO:0005515		
Immune Effector Process	GO:0002252		
Immune System Process	GO:0002376		
Cell Activation	GO:0001775		
Innate Immune Response	GO:0045087		

3.3.3 Epithelial Cellular Uptake

While the protein corona composition in nasal fluid provides insight into the biological impact of protein nanoparticles and their potential coatings, the combination of particle chemistry and nasal corona affect nanoparticle interactions with and uptake by barrier epithelial cells. Protein nanoparticles with the nasal corona were incubated with A549 epithelial cells in serum-free media to avoid a serum protein corona, and internalization was quantified by flow cytometry and confirmed by confocal microscopy (Figure 3.5).

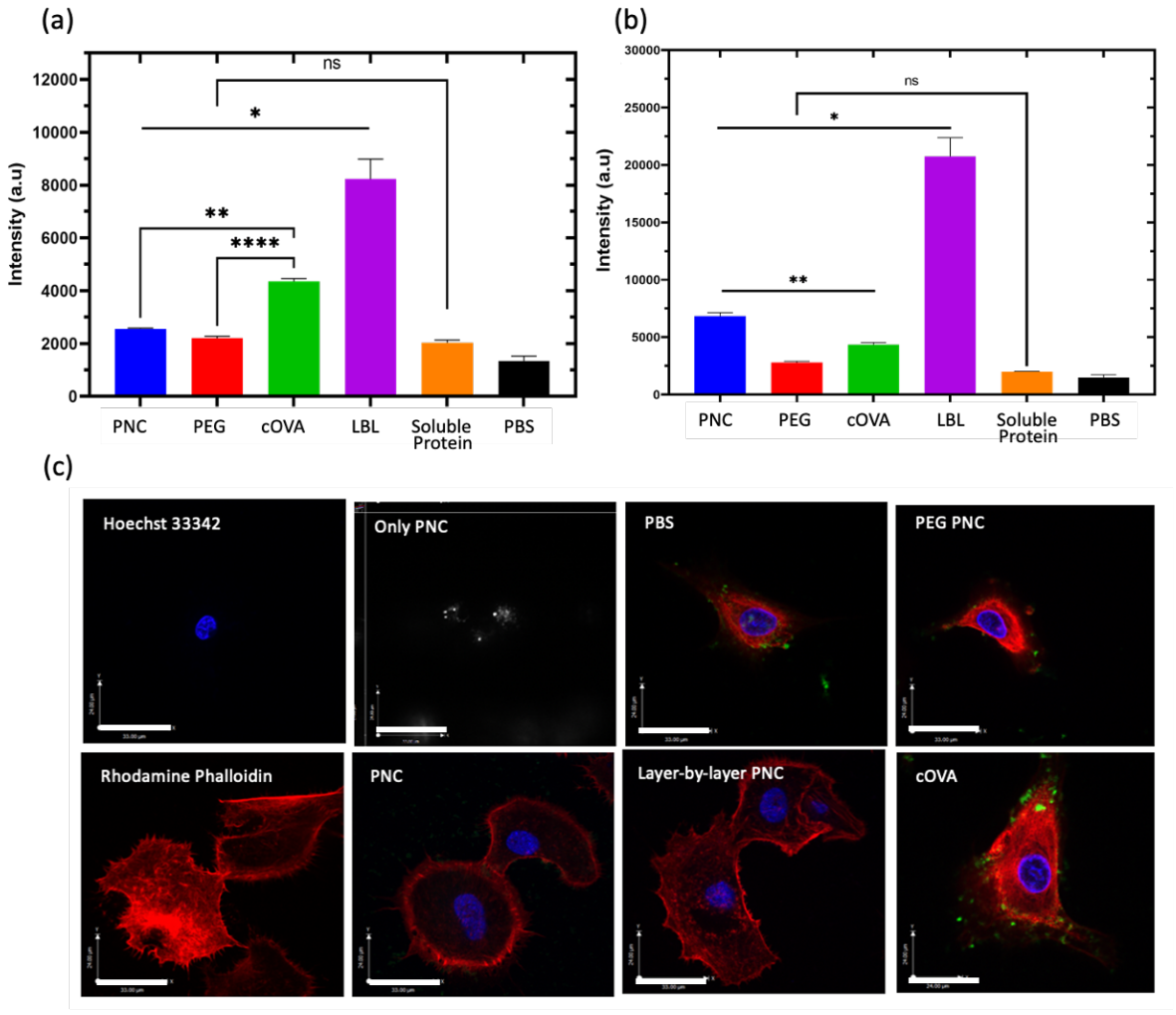

Figure 3.5: a) Summary of cellular uptake for A549 cells for 1-hour timepoint after incubation for 30 min, b) Summary of cellular uptake for A549 cells for 4-hour timepoint after incubation for 30 min each subgroup were indicated using Two-way ANOVA was used to analyze the significant difference among 3 or more groups. P-values less than 0.05 were significant (*, $p < 0.05$; **, $p < 0.005$; ***, $p < 0.001$), c) Confocal microscopy of internalized Bare OVA, cOVA PNC, PEG PNC and LBL PNC with an adsorbed protein corona. Fluorescent protein nanoparticles (0.1 ng/cell), fabricated by conjugating OVA protein with Alexa Fluor 488 prior to desolvation, were incubated with A549 cells for 4 hours at 37°C. Center slice images were obtained after nanoparticle incubation using a Perkin Elmer UltraVIEW VoX spinning disk confocal. (Scale bar – 33 µm; nanoparticles – green or white, A549 actin cytoskeleton – red, nuclei - blue)

The cellular uptake profile using A549 adenocarcinomic human alveolar basal epithelial cells indicated highest cellular uptake for layer-by-layer protein nanoparticles, which is the opposite that is shown with the JAWSII cells. It has been seen that chitosan is known to act as a tight junction

enhancer, allowing for a slight disturbance between the tight junction, causing an increase in permeability at cells adjacent to each other. [168, 169] Moreover, it has been shown that chitosan nanoparticle has shown significant improved uptake by A549 cells. Internalization of these chitosan nanoparticles by A549 cells occurred by adsorptive endocytosis initiated by nonspecific interactions between nanoparticles and cell membranes and by clathrin-mediated process. [170] Moreover, this phenomenon may increase cellular uptake based on the protein corona that could upregulate processes such as cell adhesion molecule binding and cadherin binding processes from proteins found in the corona of layer-by-layer nanoparticles. The cOVA nanoparticle is shown to have high uptake in the 1-hour timepoint with a decrease lower than bare PNC at 4-hour timepoint; this could be due to the attraction from the positive surface charge and negative charge from the cell membrane for the A549 cells. In addition, the cOVA contain proteins that has protein involved in processes such as cytoskeletal protein binding from proteins like AnxA6, which binds actin filaments. [171] As expected uptake of PEG nanoparticles is lowest, and the corona has decreased levels of proteins that regulate exocytosis and phagocytosis, compared to bare PNC, consistent with the literature. [172] Moreover, neutral particles have been shown to have less cellular uptake due to poor association to cell membranes. [172, 173]

3.3.4 Conclusions

The protein corona of nanoparticles has been well characterized for many types of nanoparticles in serum. However, little work has been done to understand the protein adsorption of nanoparticles in nasal fluids, despite the extensive work on nanoparticle-based nasal delivery for intranasal vaccines, nose-to-brain delivery, and even brain imaging via nasal delivery. [49, 50, 51, 52] To understand the adsorption of nasal proteins to nanoparticles, we characterized the composition of protein corona on model vaccine protein nanoparticles with different surface properties. Our

analysis revealed distinct corona fingerprints for different particle surface modifications as well as changes over time. The challenge in protein corona work is deriving accessible data to generalize the results to other types of nanoparticles. We demonstrated methods to modify the surface behavior of nanoparticles and determine the protein corona of each nanoparticle. Morever our findings suggest the protein corona impact in nasal fluids to assist in engineering nanoparticles for nasal route delivery methods. Each nanoparticle contain unique biological processes and a diverse array of protein from nasal fluid. For example, PEG nanoparticle is shown to contain a protein corona that could be used for neuphil activity, where cOVA and LBL demonstrate unique proteins on its corona that is responsible for cadherin-mediated binding or endocytosis. This work and our findings can be applied to both synthetic nanoparticles and biological nanoparticles using different coatings to mask the bulk material of nanoparticles. [174] Probing epithelial cells allowed to understand the potential impact of the protein corona impact on A549 cell line, and the function of coatings such as LBL that can improve permeability in epithelial cell for improve cellular uptake. Interestly, the PEG nanoparticle strong CD86 reponsive could be due to the impact of the protein corona with high neuphil assoication to the surfave leading to activiation of specific markers. Future strategies using similar surface properties or protein nanoparticles would expect similar protein corona fingerprint, which will allow to understand the biological function that the protein corona could have during an *in vivo* study.

CHAPTER 4. CONCLUSIONS AND FUTURE DIRECTIONS

4.1 Conclusions

This dissertation explored the various cell barriers associated with nasal-based delivery of nanoparticles. This work investigated the diffusion limitation phenomena of different engineered coatings on protein nanoparticles. It established the protein corona that is adsorbed onto nanoparticles during nasal fluids incubation. These studies bridge physical and biological understanding of nanoparticle delivery for intranasal administration. These results provide insight into the behavior of nanoparticles in nasal fluids. They will assist in predicting the impact during *in vivo* studies.

4.1.1 Protein Nanoparticle Diffusion and Uptake

Intranasal delivery and mucosal delivery routes have unique benefits such as invoking mucosal immunity and access to protected tissues. However, these routes face many biological barriers that significantly hinder many therapeutics and vaccines. The first barrier is mucus, which is a hydrogel-like substance known to limit the diffusion of materials. To improve delivery, nanoparticles have been used to improve cellular uptake, stability, and unique interaction with antigen-presenting cells. However, mucus and uptake on epithelial cell have been shown to significantly limit nanoparticle nasal delivery. Chapter 2 explores different coating on nanoparticles made from proteins, allowing for the high amount to be delivered based on carrier to therapeutic ratio and successful usage for vaccination. We have engineered these coatings to endow the nanoparticles with different surface properties to alter transport through the mucus. We confirmed the transport profile of each protein nanoparticle with different surface chemistry and unmodified using both a bulk diffusion analysis and multiple particles tracking analysis. We

confirmed cOVA has a low diffusion coefficient and bulk diffusion in mucus. Conversely, PEGylated protein nanoparticles rapidly diffuse across the mucus barrier. Chitosan-DNA layer-by-layer nanoparticles exhibited bimodal distribution of diffusion ability, likely due the dynamic shedding of the coated layers. Moreover, the cellular uptake on A549 and JAWSII demonstrate the striking differences between barriers. In general, nanoparticles with higher mucus diffusion had lower uptake by dendritic cells in the presence of mucus and vice versa. While the dynamic nature of the LBL particles is promising to break this trend, tuning of the layer order and shedding should be performed to match *in vivo* conditions.

4.1.2 Intranasal Proteomic

In Chapter 3, we bridged the gap in understanding the protein corona of nanoparticles with different surface charges in nasal fluids. This work providing understanding on nasal protein corona of nanoparticles, and the recruitment of proteins once nanoparticles are delivered into the nasal cavity. Many vaccines have attempted to be delivered through the intranasal route. However, little work has been done to understand the protein association that occurs during the delivery stage. Using the same nanoparticles with modified surfaces, we demonstrated that the high amount of association of protein on positive nanoparticles such as. In contrast, PEGylated nanoparticles, a standard coating often used for the nasal delivery system, adsorb far fewer proteins and recruitment of proteins that activate neutrophils based on GO theoretical analysis. Lastly, we obtained high amount of immune cell association based on their associated protein on the surface of LBL and bare nanoparticle. Interestingly, LBL protein corona could be impacted by its shedding ability as shown in Chapter 2, allowing for removing of certain proteins. Lastly, we observed that coatings such as chitosan could further enhance cellular uptake of A549, even after adsorption of a nasal corona.

4.2 Future directions

4.21 In vivo nasal delivery in Nanoparticle

The insight of nanoparticle diffusion, cellular uptake, and protein corona from nasal fluid will assist in understanding on nasal tissue uptake and cellular interactions. However in vitro analyses can only reveal key trends with the surface properties of nanoparticles and how well nanoparticles can overcome the mucus barrier. However, mucus is a flowing liquid, and the composition of nasal fluid can change over time. This is difficult to mimic in an in vitro setting, which require in vivo studies to model the geometry of the nasal cavity and fluid dynamic from cilia movement and provide intact mucus and cellular barriers. Therefore, understanding the impact of the biodistribution in an in vivo model will provide insight into the impact of coatings during intranasal delivery. We have identified key nanoparticle formulations that will be ideal to penetrate through the mucus, such as the PEG PNC and LBL nanoparticle, however, still require knowledge of these nanoparticles in a nose animal model. For this study, mice could be used with the same fabrication of nanoparticles, where mice would be administrated with OVA nanoparticles. This experiment will examine the locations of nanoparticle in the NALT, epithelium, mucus, and deeper in the nasal cavity onto other organs for the biodistribution. After a few weeks, we will examine the nasal wash, and immune organs such as lymph nodes and spleen for an immune response such as the production of antibodies. Overall, study highlight the impact of overcoming the various barriers such as the mucus and epithelium cell lines associated with nasal delivery and see the cellular impact of coatings on nanoparticles delivery. Once understanding of the impact of coatings protein nanoparticles are solidified. We aim to translation these coatings on to subunit proteins on influenza virus to generate an immune response as a

vaccine using the intranasal route. This have been previously done with M2E, extracellular domain of Matrix 2 (M2e) protein on influenza with successful protection of cross-reactive antibodies that could neutralize influenza A, however little was knowledge on the antigen amount that was ability to penetrate through the mucus to the NALT. The translating our understanding of coatings could potentially improve access of nanoparticles to the NALT.

4.2.2 Expanding coatings

While protein nanoparticle provides many advantages, these methods used in this dissertation can be allowed to many different nanoparticles systems to understand this ability to overcome mucosal barriers or understand how viruses can pass through mucosal barriers. For example, some viruses carry unique proteins such as neuraminidase that can cleave sialic acid residues from the mucin hydrogel to improve diffusion. Similar methods have been attempted by using N-acetyl-L-cysteine functionalized nanostructured lipid carrier to improve oral bioavailability of curcumin.[176] Future plans could use coatings such as the LBL with the incorporation and fabrication of conserved influenza protein such as the extracellular domain of Matrix 2 (M2e) protein, truncated hemagglutinin, and neuraminidase for protein nanoparticles for intranasal vaccination. For mice vaccination, we can challenge the mice with influenza and measure the nasal wash to produce specific IgG, IgA, or IgE antibody endpoint titers in sera, nasal washes against influenza, evaluate inflammatory cytokine levels looking at inflammatory cytokine (TNF-α, IL-12, and IL-6).

4.2.3 General Outlook

This study provided information on biomaterial's interaction with nasal fluids and their impact on different cellular carriers such as epithelial cells and immune cells. This work provides insight into how nanoparticles will provide interaction with nasal environments. The combinations of biomaterials transform due to protein adsorption, allowing rational biomaterials design to guide the future in vivo. Moreover, this work protects useful interacting of protein nanoparticle behavior in mucus to be used to tune better delivery.

Appendix

A.Code 1 For Nanoparticle Tracking

```
function D_eff = diffusion2(data, thresh)
%% Definition
%note: run such as D_eff = diffusion2("data",30)
% Calculates a diffusion coefficient from trajectory "data" using the mean
% squared displacement and the method of moments with a Random Walk
% Approximation. Reported as the average, standard deviation, and a graph
% of the distribution of diffusion coefficients

% data must be a location and name of the file directory (ex:
% 'C:\Users\TPho\Desktop\PEG MPT Trial 1.xlsx'))

% If necessary, a "threshold" for the minimum number of frames can be set
% (ex: 10). Otherwise, the second input should be 0.

%% Theory

% Random Walk Approximation:
% D = delta(x^2)/(4*delta(t))

% In terms of mean squared displacement (MSD) for 2D motion...
% D = sum(MSD)/(4*dt))
% Use finite difference approximation to achieve this


%% Parameters

% pixel conversion is 0.224 pixels per 0.5 microns
p = 4.12; % micron/Pixel
%% Organizing the Data

% Upload the data file
T = xlsread(data);

% Column 1 == Trajectory/Particle ID
% Column 2 == Frame #
% Column 3 == XPosition
% Column 4 == YPosition

% Convert T to matrix
T1 = T(:,1);
T2 = T(:,2);
T3 = T(:,3);
```

```
T4 = T(:,4);

% Number of trajectories
Num = max(T1);

% Define Deff as diffusion coefficient
D_eff = [];

% Calculate Deff for each trajectory
for i = 1:Num


    idx = find(T1 == i);
    X = T3(idx);
    Y = T4(idx);
    N = length(X);


    % Quality control to set minimum number of frames
    if  N > thresh

        for j = 2:N
            X_diff2(j-1) = (X(j)-X(j-1))^2;
            Y_diff2(j-1) = (Y(j)-Y(j-1))^2;
        end

        R2(i) = sum(X_diff2)+sum(Y_diff2);
        dt = N*0.1; % seconds
        d_eff = R2(i)/4/dt/p.^2;
        D_eff = [D_eff d_eff];

    end

end

% Find values where D_eff < 100
idx3 = find(D_eff < 100);

D_eff = D_eff(idx3);

hist(D_eff)

end
```

B.1 PNC 30 min NP Protein Corona

Protein Name	Ascension Code	MW (kDa)	Calculated PI	Normalized Peptide spectral count
14-3-3 Protein Theta	P27348	27.7	4.78	0.024
14-3-3 Protein Zeta/Delta	P63104	27.7	4.79	0.293
2-Phospho-D-Glycerate Hydro-Lyase	A0A2R8Y6G6	47.3	6.99	0.101
40S Ribosomal Protein S14	P62263	16.3	10.05	0.043
60S Ribosomal Protein L15	P61313	24.1	11.62	0.029
60S Ribosomal Protein L7	P18124	29.2	10.65	0.022
Actin, Cytoplasmic 1 (Fragment)	A0A2R8YFE2	8.8	9.2	1.536
Actin, Cytoplasmic 1	P60709	41.7	5.48	0.682
Actinin, Alpha 4, Isoform Cra_A	F5GXS2	104.8	5.44	0.039
Aldehyde Dehydrogenase, Dimeric Nadp-Preferring	P30838	50.4	6.54	0.042
Alpha-1-Acid Glycoprotein 1	P02763	23.5	5.02	0.028
Alpha-Amylase 1A	P0DUB6	57.7	6.93	0.095
Alpha-S1-Casein	P02662	24.5	5.02	0.029
Annexin A1	P04083	38.7	7.02	1.504
Annexin A5	P08758	35.9	5.05	0.039
Annexin	H0YMW4	41.9	8.13	0.952
Antibacterial Peptide Fall-39	J3KNB4	19.6	9.41	0.171
Antileukoproteinase	P03973	14.3	8.75	4.285
Apolipoprotein A-I	P02647	30.8	5.76	0.328
Apolipoprotein D (Fragment)	C9JF17	24.1	5.6	0.110
Aquaporin-5	P55064	28.3	8.62	0.049
Atp Synthase Subunit Beta, Mitochondrial	P06576	56.5	5.4	0.012
Azurocidin	P20160	26.9	9.5	0.152
Basic Salivary Proline-Rich Protein 1	G3V1M9	32.4	11.21	0.022
Basic Salivary Proline-Rich Protein 2	P02812	40.8	11.63	0.067
Beta-2-Microglobulin	P61769	13.7	6.52	0.150
Bone Marrow Proteoglycan	P13727	25.2	6.76	0.080
Bpi Fold-Containing Family B Member 1	Q8TDL5	52.4	7.23	3.051
Bpi Fold-Containing Family B Member 2	Q8N4F0	49.1	8.72	0.192
Bpi Fold-Containing Family B Member 4	A0A669KBJ0	75.3	5.36	0.341
C-X-C Motif Chemokine 17	Q6UXB2	13.8	10.96	0.145

Continued...

C4A Anaphylatoxin	A0A0G2JPR0	192.8	7.03	0.004
Cadherin-1	A0A087WXI5	100	4.79	0.007
Calmodulin-Like Protein 3	P27482	16.9	4.42	0.080
Calmodulin-Like Protein 5	Q9NZT1	15.9	4.44	1.313
Caspase-14	P31944	27.7	5.58	0.269
Catalase	P04040	59.7	7.39	0.012
Cathepsin G	P08311	28.8	11.19	0.652
Cd59 Glycoprotein	P13987	14.2	6.48	0.049
Clathrin Heavy Chain	A0A087WVQ6	191.9	5.69	0.003
Cofilin, Non-Muscle Isoform	E9PK25	22.7	8.34	0.060
Complement C3	P01024	187	6.4	0.072
Corneodesmosin	G8JLG2	51.6	8.44	0.026
Cornifelin	Q9BYD5	12.4	6.1	0.162
Cornifin-B	P22528	9.9	8.48	0.339
Cystatin-C	P01034	15.8	8.75	0.770
Cystatin-S	P01036	16.2	5.02	0.040
Cystatin-Sn	P01037	16.4	7.21	0.043
Cysteine-Rich Secretory Protein 3	J3KPA1	31	7.61	0.023
Deleted In Malignant Brain Tumors 1 Protein (Fragment)	A0A590UJF8	21.6	5.27	1.087
Desmoglein-1	Q02413	113.7	5.03	0.024
Desmoplakin	P15924	331.6	6.81	0.041
E3 Ubiquitin-Protein Ligase Trim56	Q9BRZ2	81.4	7.74	0.133
Elongation Factor 1-Alpha 1	P68104	50.1	9.01	0.188
Elongation Factor 2	P13639	95.3	6.83	0.014
Endoplasmic Reticulum Chaperone Bip	P11021	72.3	5.16	0.010
Envoplakin	K7EKI0	233.7	7.25	0.006
Eosinophil Cationic Protein	P12724	18.4	10.02	0.147
Epiplakin	P58107	555.3	5.62	0.005
Eukaryotic Initiation Factor 4A-I	P60842	46.1	5.48	0.029
Ezrin	E7EQR4	69.3	6.16	0.010
F-Box Only Protein 50	Q6ZVX7	30.8	6.62	0.045
Fatty Acid-Binding Protein 5	Q01469	15.2	7.01	1.248
Fibrinogen Beta Chain	P02675	55.9	8.27	0.145
Fibrinogen Gamma Chain (Fragment)	C9JU00	14	7.2	0.769
Filaggrin	P20930	434.9	9.25	0.011
Filaggrin-2	Q5D862	247.9	8.31	0.024
Galectin-3	P17931	26.1	8.56	0.129
Galectin-3-Binding Protein	Q08380	65.3	5.27	0.011
Galectin-7	P47929	15.1	7.62	1.256

Continued...

Gasdermin-A	Q96QA5	49.3	5.29	0.014
Gem-Interacting Protein (Fragment)	K7EJC2	33.2	6.01	0.062
Glutamine Synthetase	A0A2R8YDT1	57.1	8.37	0.011
Glyceraldehyde-3-Phosphate Dehydrogenase	P04406	36	8.46	0.318
Haptoglobin	P00738	45.2	6.58	0.135
Heat Shock 27 Kda Protein	A0A6Q8PGK1	23.7	6.4	0.342
Heat Shock 70 Kda Protein 1B	A0A0G2JIW1	70.1	5.66	0.106
Heat Shock Protein Hsp 90-Beta	P08238	83.2	5.03	0.033
Hemoglobin Subunit Alpha	P69905	15.2	8.68	0.264
Hemoglobin Subunit Beta	P68871	16	7.28	0.422
Hemoglobin Subunit Delta	P02042	16	8.05	0.041
Histidine-Rich Glycoprotein	P04196	59.5	7.5	0.068
Histone H2A	A0A0U1RRH7	18.5	11.52	0.370
Histone H2B	U3KQK0	18.8	10.54	0.573
Histone H3.3 (Fragment)	K7ES00	16.6	11.84	0.609
Histone H4	P62805	11.4	11.36	3.078
Homeobox Protein Nkx-2.3	Q8TAU0	38.4	7.49	0.017
Hornerin	Q86YZ3	282.2	10.04	0.074
Iggfc-Binding Protein	Q9Y6R7	571.6	5.34	0.104
Immunoglobulin Heavy Constant Alpha 1	P01876	37.6	6.51	4.306
Immunoglobulin Heavy Constant Alpha 2 (Fragment)	A0A0G2JMB2	36.5	6.1	0.700
Immunoglobulin Heavy Constant Gamma 1 (Fragment)	A0A0A0MS08	43.9	6.96	0.552
Immunoglobulin Heavy Constant Gamma 2 (Fragment)	A0A286YEY4	43.8	6.52	0.293
Immunoglobulin Heavy Constant Gamma 3 (Fragment)	A0A286YES1	49.1	6.87	0.028
Immunoglobulin Heavy Variable 1-2	P23083	13.1	9.13	0.103
Immunoglobulin Heavy Variable 1-69D	A0A0B4J2H0	12.7	8.47	0.374
Immunoglobulin Heavy Variable 3-49	A0A0A0MS15	13	8.62	0.104
Immunoglobulin Heavy Variable 3-72	A0A4W8ZXM2	11.2	7.97	0.778
Immunoglobulin Heavy Variable 3-74	A0A0B4J1X5	12.8	8.66	0.317
Immunoglobulin Heavy Variable 3/Or16-12 (Non-Functional) (Fragment)	A0A075B7B8	12.9	6.51	0.264

Continued...

Immunoglobulin Heavy Variable 4-30-2	A0A087WSY4	13	9.67	0.054
Immunoglobulin J Chain	P01591	18.1	5.24	4.954
Immunoglobulin Kappa Constant	P01834	11.8	6.52	6.177
Immunoglobulin Kappa Variable 1-17	P01599	12.8	8.68	0.051
Immunoglobulin Kappa Variable 1-33	A0A2Q2TTZ9	11.8	5.34	0.577
Immunoglobulin Kappa Variable 2-40	A0A087WW87	13.3	4.61	0.455
Immunoglobulin Kappa Variable 3-11	P04433	12.6	4.96	0.481
Immunoglobulin Kappa Variable 3-20	P01619	12.5	4.96	1.133
Immunoglobulin Kappa Variable 3D-7	A0A0C4DH55	13.1	5.94	0.619
Immunoglobulin Lambda Constant 2	P0DOY2	11.3	7.24	1.192
Immunoglobulin Lambda Variable 1-47	P01700	12.3	5.91	0.273
Immunoglobulin Lambda Variable 3-21	P80748	12.4	5.29	0.056
Immunoglobulin Lambda-Like Polypeptide 5	A0A0B4J231	23.1	8.84	0.966
Intelectin-2	Q8WWU7	36.2	8.28	0.019
Interleukin-1 Receptor Accessory Protein	Q9NPH3	65.4	8.12	0.010
Involucrin	P07476	68.4	4.61	0.029
Isoform 2 Of 14-3-3 Protein Sigma	P31947	24.3	4.82	0.418
Isoform 2 Of 40S Ribosomal Protein S20	P60866	16	9.32	0.044
Isoform 2 Of 6-Phosphogluconate Dehydrogenase, Decarboxylating	P52209	51.8	7.44	0.014
Isoform 2 Of Bpi Fold-Containing Family A Member 1	Q9NP55	25.2	6.06	2.064
Isoform 2 Of Carcinoembryonic Antigen-Related Cell Adhesion Molecule 5	P06731	76.7	5.92	0.027
Isoform 2 Of Fibrinogen Alpha Chain	P02671	69.7	8.06	0.009
Isoform 2 Of Fructose-Bisphosphate Aldolase A	P04075	45.2	8.25	0.014
Isoform 2 Of Immunoglobulin Heavy Constant Mu	P01871	51.9	6.15	1.120
Isoform 2 Of Interleukin-1 Receptor Antagonist Protein	P18510	17.9	5.35	0.039

Continued...

Isoform 2 Of Keratin, Type I Cytoskeletal 23	Q9C075	33.3	5.49	0.020
Isoform 2 Of Keratin, Type Ii Cytoskeletal 78	Q8N1N4	45	5.2	0.016
Isoform 2 Of Plastin-2	P13796	21.8	5.44	0.094
Isoform 2 Of Thioredoxin	P10599	9.4	6.04	0.719
Isoform 3 Of Atp Synthase Subunit Alpha, Mitochondrial	P25705	57.5	9.29	0.024
Isoform 3 Of Creb3 Regulatory Factor	Q8IUR6	72.3	4.89	0.009
Isoform 3 Of Keratin, Type I Cytoskeletal 13	P13646	45.8	4.88	1.280
Isoform 3 Of Pyruvate Kinase Pkm	P14618	56.2	8.44	0.133
Isoform 3 Of Triosephosphate Isomerase	P60174	17.9	5.58	0.151
Isoform 3 Of Tripartite Motif-Containing Protein 46	Q7Z4K8	57.4	8.69	0.619
Isoform 4 Of Leukotriene A-4 Hydrolase	P09960	66.8	6.7	0.010
Isoform 5 Of Clusterin	P10909	53.6	6.27	0.177
Isoform 5 Of Deleted In Malignant Brain Tumors 1 Protein	Q9UGM3	258.3	5.43	1.621
Isoform 5 Of L-Lactate Dehydrogenase A Chain	P00338	26.7	8.15	0.126
Isoform 5 Of Trypsin-3	P35030	25.9	5.83	0.027
Isoform Deltalf Of Lactotransferrin	P02788	73.1	7.85	9.259
Junction Plakoglobin	P14923	81.7	6.14	0.198
Kallikrein-14	Q9P0G3	29.1	9.23	0.046
Keratin, Type I Cuticular Ha3-I	O76009	45.9	4.82	0.088
Keratin, Type I Cytoskeletal 10	P13645	58.8	5.21	5.214
Keratin, Type I Cytoskeletal 12	Q99456	53.5	4.78	0.177
Keratin, Type I Cytoskeletal 14	P02533	51.5	5.16	6.093
Keratin, Type I Cytoskeletal 16	P08779	51.2	5.05	2.267
Keratin, Type I Cytoskeletal 17	Q04695	48.1	5.02	1.417
Keratin, Type I Cytoskeletal 19	P08727	44.1	5.14	1.193
Keratin, Type I Cytoskeletal 9	P35527	62	5.24	4.108
Keratin, Type Ii Cytoskeletal 1	P04264	66	8.12	4.886
Keratin, Type Ii Cytoskeletal 1B	Q7Z794	61.9	5.99	0.447
Keratin, Type Ii Cytoskeletal 2 Epidermal	P35908	65.4	8	3.154
Keratin, Type Ii Cytoskeletal 4	P19013	56.1	6.61	0.434
Keratin, Type Ii Cytoskeletal 5	P13647	62.3	7.74	2.197

Continued...

Keratin, Type Ii Cytoskeletal 6A	P02538	60	8	1.188
Keratin, Type Ii Cytoskeletal 6B	P04259	60	8	2.664
Keratin, Type Ii Cytoskeletal 6C	P48668	60	8	0.124
Keratin, Type Ii Cytoskeletal 7	P08729	51.4	5.48	0.527
Keratin, Type Ii Cytoskeletal 71	Q3SY84	57.3	6.61	0.024
Keratinocyte Proline-Rich Protein	Q5T749	64.1	8.27	0.158
Late Cornified Envelope Protein 1F	Q5T754	11.6	8.37	0.060
Late Cornified Envelope Protein 2B	O14633	11.2	8.09	0.062
Lipocalin-1	P31025	19.2	5.58	1.199
Lipocalin-15	Q6UWW0	20.4	4.94	0.398
Lysozyme C	P00698	16.2	9.07	0.170
Lysozyme C	P61626	16.5	9.16	13.492
Mammaglobin-B	O75556	10.9	5.78	0.864
Midkine	E9PLM6	16.9	9.91	0.160
Moesin	P26038	67.8	6.4	0.080
Mucin-2	A0A0G2JR65	303.2	5.88	0.004
Mucin-2	Q02817	540	5.8	0.018
Mucin-5Ac	P98088	585.2	7.02	0.665
Mucin-5B	Q9HC84	596	6.64	0.347
Mucin-7	Q8TAX7	39.1	8.78	0.086
Myeloblastin	P24158	27.8	8.35	0.144
Myeloperoxidase	P05164	83.8	8.97	0.340
Myosin-9	P35579	226.4	5.6	0.009
Neutrophil Defensin 1	P59665	10.2	6.99	3.111
Neutrophil Elastase	P08246	28.5	9.35	0.237
Neutrophil Gelatinase-Associated Lipocalin	X6R8F3	22.8	8.5	0.059
Opiorphin Prepropeptide	Q99935	27.2	10.42	0.099
Peptidoglycan Recognition Protein 1	O75594	21.7	8.59	0.032
Periplakin	O60437	204.6	5.6	0.007
Peroxiredoxin-1	Q06830	22.1	8.13	0.095
Phosphatidylinositol 3-Kinase Catalytic Subunit Type 3 (Fragment)	K7EIV6	19.9	9.54	0.511
Phosphatidylinositol 3,4,5-Trisphosphate-Dependent Rac Exchanger 2 Protein	Q70Z35	182.5	7.44	0.007
Pi-Plc X Domain-Containing Protein 1	Q9NUJ7	36.6	6.58	0.109
Polymeric Immunoglobulin Receptor	P01833	83.2	5.74	1.945
Prelamin-A/C	A0A6Q8PFJ0	80.9	8.27	0.042
Prolactin-Inducible Protein	P12273	16.6	8.05	2.078

Continued...

Proline-Rich Protein 4	A0A0J9YXF8	16.9	7.52	0.080
Prosaposin	C9JIZ6	58.4	5.17	0.012
Protein Disulfide-Isomerase	P07237	57.1	4.87	0.012
Protein Leg1 Homolog	Q6P5S2	37.9	6.15	0.125
Protein Pof1B	Q8WVV4	68	6.32	0.029
Protein S100-A14	Q9HCY8	11.7	5.24	0.171
Protein S100-A6	P06703	10.2	5.48	0.192
Protein S100-A7	P31151	11.5	6.77	1.649
Protein S100-A8	P05109	10.8	7.03	8.362
Protein S100-A9	P06702	13.2	6.13	7.883
Protein S100-P	P25815	10.4	4.88	0.067
Retinoic Acid Receptor Responder Protein 1	P49788	33.3	8.51	0.041
Rho Guanine Nucleotide Exchange Factor 17	Q96PE2	221.5	6.29	0.012
Ribonuclease 4	P34096	16.8	9.03	0.119
Secretoglobin Family 1D Member 1	O95968	9.9	9.25	0.273
Secretoglobin Family 1D Member 2	O95969	9.9	8.25	0.137
Serine Protease Htra1	Q92743	51.3	7.83	0.026
Serine/Threonine-Protein Kinase Mak	P20794	70.5	9.66	0.009
Serpin B3	P29508	44.5	6.81	0.520
Serpin B4	P48594	44.8	6.21	0.996
Serum Albumin	P02769	69.2	6.18	0.243
Serum Albumin	P02768	69.3	6.28	1.329
Sialic Acid-Binding Ig-Like Lectin 16	A6NMB1	53	9.03	0.039
Skin-Specific Protein 32	Q5T750	26.2	7.97	0.256
Small Proline-Rich Protein 2G	Q9BYE4	8.2	7.96	0.489
Spliceosome Rna Helicase Ddx39B (Fragment)	H0YCC6	16.6	5.55	0.284
Sulfhydryl Oxidase 1	O00391	82.5	8.92	0.008
Suprabasin	Q6UWP8	60.5	7.01	0.034
Synaptophysin-Like Protein 1	Q16563	28.5	8.43	0.095
T Cell Receptor Alpha Joining 56 (Fragment)	A0A075B6Z2	2.2	10.29	0.614
Tetraspanin-1	O60635	26.3	5.25	0.051
Tgc Domain-Containing Protein	A0A494C0J7	78.8	6.27	0.266
Thrombospondin-1	P07996	129.3	4.94	0.015
Thymidine Phosphorylase	P19971	49.9	5.53	0.027
Transcobalamin-1	P20061	48.2	5.03	0.028

Continued...

Transmembrane Protein 201	Q5SNT2	72.2	9.22	0.019
Tubulin Alpha Chain	F5H5D3	57.7	5.07	0.059
Tubulin Alpha-4A Chain	P68366	49.9	5.06	0.014
Tubulin Beta-4B Chain	P68371	49.8	4.89	0.095
Tumor Necrosis Factor	P01375	110.1	7.12	0.006
Ubiquitin-40S Ribosomal Protein S27A	P62979	18	9.64	0.375
Uteroglobin	P11684	10	5.06	0.070
Vitronectin	P04004	54.3	5.8	0.038
Vomeronasal Type-1 Receptor 5	Q7Z5H4	40.8	9.2	0.033
Wd Repeat-Containing Protein 1	O75083	66.2	6.65	0.010
Zinc-Alpha-2-Glycoprotein	P25311	34.2	6.05	0.040
Zymogen Granule Protein 16 Homolog B	Q96DA0	22.7	7.39	1.336

B.2 PNC 4.0 hours NP Protein Corona

Protein Name	Ascension Code	MW (kDa)	Calculated PI	Normalized Peptide spectral count
Actin-Like Protein 10	A0A7I2V3D3	39.2	8.6	0.056
Actin, Cytoplasmic 1 (Fragment)	A0A2R8YFE2	8.8	9.2	0.754
Annexin A1	P04083	38.7	7.02	1.434
Annexin	H0YMW4	41.9	8.13	0.797
Antileukoproteinase	P03973	14.3	8.75	5.281
Apolipoprotein D (Fragment)	C9JF17	24.1	5.6	0.093
Atp Synthase Subunit Beta, Mitochondrial	P06576	56.5	5.4	0.275
Bpi Fold-Containing Family B Member 1	Q8TDL5	52.4	7.23	4.410
Bpi Fold-Containing Family B Member 4	A0A669KBJ0	75.3	5.36	0.531
Cathepsin D	C9JH19	48.6	7.84	0.046
Cathepsin G	P08311	28.8	11.19	1.232
Cornifelin	Q9BYD5	12.4	6.1	0.358
Deleted In Malignant Brain Tumors 1 Protein (Fragment)	A0A590UJF8	21.6	5.27	1.648
Desmoplakin	P15924	331.6	6.81	0.013

Continued...

Dihydrolipoyllysine-Residue Succinyltransferase Component Of 2-Oxoglutarate Dehydrogenase Complex, Mitochondrial	P36957	48.7	8.95	0.730
F-Box Only Protein 50	Q6ZVX7	30.8	6.62	0.215
Fibrinogen Gamma Chain (Fragment)	C9JU00	14	7.2	0.161
Filaggrin	P20930	434.9	9.25	0.025
Filaggrin-2	Q5D862	247.9	8.31	0.063
Galectin-7	P47929	15.1	7.62	0.734
Glyceraldehyde-3-Phosphate Dehydrogenase	P04406	36	8.46	0.062
Histone H4	P62805	11.4	11.36	1.559
Hornerin	Q86YZ3	282.2	10.04	0.079
Iggfc-Binding Protein	Q9Y6R7	571.6	5.34	0.016
Immunoglobulin Heavy Constant Alpha 1	P01876	37.6	6.51	3.365
Immunoglobulin Heavy Constant Gamma 1 (Fragment)	A0A0A0MS08	43.9	6.96	0.202
Immunoglobulin Heavy Variable 3-72	A0A4W8ZXM2	11.2	7.97	0.392
Immunoglobulin J Chain	P01591	18.1	5.24	3.191
Immunoglobulin Kappa Constant	P01834	11.8	6.52	5.456
Immunoglobulin Kappa Variable 2-40	A0A087WW87	13.3	4.61	0.169
Immunoglobulin Kappa Variable 3-20	P01619	12.5	4.96	1.422
Immunoglobulin Lambda-Like Polypeptide 5	A0A0B4J231	23.1	8.84	0.769
Isoform 2 Of Bpi Fold-Containing Family A Member 1	Q9NP55	25.2	6.06	7.049
Isoform 2 Of Btb/Poz Domain-Containing Protein 1	Q9H0C5	42.1	6.98	0.052
Isoform 2 Of Electron Transfer Flavoprotein Subunit Alpha, Mitochondrial	P13804	30	8.57	0.887
Isoform 2 Of Immunoglobulin Heavy Constant Mu	P01871	51.9	6.15	0.598
Isoform 3 Of Atp Synthase Subunit Alpha, Mitochondrial	P25705	57.5	9.29	0.851
Isoform 3 Of Keratin, Type I Cytoskeletal 13	P13646	45.8	4.88	0.193
Isoform 3 Of Wap Four-Disulfide Core Domain Protein 2	Q14508	8.1	7.83	0.548
Isoform 5 Of Deleted In Malignant Brain Tumors 1 Protein	Q9UGM3	258.3	5.43	2.302
Isoform Deltalf Of Lactotransferrin	P02788	73.1	7.85	15.437

Continued...

Isoform Short Of Protocadherin Alpha-C2	Q9Y5I4	96.1	5.2	0.092
Keratin, Type I Cytoskeletal 10	P13645	58.8	5.21	7.825
Keratin, Type I Cytoskeletal 14	P02533	51.5	5.16	2.586
Keratin, Type I Cytoskeletal 16	P08779	51.2	5.05	0.738
Keratin, Type I Cytoskeletal 17	Q04695	48.1	5.02	0.276
Keratin, Type I Cytoskeletal 9	P35527	62	5.24	4.122
Keratin, Type Ii Cytoskeletal 1	P04264	66	8.12	7.132
Keratin, Type Ii Cytoskeletal 1B	Q7Z794	61.9	5.99	0.897
Keratin, Type Ii Cytoskeletal 2 Epidermal	P35908	65.4	8	3.805
Keratin, Type Ii Cytoskeletal 5	P13647	62.3	7.74	0.641
Keratin, Type Ii Cytoskeletal 6A	P02538	60	8	0.408
Keratin, Type Ii Cytoskeletal 6B	P04259	60	8	1.407
Keratin, Type Ii Cytoskeletal 7	P08729	51.4	5.48	0.605
Lipocalin-1	P31025	19.2	5.58	1.391
Lysozyme C	P61626	16.5	9.16	12.926
Midkine	E9PLM6	16.9	9.91	0.133
Mucin-2	Q02817	540	5.8	0.016
Mucin-5B	Q9HC84	596	6.64	0.254
Myeloblastin	P24158	27.8	8.35	0.162
Myeloperoxidase	P05164	83.8	8.97	0.741
Neutrophil Defensin 1	P59665	10.2	6.99	3.705
Neutrophil Elastase	P08246	28.5	9.35	0.468
Phospholipase A2, Membrane Associated	P14555	16.1	9.23	0.140
Polymeric Immunoglobulin Receptor	P01833	83.2	5.74	1.308
Prolactin-Inducible Protein	P12273	16.6	8.05	3.746
Protein Leg1 Homolog	Q6P5S2	37.9	6.15	0.058
Protein S100-A8	P05109	10.8	7.03	11.111
Protein S100-A9	P06702	13.2	6.13	12.793
Ras-Related Protein Rab-30 (Fragment)	E9PI18	8.8	5.36	0.256
Serine/Threonine-Protein Kinase Mak	P20794	70.5	9.66	0.062
Serpin B3	P29508	44.5	6.81	0.049
Serum Albumin	P02769	69.2	6.18	0.064
Serum Albumin	P02768	69.3	6.28	1.220
Suprabasin	Q6UWP8	60.5	7.01	0.037
T Cell Receptor Alpha Joining 56 (Fragment)	A0A075B6Z2	2.2	10.29	3.016
Tetraspanin-1	O60635	26.3	5.25	0.338
Transcobalamin-1	P20061	48.2	5.03	0.045

Continued...

Transcription Factor Maff	Q9ULX9	17.7	9.8	0.251
Trna (Adenine(58)-N(1))-Methyltransferase (Fragment)	H7C2E8	11.6	7.88	0.572
Zinc Finger Swim Domain-Containing Protein 6	Q9HCJ5	133.4	7.36	0.033
Zinc-Alpha-2-Glycoprotein	P25311	34.2	6.05	0.066
Zymogen Granule Protein 16 Homolog B	Q96DA0	22.7	7.39	5.086

B.3 PEG 30 minutes NP Protein Corona

Protein Name	Ascension Code	MW (kDa)	Calculated PI	Normalized Peptide spectral count
14-3-3 Protein Zeta/Delta	P63104	27.7	4.79	0.080
Actin, Cytoplasmic 1 (Fragment)	A0A2R8YFE2	8.8	9.2	1.634
Actin, Cytoplasmic 1	P60709	41.7	5.48	0.238
Alpha-Amylase 1A	P0DUB6	57.7	6.93	0.134
Annexin A1	P04083	38.7	7.02	0.114
Annexin	H0YMW4	41.9	8.13	0.080
Antileukoproteinase	P03973	14.3	8.75	2.087
Apolipoprotein A-I	P02647	30.8	5.76	0.287
Basic Salivary Proline-Rich Protein 2	P02812	40.8	11.63	0.108
Bpi Fold-Containing Family B Member 1	Q8TDL5	52.4	7.23	1.330
Bpi Fold-Containing Family B Member 2	Q8N4F0	49.1	8.72	0.135
Bpi Fold-Containing Family B Member 4	A0A669KBJ0	75.3	5.36	0.044
C-X-C Motif Chemokine 17	Q6UXB2	13.8	10.96	0.079
Calmodulin-Like Protein 5	Q9NZT1	15.9	4.44	0.210
Catalase	P04040	59.7	7.39	0.037
Cathepsin G	P08311	28.8	11.19	0.190
Complement C3	P01024	187	6.4	0.018
Coronin-1A	P31146	51	6.68	0.021
Cystatin-C	P01034	15.8	8.75	0.140
Deleted In Malignant Brain Tumors 1 Protein (Fragment)	A0A590UJF8	21.6	5.27	0.411
Desmoglein-1	Q02413	113.7	5.03	0.078
Desmoplakin	P15924	331.6	6.81	0.017

Continued...

E3 Ubiquitin-Protein Ligase Sh3Rf2	Q8TEC5	79.3	9.94	0.014
E3 Ubiquitin-Protein Ligase Trim56	Q9BRZ2	81.4	7.74	0.054
Eosinophil Cationic Protein	P12724	18.4	10.02	0.059
Extracellular Glycoprotein Lacritin	Q9GZZ8	14.2	5.5	0.311
F-Box Only Protein 50	Q6ZVX7	30.8	6.62	0.035
Fatty Acid-Binding Protein 5	Q01469	15.2	7.01	0.143
Fibrinogen Beta Chain	P02675	55.9	8.27	0.059
Fibrinogen Gamma Chain (Fragment)	C9JU00	14	7.2	0.158
Filaggrin	P20930	434.9	9.25	0.003
Filaggrin-2	Q5D862	247.9	8.31	0.036
Galectin-7	P47929	15.1	7.62	0.144
Hemoglobin Subunit Alpha	P69905	15.2	8.68	0.291
Hemoglobin Subunit Beta	P68871	16	7.28	0.899
Hemoglobin Subunit Delta	P02042	16	8.05	0.203
Histone H1.3	P16402	22.3	11.02	0.196
Histone H2A	A0A0U1RRH7	18.5	11.52	0.180
Histone H2B	U3KQK0	18.8	10.54	0.235
Histone H3.3 (Fragment)	K7ES00	16.6	11.84	0.068
Histone H4	P62805	11.4	11.36	1.163
Hornerin	Q86YZ3	282.2	10.04	0.004
Iggfc-Binding Protein	Q9Y6R7	571.6	5.34	0.033
Immunoglobulin Heavy Constant Alpha 1	P01876	37.6	6.51	1.909
Immunoglobulin Heavy Constant Alpha 2 (Fragment)	A0A0G2JMB2	36.5	6.1	0.059
Immunoglobulin Heavy Constant Gamma 1 (Fragment)	A0A0A0MS08	43.9	6.96	0.050
Immunoglobulin Heavy Constant Gamma 2 (Fragment)	A0A286YEY4	43.8	6.52	0.050
Immunoglobulin Heavy Variable 1-69D	A0A0B4J2H0	12.7	8.47	0.089
Immunoglobulin Heavy Variable 3-74	A0A0B4J1X5	12.8	8.66	0.521
Immunoglobulin J Chain	P01591	18.1	5.24	1.281
Immunoglobulin Kappa Constant	P01834	11.8	6.52	3.272
Immunoglobulin Kappa Variable 1-33	A0A2Q2TTZ9	11.8	5.34	0.374
Immunoglobulin Lambda-Like Polypeptide 5	A0A0B4J231	23.1	8.84	0.336
Isoform 2 Of Bpi Fold-Containing Family A Member 1	Q9NP55	25.2	6.06	1.138
Isoform 2 Of Immunoglobulin Heavy Constant Mu	P01871	51.9	6.15	0.170
Isoform 2 Of Keratin, Type Ii Cytoskeletal 78	Q8N1N4	45	5.2	0.073

Continued...

Isoform 2 Of Thioredoxin	P10599	9.4	6.04	0.235
Isoform 3 Of Keratin, Type I Cytoskeletal 13	P13646	45.8	4.88	1.060
Isoform 3 Of Pyruvate Kinase Pkm	P14618	56.2	8.44	0.020
Isoform 3 Of Tripartite Motif-Containing Protein 46	Q7Z4K8	57.4	8.69	3.375
Isoform 5 Of Clusterin	P10909	53.6	6.27	0.062
Isoform 5 Of Deleted In Malignant Brain Tumors 1 Protein	Q9UGM3	258.3	5.43	0.539
Isoform Deltalf Of Lactotransferrin	P02788	73.1	7.85	5.197
Isoform N3 Of Camp-Specific 3',5'-Cyclic Phosphodiesterase 4D	Q08499	23.8	9.72	0.140
Keratin, Type I Cytoskeletal 10	P13645	58.8	5.21	5.206
Keratin, Type I Cytoskeletal 12	Q99456	53.5	4.78	0.186
Keratin, Type I Cytoskeletal 14	P02533	51.5	5.16	3.001
Keratin, Type I Cytoskeletal 16	P08779	51.2	5.05	0.668
Keratin, Type I Cytoskeletal 19	P08727	44.1	5.14	0.376
Keratin, Type I Cytoskeletal 9	P35527	62	5.24	2.568
Keratin, Type Ii Cytoskeletal 1	P04264	66	8.12	3.968
Keratin, Type Ii Cytoskeletal 1B	Q7Z794	61.9	5.99	0.446
Keratin, Type Ii Cytoskeletal 2 Epidermal	P35908	65.4	8	2.128
Keratin, Type Ii Cytoskeletal 5	P13647	62.3	7.74	0.976
Keratin, Type Ii Cytoskeletal 6A	P02538	60	8	0.349
Keratin, Type Ii Cytoskeletal 6B	P04259	60	8	1.270
Keratin, Type Ii Cytoskeletal 7	P08729	51.4	5.48	0.408
Keratin, Type Ii Cytoskeletal 71	Q3SY84	57.3	6.61	0.019
Keratinocyte Proline-Rich Protein	Q5T749	64.1	8.27	0.086
Lipocalin-1	P31025	19.2	5.58	0.404
Lysozyme C	P00698	16.2	9.07	1.845
Lysozyme C	P61626	16.5	9.16	7.832
Mammaglobin-B	O75556	10.9	5.78	1.013
Mucin-5Ac	P98088	585.2	7.02	0.183
Mucin-5B	Q9HC84	596	6.64	0.284
Mucin-7	Q8TAX7	39.1	8.78	0.028
Myeloblastin	P24158	27.8	8.35	0.079
Myeloperoxidase	P05164	83.8	8.97	0.040
Myosin-9	P35579	226.4	5.6	0.005
Neutrophil Defensin 1	P59665	10.2	6.99	2.166
Neutrophil Elastase	P08246	28.5	9.35	0.155
Neutrophil Gelatinase-Associated Lipocalin	X6R8F3	22.8	8.5	0.048

Opiorphin Prepropeptide	Q99935	27.2	10.42	0.041
Phosphatidylinositol 3-Kinase Catalytic Subunit Type 3 (Fragment)	K7EIV6	19.9	9.54	0.501
Polymeric Immunoglobulin Receptor	P01833	83.2	5.74	0.585
Prolactin-Inducible Protein	P12273	16.6	8.05	1.399
Protein S100-A8	P05109	10.8	7.03	3.779
Protein S100-A9	P06702	13.2	6.13	2.085
Retinal Dehydrogenase 2	O94788	56.7	6.05	0.116
Secretoglobin Family 1D Member 1	O95968	9.9	9.25	0.446
Serpin B4	P48594	44.8	6.21	0.099
Serum Albumin	P02769	69.2	6.18	0.415
Serum Albumin	P02768	69.3	6.28	0.639
Skin-Specific Protein 32	Q5T750	26.2	7.97	0.084
Suprabasin	Q6UWP8	60.5	7.01	0.018
T Cell Receptor Alpha Joining 56 (Fragment)	A0A075B6Z2	2.2	10.29	2.008
Tgc Domain-Containing Protein	A0A494C0J7	78.8	6.27	0.014
Transmembrane Protein 201	Q5SNT2	72.2	9.22	0.015
Tumor Necrosis Factor	P01375	110.1	7.12	0.020
Uteroglobin	P11684	10	5.06	0.442
Zinc-Alpha-2-Glycoprotein	P25311	34.2	6.05	0.065
Zymogen Granule Protein 16 Homolog B	Q96DA0	22.7	7.39	0.680

B.4 PEG 4.0 hours NP Protein Corona

Protein Name	Ascension Code	MW (kDa)	Calculated PI	Normalized Peptide spectral count
Actin, Cytoplasmic 1 (Fragment)	A0A2R8YFE2	8.8	9.2	1.776
Actin, Cytoplasmic 1	P60709	41.7	5.48	0.287
Alpha-Amylase 1A	P0DUB6	57.7	6.93	0.174
Annexin A1	P04083	38.7	7.02	0.290
Annexin	H0YMW4	41.9	8.13	0.053
Antileukoproteinase	P03973	14.3	8.75	4.015
Apolipoprotein A-I	P02647	30.8	5.76	0.177
Basic Salivary Proline-Rich Protein 2	P02812	40.8	11.63	0.025
Bpi Fold-Containing Family B Member 1	Q8TDL5	52.4	7.23	1.386

Continued...

Bpi Fold-Containing Family B Member 2	Q8N4F0	49.1	8.72	0.042
Bpi Fold-Containing Family B Member 4	A0A669KBJ0	75.3	5.36	0.014
Calmodulin-Like Protein 5	Q9NZT1	15.9	4.44	0.409
Caspase-14	P31944	27.7	5.58	0.080
Catalase	P04040	59.7	7.39	0.057
Cathepsin G	P08311	28.8	11.19	0.307
Complement C3	P01024	187	6.4	0.023
Cystatin-C	P01034	15.8	8.75	0.552
Deleted In Malignant Brain Tumors 1 Protein (Fragment)	A0A590UJF8	21.6	5.27	0.615
Desmocollin-1	Q08554	99.9	5.43	0.012
Desmoglein-1	Q02413	113.7	5.03	0.048
Desmoplakin	P15924	331.6	6.81	0.007
E3 Ubiquitin-Protein Ligase Sh3Rf2	Q8TEC5	79.3	9.94	0.084
Fatty Acid-Binding Protein 5	Q01469	15.2	7.01	0.573
Fibrinogen Gamma Chain (Fragment)	C9JU00	14	7.2	0.158
Filaggrin	P20930	434.9	9.25	0.003
Filaggrin-2	Q5D862	247.9	8.31	0.036
Galectin-7	P47929	15.1	7.62	0.431
Glyceraldehyde-3-Phosphate Dehydrogenase	P04406	36	8.46	0.094
Haptoglobin	P00738	45.2	6.58	0.072
Heat Shock 70 Kda Protein 1B	A0A0G2JIW1	70.1	5.66	0.017
Hemoglobin Subunit Alpha	P69905	15.2	8.68	0.214
Hemoglobin Subunit Beta	P68871	16	7.28	0.830
Histone H2A	A0A0U1RRH7	18.5	11.52	0.120
Histone H2B	U3KQK0	18.8	10.54	0.118
Histone H4	P62805	11.4	11.36	1.165
Hornerin	Q86YZ3	282.2	10.04	0.089
Iggfc-Binding Protein	Q9Y6R7	571.6	5.34	0.005
Immunoglobulin Heavy Constant Alpha 1	P01876	37.6	6.51	1.115
Immunoglobulin Heavy Constant Alpha 2 (Fragment)	A0A0G2JMB2	36.5	6.1	0.089
Immunoglobulin Heavy Constant Gamma 1 (Fragment)	A0A0A0MS08	43.9	6.96	0.124
Immunoglobulin Heavy Variable 3/Or16-12 (Non-Functional) (Fragment)	A0A075B7B8	12.9	6.51	0.172
Immunoglobulin J Chain	P01591	18.1	5.24	1.827
Immunoglobulin Kappa Constant	P01834	11.8	6.52	4.402

Continued...

Immunoglobulin Kappa Variable 1-33	A0A2Q2TTZ9	11.8	5.34	0.088
Immunoglobulin Kappa Variable 2-40	A0A087WW87	13.3	4.61	0.244
Immunoglobulin Kappa Variable 3-20	P01619	12.5	4.96	0.094
Immunoglobulin Lambda-Like Polypeptide 5	A0A0B4J231	23.1	8.84	0.383
Isoform 2 Of Bpi Fold-Containing Family A Member 1	Q9NP55	25.2	6.06	0.796
Isoform 2 Of Carboxypeptidase A4	Q9UI42	43.5	8.34	0.024
Isoform 2 Of Dermcidin	P81605	12.4	7.97	0.095
Isoform 2 Of Immunoglobulin Heavy Constant Mu	P01871	51.9	6.15	0.108
Isoform 2 Of Keratin, Type Ii Cytoskeletal 78	Q8N1N4	45	5.2	0.023
Isoform 3 Of Keratin, Type I Cytoskeletal 13	P13646	45.8	4.88	0.889
Isoform 3 Of Tripartite Motif-Containing Protein 46	Q7Z4K8	57.4	8.69	0.108
Isoform 3 Of Wap Four-Disulfide Core Domain Protein 2	Q14508	8.1	7.83	0.273
Isoform 5 Of Clusterin	P10909	53.6	6.27	0.204
Isoform 5 Of Deleted In Malignant Brain Tumors 1 Protein	Q9UGM3	258.3	5.43	0.358
Isoform Deltalf Of Lactotransferrin	P02788	73.1	7.85	7.548
Junction Plakoglobin	P14923	81.7	6.14	0.080
Keratin, Type I Cytoskeletal 10 (Fragment)	A0A1B0GVI3	10	8.44	0.104
Keratin, Type I Cytoskeletal 10	P13645	58.8	5.21	6.993
Keratin, Type I Cytoskeletal 12	Q99456	53.5	4.78	0.097
Keratin, Type I Cytoskeletal 14	P02533	51.5	5.16	4.092
Keratin, Type I Cytoskeletal 16	P08779	51.2	5.05	0.974
Keratin, Type I Cytoskeletal 17	Q04695	48.1	5.02	0.203
Keratin, Type I Cytoskeletal 19	P08727	44.1	5.14	0.251
Keratin, Type I Cytoskeletal 9	P35527	62	5.24	4.932
Keratin, Type Ii Cytoskeletal 1	P04264	66	8.12	5.274
Keratin, Type Ii Cytoskeletal 1B	Q7Z794	61.9	5.99	0.698
Keratin, Type Ii Cytoskeletal 2 Epidermal	P35908	65.4	8	4.062
Keratin, Type Ii Cytoskeletal 4	P19013	56.1	6.61	0.060
Keratin, Type Ii Cytoskeletal 5	P13647	62.3	7.74	1.400
Keratin, Type Ii Cytoskeletal 6A	P02538	60	8	0.566
Keratin, Type Ii Cytoskeletal 6B	P04259	60	8	1.840
Keratin, Type Ii Cytoskeletal 7	P08729	51.4	5.48	0.663

Continued...

Keratin, Type Ii Cytoskeletal 71	Q3SY84	57.3	6.61	0.018
Keratinocyte Proline-Rich Protein	Q5T749	64.1	8.27	0.065
Lipocalin-1	P31025	19.2	5.58	0.792
Lipocalin-15	Q6UWW0	20.4	4.94	0.051
Lysozyme C	P00698	16.2	9.07	1.640
Lysozyme C	P61626	16.5	9.16	9.985
Mammaglobin-B	O75556	10.9	5.78	1.745
Mucin-5Ac	P98088	585.2	7.02	0.036
Mucin-5B	Q9HC84	596	6.64	0.159
Mucin-7	Q8TAX7	39.1	8.78	0.027
Myeloperoxidase	P05164	83.8	8.97	0.291
Myosin-9	P35579	226.4	5.6	0.005
Neutrophil Defensin 1	P59665	10.2	6.99	2.489
Neutrophil Elastase	P08246	28.5	9.35	0.078
Phosphatidylinositol 3-Kinase Catalytic Subunit Type 3 (Fragment)	K7EIV6	19.9	9.54	0.261
Polymeric Immunoglobulin Receptor	P01833	83.2	5.74	0.687
Prolactin-Inducible Protein	P12273	16.6	8.05	1.262
Protein Leg1 Homolog	Q6P5S2	37.9	6.15	0.086
Protein Pof1B	Q8WVV4	68	6.32	0.033
Protein S100-A8	P05109	10.8	7.03	3.458
Protein S100-A9	P06702	13.2	6.13	0.650
Retinal Dehydrogenase 2	O94788	56.7	6.05	0.037
Secretoglobin Family 1D Member 1	O95968	9.9	9.25	0.105
Serine Protease Htra1	Q92743	51.3	7.83	0.020
Serpin B4	P48594	44.8	6.21	0.049
Serum Albumin	P02769	69.2	6.18	0.497
Serum Albumin	P02768	69.3	6.28	0.971
Skin-Specific Protein 32	Q5T750	26.2	7.97	0.253
Suprabasin	Q6UWP8	60.5	7.01	0.093
T Cell Receptor Alpha Joining 56 (Fragment)	A0A075B6Z2	2.2	10.29	3.018
Tgc Domain-Containing Protein	A0A494C0J7	78.8	6.27	0.013
Tumor Necrosis Factor	P01375	110.1	7.12	0.009
Ubiquitin-40S Ribosomal Protein S27A	P62979	18	9.64	0.058
Uteroglobin	P11684	10	5.06	0.443
Zinc-Alpha-2-Glycoprotein	P25311	34.2	6.05	0.129
Zymogen Granule Protein 16 Homolog B	Q96DA0	22.7	7.39	1.170

B.5 cOVA 30 mins NP Protein Corona

Protein Name	Ascension Code	MW (kDa)	Calculated PI	Normalized Peptide spectral count
14-3-3 Protein Beta/Alpha	P31946	28.1	4.83	0.041
14-3-3 Protein Theta	P27348	27.7	4.78	0.020
14-3-3 Protein Zeta/Delta	P63104	27.7	4.79	0.439
2-Phospho-D-Glycerate Hydro-Lyase	A0A2R8Y6G6	47.3	6.99	0.085
Actin-Related Protein 3	P61158	47.3	5.88	0.024
Actin, Cytoplasmic 1 (Fragment)	A0A2R8YFE2	8.8	9.2	3.869
Actin, Cytoplasmic 1	P60709	41.7	5.48	0.884
Actinin, Alpha 4, Isoform Cra_A	F5GXS2	104.8	5.44	0.132
Aldehyde Dehydrogenase Family 3 Member B1	P43353	51.8	7.62	0.044
Aldehyde Dehydrogenase, Dimeric Nadp-Preferring	P30838	50.4	6.54	0.136
Alpha-1-Acid Glycoprotein 1	P02763	23.5	5.02	0.073
Alpha-1-Antichymotrypsin	P01011	47.6	5.52	0.692
Alpha-2-Macroglobulin	P01023	163.2	6.46	0.304
Alpha-Amylase 1A	P0DUB6	57.7	6.93	1.452
Alpha-S1-Casein	P02662	24.5	5.02	0.189
Annexin A1	P04083	38.7	7.02	1.029
Annexin A3	P12429	36.4	5.92	0.127
Annexin A5	P08758	35.9	5.05	0.081
Annexin	H0YMW4	41.9	8.13	0.746
Anterior Gradient Protein 2 Homolog	B5MC07	21.4	8.1	0.053
Antibacterial Peptide Fall-39	J3KNB4	19.6	9.41	0.147
Antileukoproteinase	P03973	14.3	8.75	0.887
Antithrombin-Iii	P01008	52.6	6.71	0.065
Apolipoprotein A-I	P02647	30.8	5.76	1.427
Apolipoprotein B-100	P04114	515.3	7.05	0.002
Apolipoprotein D (Fragment)	C9JF17	24.1	5.6	0.023
Apolipoprotein E	P02649	36.1	5.73	0.016
Aquaporin-5	P55064	28.3	8.62	0.061
Azurocidin	P20160	26.9	9.5	0.021
Bactericidal Permeability-Increasing Protein	P17213	53.9	9.38	0.011
Basement Membrane-Specific Heparan Sulfate Proteoglycan Core Protein	P98160	468.5	6.51	0.012
Basic Salivary Proline-Rich Protein 2	P02812	40.8	11.63	0.128

Continued...

Beta-1,4-Galactosyltransferase 1	P15291	43.9	8.65	0.026
Beta-2-Microglobulin	P61769	13.7	6.52	0.210
Bpi Fold-Containing Family B Member 1	Q8TDL5	52.4	7.23	4.047
Bpi Fold-Containing Family B Member 2	Q8N4F0	49.1	8.72	0.823
Bpi Fold-Containing Family B Member 3	P59826	50.3	6.74	0.023
Bpi Fold-Containing Family B Member 4	A0A669KBJ0	75.3	5.36	0.713
C3/C5 Convertase	B4E1Z4	140.9	7.18	0.016
C4A Anaphylatoxin	A0A0G2JPR0	192.8	7.03	0.135
Calcyphosin	Q13938	30.2	6.04	0.116
Calmodulin-Like Protein 5	Q9NZT1	15.9	4.44	0.145
Carboxypeptidase	X6R8A1	56.2	6.61	0.011
Caspase-14	P31944	27.7	5.58	0.436
Catalase	P04040	59.7	7.39	0.049
Cathepsin D	C9JH19	48.6	7.84	0.059
Cathepsin G	P08311	28.8	11.19	0.061
Cathepsin Z	Q9UBR2	33.8	7.11	0.018
Cd63 Antigen	P08962	25.6	7.81	0.022
Ceruloplasmin	P00450	122.1	5.72	0.171
Chloride Intracellular Channel Protein 1	O00299	26.9	5.17	0.022
Choline Transporter-Like Protein 4	Q53GD3	79.2	8.59	0.029
Complement C1Q Subcomponent Subunit B	P02746	26.7	8.63	0.043
Complement C1Q Subcomponent Subunit C	P02747	25.8	8.41	0.068
Complement C3	P01024	187	6.4	0.977
Complement Component C7	P10643	93.5	6.48	0.006
Complement Factor H	P08603	139	6.61	0.013
Coronin-1A	P31146	51	6.68	0.011
Cystatin-C	P01034	15.8	8.75	1.281
Cystatin-S	P01036	16.2	5.02	0.746
Cystatin-Sn	P01037	16.4	7.21	0.070
Deleted In Malignant Brain Tumors 1 Protein (Fragment)	A0A590UJF8	21.6	5.27	1.660
Desmoglein-1	Q02413	113.7	5.03	0.010
Desmoplakin	P15924	331.6	6.81	0.030
E3 Ubiquitin-Protein Ligase Trim56	Q9BRZ2	81.4	7.74	0.185
Elongation Factor 1-Alpha 1	P68104	50.1	9.01	0.127
Elongation Factor 2	P13639	95.3	6.83	0.006

Continued...

Eosinophil Peroxidase	P11678	81	10.29	0.014
Extracellular Glycoprotein Lacritin	Q9GZZ8	14.2	5.5	0.367
Ezrin	E7EQR4	69.3	6.16	0.175
Fatty Acid-Binding Protein 5	Q01469	15.2	7.01	0.454
Fibrinogen Beta Chain	P02675	55.9	8.27	1.126
Fibrinogen Gamma Chain (Fragment)	C9JU00	14	7.2	2.188
Fibrinogen Gamma Chain	C9JC84	52.3	5.63	0.386
Fibromodulin	Q06828	43.2	6.04	0.014
Filaggrin	P20930	434.9	9.25	0.012
Filaggrin-2	Q5D862	247.9	8.31	0.026
Galectin-3	P17931	26.1	8.56	0.200
Galectin-3-Binding Protein	Q08380	65.3	5.27	0.336
Galectin-7	P47929	15.1	7.62	0.192
Gamma-Glutamylcyclotransferase	O75223	21	5.14	0.028
Gelsolin	P06396	85.6	6.28	0.230
Glucose-6-Phosphate 1-Dehydrogenase	P11413	59.2	6.84	0.010
Glucose-6-Phosphate Isomerase	A0A2U3TZU2	67.2	8.97	0.060
Glutathione S-Transferase P	P09211	23.3	5.64	0.325
Glyceraldehyde-3-Phosphate Dehydrogenase	P04406	36	8.46	0.321
Grancalcin	P28676	24	5.21	0.074
Haptoglobin	P00738	45.2	6.58	1.175
Heat Shock 27 Kda Protein	A0A6Q8PGK1	23.7	6.4	0.170
Heat Shock 70 Kda Protein 1B	A0A0G2JIW1	70.1	5.66	0.083
Hemoglobin Subunit Alpha	P69905	15.2	8.68	2.090
Hemoglobin Subunit Beta	P68871	16	7.28	1.080
Hemoglobin Subunit Delta	P02042	16	8.05	0.396
Hemopexin	P02790	51.6	7.02	0.034
Heparin Cofactor 2	P05546	57	6.9	0.020
Histidine-Rich Glycoprotein	P04196	59.5	7.5	0.009
Histone H2A	A0A0U1RRH7	18.5	11.52	0.405
Histone H2B	U3KQK0	18.8	10.54	0.151
Histone H3.3 (Fragment)	K7ES00	16.6	11.84	0.625
Histone H4	P62805	11.4	11.36	2.074
Hornerin	Q86YZ3	282.2	10.04	0.073
Iggfc-Binding Protein	Q9Y6R7	571.6	5.34	0.159
Immunoglobulin Heavy Constant Alpha 1	P01876	37.6	6.51	4.670
Immunoglobulin Heavy Constant Alpha 2 (Fragment)	A0A0G2JMB2	36.5	6.1	0.964

Continued...

Immunoglobulin Heavy Constant Gamma 1 (Fragment)	A0A0A0MS08	43.9	6.96	0.644
Immunoglobulin Heavy Constant Gamma 2 (Fragment)	A0A286YEY4	43.8	6.52	0.699
Immunoglobulin Heavy Constant Gamma 3 (Fragment)	A0A286YES1	49.1	6.87	0.024
Immunoglobulin Heavy Variable 1-2	P23083	13.1	9.13	0.176
Immunoglobulin Heavy Variable 1-69D	A0A0B4J2H0	12.7	8.47	0.320
Immunoglobulin Heavy Variable 3-49	A0A0A0MS15	13	8.62	0.132
Immunoglobulin Heavy Variable 3-72	A0A4W8ZXM2	11.2	7.97	1.185
Immunoglobulin Heavy Variable 3-74	A0A0B4J1X5	12.8	8.66	0.359
Immunoglobulin Heavy Variable 3/Or16-12 (Non-Functional) (Fragment)	A0A075B7B8	12.9	6.51	0.358
Immunoglobulin Heavy Variable 4-30-2	A0A087WSY4	13	9.67	0.043
Immunoglobulin Heavy Variable 4-39	P01824	13.9	9.26	0.083
Immunoglobulin Heavy Variable 5-51	A0A0C4DH38	12.7	8.27	0.273
Immunoglobulin J Chain	P01591	18.1	5.24	5.451
Immunoglobulin Kappa Constant (Fragment)	A0A5H1ZRQ3	11.7	5.87	0.198
Immunoglobulin Kappa Constant	P01834	11.8	6.52	9.895
Immunoglobulin Kappa Variable 1-17	P01599	12.8	8.68	0.090
Immunoglobulin Kappa Variable 1-33	A0A2Q2TTZ9	11.8	5.34	1.665
Immunoglobulin Kappa Variable 1-6	A0A0C4DH72	12.7	8.29	0.322
Immunoglobulin Kappa Variable 2-40	A0A087WW87	13.3	4.61	0.782
Immunoglobulin Kappa Variable 3-11	P04433	12.6	4.96	0.640
Immunoglobulin Kappa Variable 3-20	P01619	12.5	4.96	0.834
Immunoglobulin Kappa Variable 3D-7	A0A0C4DH55	13.1	5.94	0.751
Immunoglobulin Lambda Constant 2	P0DOY2	11.3	7.24	2.147
Immunoglobulin Lambda Variable 1-47	P01700	12.3	5.91	0.282
Immunoglobulin Lambda Variable 3-10	A0A075B6K4	12.4	4.83	0.139
Immunoglobulin Lambda Variable 3-21	P80748	12.4	5.29	0.745
Immunoglobulin Lambda-Like Polypeptide 5	A0A0B4J231	23.1	8.84	2.451
Integrin Alpha-M	P11215	127.1	7.23	0.005
Intelectin-1	Q8WWA0	34.9	6.01	0.463
Intelectin-2	Q8WWU7	36.2	8.28	0.271
Inter-Alpha-Trypsin Inhibitor Heavy Chain H2	P19823	106.4	6.86	0.027
Isoform 2 Of 6-Phosphogluconate Dehydrogenase, Decarboxylating	P52209	51.8	7.44	0.089
Isoform 2 Of Alpha-1-Antitrypsin	P01009	40.2	5.47	0.419

Continued...

Isoform 2 Of Bpi Fold-Containing Family A Member 1	Q9NP55	25.2	6.06	3.346
Isoform 2 Of Carboxypeptidase A4	Q9UI42	43.5	8.34	0.027
Isoform 2 Of Carcinoembryonic Antigen-Related Cell Adhesion Molecule 5	P06731	76.7	5.92	0.060
Isoform 2 Of Diencephalon/Mesencephalon Homeobox Protein 1	Q8NFW5	40.6	8.7	0.015
Isoform 2 Of Egf-Containing Fibulin-Like Extracellular Matrix Protein 1	Q12805	53.7	5.02	0.022
Isoform 2 Of Fibrinogen Alpha Chain	P02671	69.7	8.06	0.124
Isoform 2 Of Fructose-Bisphosphate Aldolase A	P04075	45.2	8.25	0.064
Isoform 2 Of Heat Shock Protein Hsp 90-Alpha	P07900	98.1	5.16	0.006
Isoform 2 Of Immunoglobulin Heavy Constant Mu	P01871	51.9	6.15	1.503
Isoform 2 Of Keratin, Type Ii Cytoskeletal 78	Q8N1N4	45	5.2	0.013
Isoform 2 Of Myosin-14	Q7Z406	231.9	5.6	0.008
Isoform 2 Of Neutral Alpha-Glucosidase Ab	Q14697	109.4	6.24	0.011
Isoform 2 Of Nucleobindin-2	P80303	50.2	5.12	0.046
Isoform 2 Of Peroxiredoxin-2	P32119	15.8	9.06	0.037
Isoform 2 Of Plastin-2	P13796	21.8	5.44	0.531
Isoform 2 Of Transketolase	P29401	68.8	7.52	0.133
Isoform 2 Of Vitamin D-Binding Protein	P02774	39.5	5.2	0.029
Isoform 3 Of Actin-Related Protein 2/3 Complex Subunit 4	P59998	21.6	8.59	0.027
Isoform 3 Of Alpha-Actinin-1	P12814	105.5	5.41	0.027
Isoform 3 Of Keratin, Type I Cytoskeletal 13	P13646	45.8	4.88	0.466
Isoform 3 Of Phospholipid Transfer Protein	P55058	44.1	6.55	0.158
Isoform 3 Of Pyruvate Kinase Pkm	P14618	56.2	8.44	0.152
Isoform 3 Of Triosephosphate Isomerase	P60174	17.9	5.58	0.065
Isoform 3 Of Tripartite Motif-Containing Protein 46	Q7Z4K8	57.4	8.69	0.182
Isoform 3 Of Vitelline Membrane Outer Layer Protein 1 Homolog	Q7Z5L0	10.8	5.83	0.585

Continued...

Isoform 3 Of Wap Four-Disulfide Core Domain Protein 2	Q14508	8.1	7.83	0.358
Isoform 35 Of Voltage-Dependent T-Type Calcium Channel Subunit Alpha-1G	O43497	248.4	7.02	0.005
Isoform 4 Of Leukotriene A-4 Hydrolase	P09960	66.8	6.7	0.043
Isoform 5 Of Clusterin	P10909	53.6	6.27	0.463
Isoform 5 Of Deleted In Malignant Brain Tumors 1 Protein	Q9UGM3	258.3	5.43	1.735
Isoform 5 Of L-Lactate Dehydrogenase A Chain	P00338	26.7	8.15	0.260
Isoform 8 Of Fibronectin	P02751	252.7	5.94	0.064
Isoform Deltalf Of Lactotransferrin	P02788	73.1	7.85	6.523
Isoform F Of Mucin-1	P15941	21.5	8.66	0.241
Itih4 Protein	B7ZKJ8	103.8	6.89	0.011
Junction Plakoglobin	P14923	81.7	6.14	0.113
Keratin, High-Sulfur Matrix Protein, Iiia3	P02441	14.2	8.12	0.163
Keratin, Type I Cuticular Ha1	Q15323	47.2	4.88	0.452
Keratin, Type I Cuticular Ha3-I	O76009	45.9	4.82	1.752
Keratin, Type I Cuticular Ha3-Ii	Q14525	46.2	4.84	0.012
Keratin, Type I Cuticular Ha4	A0A140TA69	49.4	5.06	0.257
Keratin, Type I Cytoskeletal 10	P13645	58.8	5.21	4.646
Keratin, Type I Cytoskeletal 12	Q99456	53.5	4.78	0.022
Keratin, Type I Cytoskeletal 14	P02533	51.5	5.16	2.962
Keratin, Type I Cytoskeletal 16	P08779	51.2	5.05	0.666
Keratin, Type I Cytoskeletal 17	Q04695	48.1	5.02	0.145
Keratin, Type I Cytoskeletal 19	P08727	44.1	5.14	1.375
Keratin, Type I Cytoskeletal 9	P35527	62	5.24	3.942
Keratin, Type Ii Cuticular Hb1	Q14533	54.9	5.47	0.504
Keratin, Type Ii Cuticular Hb2	Q9NSB4	56.6	6.74	0.020
Keratin, Type Ii Cuticular Hb3	P78385	54.2	5.64	0.085
Keratin, Type Ii Cuticular Hb5	P78386	55.8	6.55	0.341
Keratin, Type Ii Cuticular Hb6	O43790	53.5	5.66	0.139
Keratin, Type Ii Cytoskeletal 1	P04264	66	8.12	4.192
Keratin, Type Ii Cytoskeletal 1B	Q7Z794	61.9	5.99	0.457
Keratin, Type Ii Cytoskeletal 2 Epidermal	P35908	65.4	8	3.116
Keratin, Type Ii Cytoskeletal 4	P19013	56.1	6.61	0.062
Keratin, Type Ii Cytoskeletal 5	P13647	62.3	7.74	1.011
Keratin, Type Ii Cytoskeletal 6A	P02538	60	8	0.557

Continued...

Keratin, Type Ii Cytoskeletal 6B	P04259	60	8	0.839
Keratin, Type Ii Cytoskeletal 7	P08729	51.4	5.48	0.573
Keratin, Type Ii Cytoskeletal 71	Q3SY84	57.3	6.61	0.010
Keratin, Type Ii Cytoskeletal 8	P05787	53.7	5.59	0.032
Keratin, Type Ii Microfibrillar, Component 7C	P15241	53.6	5.57	0.485
Keratinocyte Proline-Rich Protein	Q5T749	64.1	8.27	0.009
Kinesin-Like Protein	A0A1W2PPS5	71.1	8.85	0.008
Lactoperoxidase	P22079	80.2	8.62	0.065
Leukocyte Elastase Inhibitor	P30740	42.7	6.28	0.176
Lipocalin-1	P31025	19.2	5.58	2.222
Lipocalin-15	Q6UWW0	20.4	4.94	0.937
Lysozyme C	P61626	16.5	9.16	2.033
Mammaglobin-B	O75556	10.9	5.78	0.584
Matrix Metalloproteinase-9	P14780	78.4	6.06	0.029
Metalloproteinase Inhibitor 1	P01033	23.2	8.1	0.024
Moesin	P26038	67.8	6.4	0.119
Monocyte Differentiation Antigen Cd14	P08571	40.1	6.23	0.072
Mucin-2	A0A0G2JR65	303.2	5.88	0.006
Mucin-2	Q02817	540	5.8	0.013
Mucin-5Ac	P98088	585.2	7.02	0.371
Mucin-5B	Q9HC84	596	6.64	0.549
Mucin-7	Q8TAX7	39.1	8.78	0.133
Myeloid Cell Nuclear Differentiation Antigen	P41218	45.8	9.76	0.038
Myeloperoxidase	P05164	83.8	8.97	0.649
Myosin Regulatory Light Chain 12A	J3QRS3	20.4	4.75	0.028
Myosin-9	P35579	226.4	5.6	0.039
Neutrophil Collagenase	P22894	53.4	6.87	0.011
Neutrophil Defensin 1	P59665	10.2	6.99	1.243
Neutrophil Elastase	P08246	28.5	9.35	0.081
Neutrophil Gelatinase-Associated Lipocalin	X6R8F3	22.8	8.5	0.329
Olfactory Receptor 6N2	Q8NGY6	35.7	8.82	0.080
Opiorphin Prepropeptide	Q99935	27.2	10.42	0.127
Peroxiredoxin-1	Q06830	22.1	8.13	0.131
Peroxiredoxin-6	P30041	25	6.38	0.070
Phosphatidylinositol 3-Kinase Catalytic Subunit Type 3 (Fragment)	K7EIV6	19.9	9.54	0.406
Phosphoglycerate Mutase 1	P18669	28.8	7.18	0.020
Pi-Plc X Domain-Containing Protein 1	Q9NUJ7	36.6	6.58	0.191

Continued...

Pigment Epithelium-Derived Factor	P36955	46.3	6.38	0.062
Plasma Protease C1 Inhibitor	E9PGN7	59.5	6.76	0.049
Polymeric Immunoglobulin Receptor	P01833	83.2	5.74	2.833
Prelamin-A/C	A0A6Q8PFJ0	80.9	8.27	0.022
Probable Non-Functional Immunoglobulin Kappa Variable 2D-24	A0A075B6R9	13.1	8.87	0.529
Profilin-1	P07737	15	8.27	0.039
Prolactin-Inducible Protein	P12273	16.6	8.05	1.949
Proline-Rich Protein 4	A0A0J9YXF8	16.9	7.52	0.170
Prominin-1	O43490	97.1	7.27	0.071
Prostate Stem Cell Antigen	O43653	12	4.94	0.385
Protein Disulfide-Isomerase	P07237	57.1	4.87	0.020
Protein Leg1 Homolog	Q6P5S2	37.9	6.15	0.822
Protein Mal2	Q969L2	19.1	6.24	0.060
Protein S100-A4	P26447	11.7	6.11	0.099
Protein S100-A6	P06703	10.2	5.48	0.282
Protein S100-A7	P31151	11.5	6.77	0.500
Protein S100-A8	P05109	10.8	7.03	6.044
Protein S100-A9	P06702	13.2	6.13	3.286
Protein S100-P	P25815	10.4	4.88	0.168
Protein-Arginine Deiminase Type-4	Q9UM07	74	6.58	0.016
Ras Gtpase-Activating-Like Protein Iqgap1	P46940	189.1	6.48	0.006
Ras-Related Protein Rab-10	P61026	22.5	8.38	0.051
Retinal Dehydrogenase 1	P00352	54.8	6.73	0.031
Retinoic Acid Receptor Responder Protein 1	P49788	33.3	8.51	0.244
Retinol-Binding Protein 4	P02753	23	6.07	0.050
Rho Guanine Nucleotide Exchange Factor 17	Q96PE2	221.5	6.29	0.018
Secretoglobin Family 1D Member 1	O95968	9.9	9.25	0.350
Secretoglobin Family 1D Member 2	O95969	9.9	8.25	0.410
Serine Protease Htra1	Q92743	51.3	7.83	0.158
Serpin B3	P29508	44.5	6.81	0.469
Serpin B4	P48594	44.8	6.21	0.271
Serum Albumin	P02769	69.2	6.18	1.042
Serum Albumin	P02768	69.3	6.28	4.697
Sialic Acid-Binding Ig-Like Lectin 16	A6NMB1	53	9.03	0.207
Skin-Specific Protein 32	Q5T750	26.2	7.97	0.045
Small Integral Membrane Protein 22	A0A4V7I672	14.6	6.52	0.158

Continued...

Submaxillary Gland Androgen-Regulated Protein 3A	Q99954	14	9.57	0.040
Sulfhydryl Oxidase 1	O00391	82.5	8.92	0.195
Suprabasin	Q6UWP8	60.5	7.01	0.047
Synaptophysin-Like Protein 1	Q16563	28.5	8.43	0.081
T Cell Receptor Alpha Joining 56 (Fragment)	A0A075B6Z2	2.2	10.29	8.378
Tetraspanin-1	O60635	26.3	5.25	0.176
Tgc Domain-Containing Protein	A0A494C0J7	78.8	6.27	0.015
Thrombospondin-1	P07996	129.3	4.94	0.045
Transcobalamin-1	P20061	48.2	5.03	0.156
Transthyretin	P02766	15.9	5.76	0.363
Tropomyosin Alpha-3 Chain	P06753	32.9	4.72	0.070
Tubulin Beta-4B Chain	P68371	49.8	4.89	0.081
Tumor Necrosis Factor	P01375	110.1	7.12	0.205
Ubiquitin-40S Ribosomal Protein S27A	P62979	18	9.64	0.288
Vimentin	P08670	53.6	5.12	0.011
Vitronectin	P04004	54.3	5.8	0.032
Wd Repeat-Containing Protein 1	O75083	66.2	6.65	0.017
Zinc-Alpha-2-Glycoprotein	P25311	34.2	6.05	1.658
Zymogen Granule Protein 16 Homolog B	Q96DA0	22.7	7.39	1.147

B.6 cOVA 4.0 hours NP Protein Corona

Protein Name	Ascension Code	MW (kDa)	Calculated PI	Normalized Peptide spectral count
14-3-3 Protein Beta/Alpha	P31946	28.1	4.83	0.192
14-3-3 Protein Zeta/Delta	P63104	27.7	4.79	0.494
2-Phospho-D-Glycerate Hydro-Lyase	A0A2R8Y6G6	47.3	6.99	0.218
Actin-Related Protein 3	P61158	47.3	5.88	0.041
Actin, Alpha Cardiac Muscle 1	P68032	42	5.39	0.070
Actin, Cytoplasmic 1 (Fragment)	A0A2R8YFE2	8.8	9.2	3.500
Actin, Cytoplasmic 1	P60709	41.7	5.48	1.114
Actinin, Alpha 4, Isoform Cra_A	F5GXS2	104.8	5.44	0.192

Continued...

Adenylyl Cyclase-Associated Protein 1	Q01518	51.9	8.06	0.009
Aldehyde Dehydrogenase Family 3 Member B1	P43353	51.8	7.62	0.076
Aldehyde Dehydrogenase, Dimeric Nadp-Preferring	P30838	50.4	6.54	0.165
Aldo-Keto Reductase Family 1 Member C3	A0A0A0MSS8	36.8	7.94	0.013
Alpha-1-Acid Glycoprotein 1	P02763	23.5	5.02	0.271
Alpha-1-Antichymotrypsin	P01011	47.6	5.52	0.822
Alpha-2-Hs-Glycoprotein	C9JV77	39.4	5.72	0.012
Alpha-2-Macroglobulin	P01023	163.2	6.46	0.507
Alpha-Amylase 1A	P0DUB6	57.7	6.93	1.779
Alpha-N-Acetylglucosaminidase	P54802	82.2	6.65	0.006
Alpha-S1-Casein	P02662	24.5	5.02	0.280
Aminopeptidase N	P15144	109.5	5.48	0.022
Angiotensinogen	P01019	53.1	6.32	0.018
Annexin A1	P04083	38.7	7.02	1.288
Annexin A11	P50995	54.4	7.65	0.027
Annexin A3	P12429	36.4	5.92	0.618
Annexin A5	P08758	35.9	5.05	0.313
Annexin A6	P08133	75.8	5.6	0.019
Annexin A7	P20073	52.7	5.68	0.009
Annexin	H0YMW4	41.9	8.13	1.132
Anterior Gradient Protein 2 Homolog	B5MC07	21.4	8.1	0.136
Antibacterial Peptide Fall-39	J3KNB4	19.6	9.41	0.200
Antileukoproteinase	P03973	14.3	8.75	0.890
Antithrombin-Iii	P01008	52.6	6.71	0.093
Apolipoprotein A-I	P02647	30.8	5.76	1.684
Apolipoprotein A-Ii	V9GYM3	14.9	8.27	0.098
Apolipoprotein A-Iv	P06727	45.3	5.38	0.033
Apolipoprotein B-100	P04114	515.3	7.05	0.031
Apolipoprotein D (Fragment)	C9JF17	24.1	5.6	0.082
Apolipoprotein E	P02649	36.1	5.73	0.054
Aquaporin-5	P55064	28.3	8.62	0.190
Azurocidin	P20160	26.9	9.5	0.219
Bactericidal Permeability-Increasing Protein	P17213	53.9	9.38	0.054
Basement Membrane-Specific Heparan Sulfate Proteoglycan Core Protein	P98160	468.5	6.51	0.038
Basic Salivary Proline-Rich Protein 1	G3V1M9	32.4	11.21	0.030
Basic Salivary Proline-Rich Protein 2	P02812	40.8	11.63	0.108

Continued...

Beta-1,3-Galactosyl-O-Glycosyl-Glycoprotein Beta-1,6-N-Acetylglucosaminyltransferase 3	O95395	50.8	8.25	0.039
Beta-1,4-Galactosyltransferase 1	P15291	43.9	8.65	0.022
Beta-2-Microglobulin	P61769	13.7	6.52	0.358
Beta-Hexosaminidase	H3BP20	62	5.21	0.008
Beta-Hexosaminidase Subunit Beta	P07686	63.1	6.76	0.008
Bpi Fold-Containing Family B Member 1	Q8TDL5	52.4	7.23	5.857
Bpi Fold-Containing Family B Member 2	Q8N4F0	49.1	8.72	0.966
Bpi Fold-Containing Family B Member 3	P59826	50.3	6.74	0.165
Bpi Fold-Containing Family B Member 4	A0A669KBJ0	75.3	5.36	0.831
Brain Acid Soluble Protein 1	P80723	22.7	4.63	0.022
Bri3-Binding Protein	A0A5F9ZHY7	31.4	10.32	0.015
C3/C5 Convertase	B4E1Z4	140.9	7.18	0.031
C4A Anaphylatoxin	A0A0G2JPR0	192.8	7.03	0.185
Calcyphosin	Q13938	30.2	6.04	0.210
Calmodulin-3	P0DP25	16.8	4.22	0.087
Calmodulin-Like Protein 3	P27482	16.9	4.42	0.087
Calmodulin-Like Protein 5	Q9NZT1	15.9	4.44	0.309
Calpain-1 Catalytic Subunit	P07384	81.8	5.67	0.006
Calreticulin	P27797	48.1	4.44	0.020
Carcinoembryonic Antigen-Related Cell Adhesion Molecule 6	P40199	37.2	5.82	0.013
Caspase-14	P31944	27.7	5.58	0.282
Catalase	P04040	59.7	7.39	0.148
Cathepsin B	E9PHZ5	41.3	6.58	0.012
Cathepsin D	C9JH19	48.6	7.84	0.141
Cathepsin G	P08311	28.8	11.19	0.102
Cathepsin Z	Q9UBR2	33.8	7.11	0.073
Cd5 Antigen-Like	O43866	38.1	5.47	0.013
Cd59 Glycoprotein	P13987	14.2	6.48	0.275
Cd9 Antigen	F5GXT1	29.9	7.52	0.049
Cell Division Control Protein 42 Homolog	P60953	21.2	6.55	0.023
Ceruloplasmin	P00450	122.1	5.72	0.324
Chloride Intracellular Channel Protein 1	O00299	26.9	5.17	0.036
Choline Transporter-Like Protein 4	Q53GD3	79.2	8.59	0.019

Continued...

Clathrin Heavy Chain	A0A087WVQ6	191.9	5.69	0.003
Coagulation Factor V	A0A0A0MRJ7	252.1	6.05	0.016
Cofilin, Non-Muscle Isoform	E9PK25	22.7	8.34	0.043
Complement C1Q Subcomponent Subunit B	P02746	26.7	8.63	0.055
Complement C1Q Subcomponent Subunit C	P02747	25.8	8.41	0.076
Complement C3	P01024	187	6.4	1.240
Complement Factor H	P08603	139	6.61	0.011
Coronin-1A	P31146	51	6.68	0.058
Cystatin-C	P01034	15.8	8.75	0.867
Cystatin-S	P01036	16.2	5.02	1.419
Cystatin-Sn	P01037	16.4	7.21	0.119
Cysteine-Rich Secretory Protein 3	J3KPA1	31	7.61	0.016
Deleted In Malignant Brain Tumors 1 Protein (Fragment)	A0A590UJF8	21.6	5.27	1.491
Delta(14)-Sterol Reductase Lbr	Q14739	70.7	9.36	0.007
Desmocollin-1	Q08554	99.9	5.43	0.005
Desmoglein-1	Q02413	113.7	5.03	0.022
Desmoplakin	P15924	331.6	6.81	0.007
Dnaj Homolog Subfamily C Member 3	Q13217	57.5	6.15	0.026
Dnaj Homolog Subfamily C Member 5	Q9H3Z4	22.1	5.07	0.022
E3 Ubiquitin-Protein Ligase Trim56	Q9BRZ2	81.4	7.74	0.102
Elongation Factor 1-Alpha 1	P68104	50.1	9.01	0.108
Elongation Factor 2	P13639	95.3	6.83	0.005
Extracellular Glycoprotein Lacritin	Q9GZZ8	14.2	5.5	0.827
Ezrin	E7EQR4	69.3	6.16	0.219
Fatty Acid-Binding Protein 5	Q01469	15.2	7.01	0.577
Fibrinogen Beta Chain	P02675	55.9	8.27	1.460
Fibrinogen Gamma Chain (Fragment)	C9JU00	14	7.2	2.690
Fibrinogen Gamma Chain	C9JC84	52.3	5.63	0.505
Fibromodulin	Q06828	43.2	6.04	0.023
Filaggrin	P20930	434.9	9.25	0.006
Filaggrin-2	Q5D862	247.9	8.31	0.012
G-Protein Coupled Receptor Family C Group 5 Member B	Q9NZH0	44.8	8.24	0.011
Galectin-3	P17931	26.1	8.56	0.169
Galectin-3-Binding Protein	Q08380	65.3	5.27	0.390
Galectin-7	P47929	15.1	7.62	0.032
Gamma-Glutamylcyclotransferase	O75223	21	5.14	0.047
Gelsolin	P06396	85.6	6.28	0.366

Continued...

Glucose-6-Phosphate Isomerase	A0A2U3TZU2	67.2	8.97	0.124
Glutathione S-Transferase P	P09211	23.3	5.64	0.525
Glyceraldehyde-3-Phosphate Dehydrogenase	P04406	36	8.46	0.285
Glycogen Phosphorylase, Liver Form	P06737	97.1	7.17	0.015
Grancalcin	P28676	24	5.21	0.204
Haptoglobin	P00738	45.2	6.58	1.666
Heat Shock 27 Kda Protein	A0A6Q8PGK1	23.7	6.4	0.187
Heat Shock 70 Kda Protein 1B	A0A0G2JIW1	70.1	5.66	0.147
Heat Shock Cognate 71 Kda Protein	P11142	70.9	5.52	0.021
Heat Shock Protein Hsp 90-Beta	P08238	83.2	5.03	0.006
Hemoglobin Subunit Alpha	P69905	15.2	8.68	2.188
Hemoglobin Subunit Beta	P68871	16	7.28	1.559
Hemoglobin Subunit Delta	P02042	16	8.05	0.795
Hemopexin	P02790	51.6	7.02	0.114
Heparin Cofactor 2	P05546	57	6.9	0.034
Histidine-Rich Glycoprotein	P04196	59.5	7.5	0.008
Histone H2A	A0A0U1RRH7	18.5	11.52	0.847
Histone H2B	U3KQK0	18.8	10.54	0.207
Histone H3.3 (Fragment)	K7ES00	16.6	11.84	0.500
Histone H4	P62805	11.4	11.36	2.101
Hornerin	Q86YZ3	282.2	10.04	0.038
Ig-Like Domain-Containing Protein (Fragment)	A0A0J9YY99	13	8.92	0.112
Iggfc-Binding Protein	Q9Y6R7	571.6	5.34	0.263
Immunoglobulin Heavy Constant Alpha 1	P01876	37.6	6.51	4.538
Immunoglobulin Heavy Constant Alpha 2 (Fragment)	A0A0G2JMB2	36.5	6.1	0.910
Immunoglobulin Heavy Constant Gamma 1 (Fragment)	A0A0A0MS08	43.9	6.96	0.869
Immunoglobulin Heavy Constant Gamma 2 (Fragment)	A0A286YEY4	43.8	6.52	0.782
Immunoglobulin Heavy Constant Gamma 3 (Fragment)	A0A286YES1	49.1	6.87	0.060
Immunoglobulin Heavy Variable 1-2	P23083	13.1	9.13	0.261
Immunoglobulin Heavy Variable 1-69D	A0A0B4J2H0	12.7	8.47	0.385
Immunoglobulin Heavy Variable 1/Or15-1 (Non-Functional) (Fragment)	A0A075B7D0	13	9.13	0.037
Immunoglobulin Heavy Variable 3-49	A0A0A0MS15	13	8.62	0.264
Immunoglobulin Heavy Variable 3-72	A0A4W8ZXM2	11.2	7.97	1.530

Continued...

Immunoglobulin Heavy Variable 3-74	A0A0B4J1X5	12.8	8.66	0.343
Immunoglobulin Heavy Variable 3/Or16-12 (Non-Functional) (Fragment)	A0A075B7B8	12.9	6.51	0.303
Immunoglobulin Heavy Variable 4-30-2	A0A087WSY4	13	9.67	0.152
Immunoglobulin Heavy Variable 4-39	P01824	13.9	9.26	0.070
Immunoglobulin Heavy Variable 5-51	A0A0C4DH38	12.7	8.27	0.231
Immunoglobulin Heavy Variable 6-1	A0A0B4J1U7	13.5	9.2	0.110
Immunoglobulin J Chain	P01591	18.1	5.24	4.861
Immunoglobulin Kappa Constant (Fragment)	A0A5H1ZRQ3	11.7	5.87	0.251
Immunoglobulin Kappa Constant	P01834	11.8	6.52	8.613
Immunoglobulin Kappa Variable 1-17	P01599	12.8	8.68	0.306
Immunoglobulin Kappa Variable 1-33	A0A2Q2TTZ9	11.8	5.34	1.698
Immunoglobulin Kappa Variable 1-6	A0A0C4DH72	12.7	8.29	0.153
Immunoglobulin Kappa Variable 2-40	A0A087WW87	13.3	4.61	0.698
Immunoglobulin Kappa Variable 2D-28	A0A5H1ZRS2	11	5.24	0.178
Immunoglobulin Kappa Variable 3-11	P04433	12.6	4.96	0.583
Immunoglobulin Kappa Variable 3-20	P01619	12.5	4.96	0.821
Immunoglobulin Kappa Variable 3D-20	A0A0C4DH25	12.5	4.59	0.235
Immunoglobulin Kappa Variable 3D-7	A0A0C4DH55	13.1	5.94	0.747
Immunoglobulin Lambda Constant 2	P0DOY2	11.3	7.24	2.077
Immunoglobulin Lambda Variable 1-47	P01700	12.3	5.91	0.398
Immunoglobulin Lambda Variable 3-10	A0A075B6K4	12.4	4.83	0.198
Immunoglobulin Lambda Variable 3-21	P80748	12.4	5.29	0.670
Immunoglobulin Lambda Variable 9-49	A0A0B4J1Y8	13	7.28	0.037
Immunoglobulin Lambda-Like Polypeptide 5	A0A0B4J231	23.1	8.84	2.244
Integrin Alpha-M	P11215	127.1	7.23	0.023
Integrin Beta	A0A494C0X7	84.7	6.98	0.035
Intelectin-1	Q8WWA0	34.9	6.01	0.630
Intelectin-2	Q8WWU7	36.2	8.28	0.338
Inter-Alpha-Trypsin Inhibitor Heavy Chain H2	P19823	106.4	6.86	0.064
Isocitrate Dehydrogenase [Nadp] Cytoplasmic	O75874	46.6	7.01	0.021

Continued...

Isoform 2 Of 6-Phosphogluconate Dehydrogenase, Decarboxylating	P52209	51.8	7.44	0.180
Isoform 2 Of Alpha-1-Antitrypsin	P01009	40.2	5.47	0.986
Isoform 2 Of Bpi Fold-Containing Family A Member 1	Q9NP55	25.2	6.06	5.296
Isoform 2 Of Calcium And Integrin-Binding Protein 1	Q99828	26	4.86	0.038
Isoform 2 Of Carboxypeptidase A4	Q9UI42	43.5	8.34	0.045
Isoform 2 Of Carcinoembryonic Antigen-Related Cell Adhesion Molecule 5	P06731	76.7	5.92	0.089
Isoform 2 Of Diencephalon/Mesencephalon Homeobox Protein 1	Q8NFW5	40.6	8.7	0.024
Isoform 2 Of Egf-Containing Fibulin-Like Extracellular Matrix Protein 1	Q12805	53.7	5.02	0.027
Isoform 2 Of Fibrinogen Alpha Chain	P02671	69.7	8.06	0.161
Isoform 2 Of Filamin-A	P21333	279.8	6.05	0.003
Isoform 2 Of Fructose-Bisphosphate Aldolase A	P04075	45.2	8.25	0.043
Isoform 2 Of Guanine Nucleotide-Binding Protein G(I)/G(S)/G(T) Subunit Beta-3	P16520	32.6	6.42	0.030
Isoform 2 Of Heat Shock Protein Hsp 90-Alpha	P07900	98.1	5.16	0.030
Isoform 2 Of Immunoglobulin Heavy Constant Mu	P01871	51.9	6.15	1.620
Isoform 2 Of Myosin-14	Q7Z406	231.9	5.6	0.015
Isoform 2 Of Neutral Alpha-Glucosidase Ab	Q14697	109.4	6.24	0.018
Isoform 2 Of Nitric Oxide Synthase, Inducible	P35228	126.7	7.96	0.016
Isoform 2 Of Nucleobindin-2	P80303	50.2	5.12	0.049
Isoform 2 Of Peroxiredoxin-2	P32119	15.8	9.06	0.031
Isoform 2 Of Plastin-2	P13796	21.8	5.44	1.034
Isoform 2 Of Poly(Rc)-Binding Protein 3	P57721	36.8	7.2	0.027
Isoform 2 Of Ras-Related Protein Rab-1A	P62820	15.3	8.13	0.032
Isoform 2 Of Sodium/Glucose Cotransporter 1	P13866	60.1	7.49	0.041
Isoform 2 Of Solute Carrier Family 2, Facilitated Glucose Transporter Member 14	Q8TDB8	54	7.52	0.009

Continued...

Isoform 2 Of Thioredoxin	P10599	9.4	6.04	0.155
Isoform 2 Of Transketolase	P29401	68.8	7.52	0.185
Isoform 2 Of Vitamin D-Binding Protein	P02774	39.5	5.2	0.061
Isoform 3 Of Actin-Related Protein 2/3 Complex Subunit 4	P59998	21.6	8.59	0.091
Isoform 3 Of Alpha-Actinin-1	P12814	105.5	5.41	0.074
Isoform 3 Of Carbonic Anhydrase 6	P23280	28.7	6.93	0.034
Isoform 3 Of Guanine Nucleotide-Binding Protein G(I) Subunit Alpha-2	P04899	36.4	5.59	0.040
Isoform 3 Of Keratin, Type I Cytoskeletal 13	P13646	45.8	4.88	0.374
Isoform 3 Of Mesothelin	Q13421	71.4	7.36	0.069
Isoform 3 Of Peroxiredoxin-5, Mitochondrial	P30044	17.4	8.94	0.056
Isoform 3 Of Phospholipid Transfer Protein	P55058	44.1	6.55	0.499
Isoform 3 Of Pyruvate Kinase Pkm	P14618	56.2	8.44	0.261
Isoform 3 Of Triosephosphate Isomerase	P60174	17.9	5.58	0.055
Isoform 3 Of Tripartite Motif-Containing Protein 46	Q7Z4K8	57.4	8.69	0.051
Isoform 3 Of Vitelline Membrane Outer Layer Protein 1 Homolog	Q7Z5L0	10.8	5.83	0.997
Isoform 3 Of Wap Four-Disulfide Core Domain Protein 2	Q14508	8.1	7.83	0.784
Isoform 4 Of Biotinidase	P43251	58.9	5.85	0.008
Isoform 4 Of Leukotriene A-4 Hydrolase	P09960	66.8	6.7	0.044
Isoform 5 Of Clusterin	P10909	53.6	6.27	0.502
Isoform 5 Of Deleted In Malignant Brain Tumors 1 Protein	Q9UGM3	258.3	5.43	1.787
Isoform 5 Of L-Lactate Dehydrogenase A Chain	P00338	26.7	8.15	0.202
Isoform 8 Of Fibronectin	P02751	252.7	5.94	0.118
Isoform Deltalf Of Lactotransferrin	P02788	73.1	7.85	6.655
Isoform F Of Mucin-1	P15941	21.5	8.66	0.432
Itih4 Protein	B7ZKJ8	103.8	6.89	0.019
Junction Plakoglobin	P14923	81.7	6.14	0.012
Keratin, Type I Cuticular Ha3-I	O76009	45.9	4.82	0.053
Keratin, Type I Cytoskeletal 10	P13645	58.8	5.21	1.995
Keratin, Type I Cytoskeletal 12	Q99456	53.5	4.78	0.027
Keratin, Type I Cytoskeletal 14	P02533	51.5	5.16	1.880

Continued...

Keratin, Type I Cytoskeletal 16	P08779	51.2	5.05	0.296
Keratin, Type I Cytoskeletal 17	Q04695	48.1	5.02	0.081
Keratin, Type I Cytoskeletal 19	P08727	44.1	5.14	1.609
Keratin, Type I Cytoskeletal 9	P35527	62	5.24	2.555
Keratin, Type Ii Cytoskeletal 1	P04264	66	8.12	2.355
Keratin, Type Ii Cytoskeletal 1B	Q7Z794	61.9	5.99	0.261
Keratin, Type Ii Cytoskeletal 2 Epidermal	P35908	65.4	8	1.398
Keratin, Type Ii Cytoskeletal 4	P19013	56.1	6.61	0.078
Keratin, Type Ii Cytoskeletal 5	P13647	62.3	7.74	0.667
Keratin, Type Ii Cytoskeletal 6A	P02538	60	8	0.285
Keratin, Type Ii Cytoskeletal 6B	P04259	60	8	0.612
Keratin, Type Ii Cytoskeletal 7	P08729	51.4	5.48	0.314
Keratin, Type Ii Cytoskeletal 8	P05787	53.7	5.59	0.100
Kinesin-Like Protein	A0A1W2PPS5	71.1	8.85	0.021
Lactoperoxidase	P22079	80.2	8.62	0.183
Leukocyte Elastase Inhibitor	P30740	42.7	6.28	0.333
Lipocalin-1	P31025	19.2	5.58	2.544
Lipocalin-15	Q6UWW0	20.4	4.94	1.224
Lipopolysaccharide-Binding Protein	P18428	53.4	6.7	0.009
Lysozyme C	P61626	16.5	9.16	2.489
Mammaglobin-B	O75556	10.9	5.78	0.583
Mast Cell-Expressed Membrane Protein 1	Q8IX19	21.2	8.87	0.023
Matrix Metalloproteinase-9	P14780	78.4	6.06	0.063
Metalloproteinase Inhibitor 1	P01033	23.2	8.1	0.063
Moesin	P26038	67.8	6.4	0.166
Monocyte Differentiation Antigen Cd14	P08571	40.1	6.23	0.244
Mucin-16	Q8WXI7	1518.2	5.26	0.002
Mucin-2	A0A0G2JR65	303.2	5.88	0.006
Mucin-2	Q02817	540	5.8	0.059
Mucin-4	A0A0G2JS65	734.2	5.24	0.001
Mucin-5Ac	P98088	585.2	7.02	0.431
Mucin-5B	Q9HC84	596	6.64	0.526
Mucin-7	Q8TAX7	39.1	8.78	0.063
Myeloblastin	P24158	27.8	8.35	0.212
Myeloid Cell Nuclear Differentiation Antigen	P41218	45.8	9.76	0.086
Myeloperoxidase	P05164	83.8	8.97	1.016
Myosin Regulatory Light Chain 12A	J3QRS3	20.4	4.75	0.096

Continued...

Myosin-9	P35579	226.4	5.6	0.078
Neutrophil Defensin 1	P59665	10.2	6.99	0.910
Neutrophil Elastase	P08246	28.5	9.35	0.275
Neutrophil Gelatinase-Associated Lipocalin	X6R8F3	22.8	8.5	0.343
Nicotinamide Phosphoribosyltransferase	P43490	55.5	7.15	0.062
Nucleobindin-1	Q02818	53.8	5.25	0.036
Olfactory Receptor 6N2	Q8NGY6	35.7	8.82	0.041
Opiorphin Prepropeptide	Q99935	27.2	10.42	0.144
Peptidyl-Prolyl Cis-Trans Isomerase A	P62937	18	7.81	0.191
Peptidyl-Prolyl Cis-Trans Isomerase B	P23284	23.7	9.41	0.041
Peroxiredoxin-1	Q06830	22.1	8.13	0.199
Peroxiredoxin-6	P30041	25	6.38	0.078
Phosphatidylinositol 3-Kinase Catalytic Subunit Type 3 (Fragment)	K7EIV6	19.9	9.54	0.319
Phosphoglycerate Kinase 1	P00558	44.6	8.1	0.011
Phosphoglycerate Mutase 1	P18669	28.8	7.18	0.017
Pi-Plc X Domain-Containing Protein 1	Q9NUJ7	36.6	6.58	0.214
Pigment Epithelium-Derived Factor	P36955	46.3	6.38	0.243
Plasma Protease C1 Inhibitor	E9PGN7	59.5	6.76	0.082
Plasminogen	P00747	90.5	7.24	0.016
Polymeric Immunoglobulin Receptor	P01833	83.2	5.74	2.656
Polyunsaturated Fatty Acid Lipoxygenase Alox15	P16050	74.8	6.58	0.006
Prelamin-A/C	A0A6Q8PFJ0	80.9	8.27	0.012
Probable Non-Functional Immunoglobulin Heavy Variable 3-38	A0A0C4DH36	12.8	9.25	0.038
Probable Non-Functional Immunoglobulin Kappa Variable 2D-24	A0A075B6R9	13.1	8.87	0.261
Profilin-1	P07737	15	8.27	0.228
Programmed Cell Death Protein 6	O75340	21.9	5.4	0.023
Prolactin-Inducible Protein	P12273	16.6	8.05	2.034
Proline-Rich Protein 4	A0A0J9YXF8	16.9	7.52	0.145
Prominin-1	O43490	97.1	7.27	0.126
Prosaposin	C9JIZ6	58.4	5.17	0.008
Prostate Stem Cell Antigen	O43653	12	4.94	0.408
Protein Disulfide-Isomerase	P07237	57.1	4.87	0.034
Protein Leg1 Homolog	Q6P5S2	37.9	6.15	1.380
Protein Mal2	Q969L2	19.1	6.24	0.154
Protein S100-A14	Q9HCY8	11.7	5.24	0.041

Continued...

Protein S100-A4	P26447	11.7	6.11	0.251
Protein S100-A6	P06703	10.2	5.48	0.431
Protein S100-A7	P31151	11.5	6.77	0.553
Protein S100-A8	P05109	10.8	7.03	6.071
Protein S100-A9	P06702	13.2	6.13	3.525
Protein S100-P	P25815	10.4	4.88	0.234
Protein-Arginine Deiminase Type-4	Q9UM07	74	6.58	0.060
Ras Gtpase-Activating-Like Protein Iqgap1	P46940	189.1	6.48	0.010
Ras-Related C3 Botulinum Toxin Substrate 2	P15153	21.4	7.61	0.092
Ras-Related Protein Rab-10	P61026	22.5	8.38	0.065
Retinal Dehydrogenase 1	P00352	54.8	6.73	0.170
Retinoic Acid Receptor Responder Protein 1	P49788	33.3	8.51	0.264
Retinoic Acid-Induced Protein 3	Q8NFJ5	40.2	8.15	0.012
Retinol-Binding Protein 4	P02753	23	6.07	0.128
Rho Gdp-Dissociation Inhibitor 1	J3QQX2	25.8	7.44	0.019
Rho Gdp-Dissociation Inhibitor 2	P52566	23	5.21	0.043
Rho Guanine Nucleotide Exchange Factor 17	Q96PE2	221.5	6.29	0.009
Secretoglobin Family 1D Member 1	O95968	9.9	9.25	0.248
Secretoglobin Family 1D Member 2	O95969	9.9	8.25	0.643
Serine Protease Htra1	Q92743	51.3	7.83	0.171
Serine/Threonine-Protein Phosphatase Pp1-Alpha Catalytic Subunit	P62136	37.5	6.33	0.013
Serpin B3	P29508	44.5	6.81	0.682
Serpin B4	P48594	44.8	6.21	0.513
Serum Albumin	P02769	69.2	6.18	0.891
Serum Albumin	P02768	69.3	6.28	4.225
Sh3 Domain-Binding Glutamic Acid-Rich-Like Protein 3	Q9H299	10.4	4.93	0.046
Sialic Acid-Binding Ig-Like Lectin 16	A6NMB1	53	9.03	0.194
Small Integral Membrane Protein 22	A0A4V7I672	14.6	6.52	0.268
Sodium-Coupled Monocarboxylate Transporter 1	Q8N695	66.5	7.75	0.007
Stomatin	P27105	31.7	7.88	0.031
Stromelysin-2	P09238	54.1	5.8	0.045
Submaxillary Gland Androgen-Regulated Protein 3A	Q99954	14	9.57	0.490
Sulfhydryl Oxidase 1	O00391	82.5	8.92	0.284
Synaptophysin-Like Protein 1	Q16563	28.5	8.43	0.052

Continued...

T Cell Receptor Alpha Joining 56 (Fragment)	A0A075B6Z2	2.2	10.29	5.535
Tetraspanin-1	O60635	26.3	5.25	0.149
Tgc Domain-Containing Protein	A0A494C0J7	78.8	6.27	0.012
Thrombospondin-1	P07996	129.3	4.94	0.068
Transcobalamin-1	P20061	48.2	5.03	0.396
Transitional Endoplasmic Reticulum Atpase	P55072	89.3	5.26	0.005
Transthyretin	P02766	15.9	5.76	0.894
Tropomyosin Alpha-3 Chain	P06753	32.9	4.72	0.015
Tubulin Alpha Chain	F5H5D3	57.7	5.07	0.042
Tubulin Beta-4B Chain	P68371	49.8	4.89	0.186
Tumor Necrosis Factor	P01375	110.1	7.12	0.289
Tumor-Associated Calcium Signal Transducer 2	P09758	35.7	8.87	0.014
Ubiquitin-40S Ribosomal Protein S27A	P62979	18	9.64	0.462
Uncharacterized Protein	F5H423	23.3	8.6	0.042
Uroplakin-3B-Like Protein 2	E5RIL1	28.4	8.21	0.034
Uteroglobin	P11684	10	5.06	0.196
Vimentin	P08670	53.6	5.12	0.109
Vitronectin	P04004	54.3	5.8	0.045
Wd Repeat-Containing Protein 1	O75083	66.2	6.65	0.015
Zinc Finger Protein 398	Q8TD17	71.3	6.67	0.007
Zinc-Alpha-2-Glycoprotein	P25311	34.2	6.05	2.332
Zymogen Granule Protein 16 Homolog B	Q96DA0	22.7	7.39	1.336

B.7 LBL 30 mins NP Protein Corona

Protein Name	Ascension Code	MW (kDa)	Calculated PI	Normalized Peptide spectral count
14-3-3 Protein Zeta/Delta	P63104	27.7	4.79	0.142
2-Phospho-D-Glycerate Hydro-Lyase	A0A2R8Y6G6	47.3	6.99	0.033
Actin-Like Protein 10	A0A7I2V3D3	39.2	8.6	0.059
Actin, Cytoplasmic 1 (Fragment)	A0A2R8YFE2	8.8	9.2	0.354
Actin, Cytoplasmic 1	P60709	41.7	5.48	0.113
Actinin, Alpha 4, Isoform Cra_A	F5GXS2	104.8	5.44	0.082
Alpha-1-Acid Glycoprotein 1	P02763	23.5	5.02	1.594

Continued...

Alpha-1-Antichymotrypsin	P01011	47.6	5.52	0.295
Alpha-2-Macroglobulin	P01023	163.2	6.46	0.148
Alpha-Amylase 1A	P0DUB6	57.7	6.93	0.162
Alpha-S1-Casein	P02662	24.5	5.02	0.064
Annexin A1	P04083	38.7	7.02	0.121
Annexin	H0YMW4	41.9	8.13	0.038
Antileukoproteinase	P03973	14.3	8.75	0.654
Antithrombin-Iii	P01008	52.6	6.71	0.044
Apolipoprotein A-I	P02647	30.8	5.76	0.835
Apolipoprotein D (Fragment)	C9JF17	24.1	5.6	0.161
Aquaporin-5	P55064	28.3	8.62	0.027
Atp Synthase Subunit Beta, Mitochondrial	P06576	56.5	5.4	0.262
Azurocidin	P20160	26.9	9.5	0.029
Beta/Gamma Crystallin Domain-Containing Protein 1	A0A0J9YWL0	231.6	5.81	0.007
Bpi Fold-Containing Family B Member 1	Q8TDL5	52.4	7.23	3.111
Bpi Fold-Containing Family B Member 2	Q8N4F0	49.1	8.72	0.254
Bpi Fold-Containing Family B Member 4	A0A669KBJ0	75.3	5.36	0.145
C4A Anaphylatoxin	A0A0G2JPR0	192.8	7.03	0.004
C4B-Binding Protein Alpha Chain	P04003	67	7.3	0.012
Cadherin-1	A0A087WXI5	100	4.79	0.016
Cadherin-Related Family Member 1 (Fragment)	A0A0A6YYA3	65.1	6.71	0.012
Calmodulin-Like Protein 5	Q9NZT1	15.9	4.44	0.147
Cathepsin G	P08311	28.8	11.19	0.947
Cd59 Glycoprotein	P13987	14.2	6.48	0.165
Cd9 Antigen	F5GXT1	29.9	7.52	0.052
Ceruloplasmin	P00450	122.1	5.72	0.064
Choline Transporter-Like Protein 4	Q53GD3	79.2	8.59	0.020
Complement C3	P01024	187	6.4	0.079
Complement Factor H	P08603	139	6.61	0.034
Cystatin-S	P01036	16.2	5.02	0.384
Deleted In Malignant Brain Tumors 1 Protein (Fragment)	A0A590UJF8	21.6	5.27	0.471
Deleted In Malignant Brain Tumors 1 Protein (Fragment)	A0A590UK99	13.9	4.7	0.280
Desmocollin-1	Q08554	99.9	5.43	0.008
Desmoplakin	P15924	331.6	6.81	0.007

Continued...

E3 Ubiquitin-Protein Ligase Trim56	Q9BRZ2	81.4	7.74	0.144
Elongation Factor 1-Alpha 1	P68104	50.1	9.01	0.047
Extracellular Glycoprotein Lacritin	Q9GZZ8	14.2	5.5	0.220
Fatty Acid-Binding Protein 5	Q01469	15.2	7.01	0.153
Fibrinogen Beta Chain	P02675	55.9	8.27	0.056
Fibrinogen Gamma Chain (Fragment)	C9JU00	14	7.2	0.221
Filaggrin	P20930	434.9	9.25	0.007
Filaggrin-2	Q5D862	247.9	8.31	0.013
Flavin-Containing Monooxygenase 5	P49326	60.2	8.21	0.078
Galectin-3-Binding Protein	Q08380	65.3	5.27	0.191
Galectin-7	P47929	15.1	7.62	0.207
Glyceraldehyde-3-Phosphate Dehydrogenase	P04406	36	8.46	0.043
Haptoglobin	P00738	45.2	6.58	1.120
Heat Shock 27 Kda Protein	A0A6Q8PGK1	23.7	6.4	0.197
Heat Shock Cognate 71 Kda Protein	P11142	70.9	5.52	0.033
Hemoglobin Subunit Alpha	P69905	15.2	8.68	1.334
Hemoglobin Subunit Beta	P68871	16	7.28	0.732
Hemoglobin Subunit Delta	P02042	16	8.05	0.243
Histidine-Rich Glycoprotein	P04196	59.5	7.5	0.066
Histone H2A	A0A0U1RRH7	18.5	11.52	0.210
Histone H2B	U3KQK0	18.8	10.54	0.166
Histone H3.3 (Fragment)	K7ES00	16.6	11.84	0.329
Histone H4	P62805	11.4	11.36	1.643
Hornerin	Q86YZ3	282.2	10.04	0.033
Iggfc-Binding Protein	Q9Y6R7	571.6	5.34	0.254
Immunoglobulin Heavy Constant Alpha 1	P01876	37.6	6.51	7.297
Immunoglobulin Heavy Constant Alpha 2 (Fragment)	A0A0G2JMB2	36.5	6.1	0.961
Immunoglobulin Heavy Constant Gamma 1 (Fragment)	A0A0A0MS08	43.9	6.96	0.515
Immunoglobulin Heavy Constant Gamma 2 (Fragment)	A0A286YEY4	43.8	6.52	0.515
Immunoglobulin Heavy Variable 1-2	P23083	13.1	9.13	0.238
Immunoglobulin Heavy Variable 1-69D	A0A0B4J2H0	12.7	8.47	0.183
Immunoglobulin Heavy Variable 1/Or15-1 (Non-Functional) (Fragment)	A0A075B7D0	13	9.13	0.539
Immunoglobulin Heavy Variable 3-49	A0A0A0MS15	13	8.62	0.120
Immunoglobulin Heavy Variable 3-72	A0A4W8ZXM2	11.2	7.97	1.322
Immunoglobulin Heavy Variable 3-74	A0A0B4J1X5	12.8	8.66	0.549

Continued...

Immunoglobulin Heavy Variable 3/Or16-12 (Non-Functional) (Fragment)	A0A075B7B8	12.9	6.51	0.302
Immunoglobulin J Chain	P01591	18.1	5.24	7.235
Immunoglobulin Kappa Constant	P01834	11.8	6.52	9.650
Immunoglobulin Kappa Variable 1-33	A0A2Q2TTZ9	11.8	5.34	1.584
Immunoglobulin Kappa Variable 2-40	A0A087WW87	13.3	4.61	0.822
Immunoglobulin Kappa Variable 3-20	P01619	12.5	4.96	0.314
Immunoglobulin Kappa Variable 3D-7	A0A0C4DH55	13.1	5.94	0.416
Immunoglobulin Kappa Variable 4-1	P06312	13.4	5.25	0.233
Immunoglobulin Lambda Constant 2	P0DOY2	11.3	7.24	2.142
Immunoglobulin Lambda Variable 3-21	P80748	12.4	5.29	0.503
Immunoglobulin Lambda-Like Polypeptide 5	A0A0B4J231	23.1	8.84	1.249
Intelectin-1	Q8WWA0	34.9	6.01	0.357
Intelectin-2	Q8WWU7	36.2	8.28	0.151
Isoform 2 Of Alpha-1-Antitrypsin	P01009	40.2	5.47	0.388
Isoform 2 Of Bpi Fold-Containing Family A Member 1	Q9NP55	25.2	6.06	1.517
Isoform 2 Of Carcinoembryonic Antigen-Related Cell Adhesion Molecule 5	P06731	76.7	5.92	0.051
Isoform 2 Of Immunoglobulin Heavy Constant Mu	P01871	51.9	6.15	1.036
Isoform 2 Of Keratin, Type Ii Cytoskeletal 78	Q8N1N4	45	5.2	0.018
Isoform 2 Of Map Kinase-Activated Protein Kinase 5	Q8IW41	54	7.61	0.058
Isoform 2 Of Plastin-2	P13796	21.8	5.44	0.107
Isoform 2 Of Thioredoxin Domain-Containing Protein 5	Q8NBS9	36.2	5.47	0.043
Isoform 2 Of Thioredoxin	P10599	9.4	6.04	0.250
Isoform 2 Of Vitamin D-Binding Protein	P02774	39.5	5.2	0.099
Isoform 3 Of Atp Synthase Subunit Alpha, Mitochondrial	P25705	57.5	9.29	0.230
Isoform 3 Of Keratin, Type I Cytoskeletal 13	P13646	45.8	4.88	0.545
Isoform 3 Of Tripartite Motif-Containing Protein 46	Q7Z4K8	57.4	8.69	0.232
Isoform 3 Of Wap Four-Disulfide Core Domain Protein 2	Q14508	8.1	7.83	3.081

Continued...

Isoform 4 Of Leukotriene A-4 Hydrolase	P09960	66.8	6.7	0.023
Isoform 5 Of Clusterin	P10909	53.6	6.27	0.189
Isoform 5 Of Deleted In Malignant Brain Tumors 1 Protein	Q9UGM3	258.3	5.43	1.975
Isoform 5 Of L-Lactate Dehydrogenase A Chain	P00338	26.7	8.15	0.058
Isoform 6 Of Ef-Hand Calcium-Binding Domain-Containing Protein 6	Q5THR3	48.4	9.63	0.016
Isoform 8 Of Fibronectin	P02751	252.7	5.94	0.040
Isoform Alpha Of Pancreatic Secretory Granule Membrane Major Glycoprotein Gp2	P55259	59.1	5.17	0.039
Isoform Deltalf Of Lactotransferrin	P02788	73.1	7.85	5.877
Isoform Lmw Of Kininogen-1	P01042	47.9	6.65	0.016
Junction Plakoglobin	P14923	81.7	6.14	0.066
Junctophilin-3	Q8WXH2	81.4	9.39	0.009
Keratin, Type I Cytoskeletal 10	P13645	58.8	5.21	4.548
Keratin, Type I Cytoskeletal 12	Q99456	53.5	4.78	0.102
Keratin, Type I Cytoskeletal 14	P02533	51.5	5.16	2.679
Keratin, Type I Cytoskeletal 16	P08779	51.2	5.05	0.564
Keratin, Type I Cytoskeletal 17	Q04695	48.1	5.02	0.065
Keratin, Type I Cytoskeletal 19	P08727	44.1	5.14	0.337
Keratin, Type I Cytoskeletal 9	P35527	62	5.24	2.238
Keratin, Type Ii Cytoskeletal 1	P04264	66	8.12	3.261
Keratin, Type Ii Cytoskeletal 1B	Q7Z794	61.9	5.99	0.416
Keratin, Type Ii Cytoskeletal 2 Epidermal	P35908	65.4	8	1.549
Keratin, Type Ii Cytoskeletal 4	P19013	56.1	6.61	0.056
Keratin, Type Ii Cytoskeletal 5	P13647	62.3	7.74	0.689
Keratin, Type Ii Cytoskeletal 6A	P02538	60	8	0.442
Keratin, Type Ii Cytoskeletal 6B	P04259	60	8	1.117
Keratin, Type Ii Cytoskeletal 7	P08729	51.4	5.48	0.379
Keratin, Type Ii Cytoskeletal 71	Q3SY84	57.3	6.61	0.082
Keratinocyte Proline-Rich Protein	Q5T749	64.1	8.27	0.036
Lactoperoxidase	P22079	80.2	8.62	0.019
Leukocyte Elastase Inhibitor	P30740	42.7	6.28	0.018
Lipocalin-1	P31025	19.2	5.58	3.857
Lipocalin-15	Q6UWW0	20.4	4.94	1.070
Lysozyme C	P00698	16.2	9.07	0.770
Lysozyme C	P61626	16.5	9.16	2.173
Mammaglobin-B	O75556	10.9	5.78	0.715

Continued...

Matrix Metalloproteinase-9	P14780	78.4	6.06	0.010
Metalloproteinase Inhibitor 1	P01033	23.2	8.1	0.100
Moesin	P26038	67.8	6.4	0.046
Mucin-2	Q02817	540	5.8	0.004
Mucin-5Ac	P98088	585.2	7.02	0.281
Mucin-5B	Q9HC84	596	6.64	0.748
Myeloblastin	P24158	27.8	8.35	0.420
Myeloperoxidase	P05164	83.8	8.97	0.018
Myomesin-2	P54296	164.8	6.19	0.019
Neutrophil Defensin 1	P59665	10.2	6.99	2.292
Neutrophil Elastase	P08246	28.5	9.35	0.055
Neutrophil Gelatinase-Associated Lipocalin	X6R8F3	22.8	8.5	0.068
Opiorphin Prepropeptide	Q99935	27.2	10.42	0.115
Peptidoglycan Recognition Protein 1	O75594	21.7	8.59	0.108
Peroxiredoxin-1	Q06830	22.1	8.13	0.035
Phosphatidylinositol 3-Kinase Catalytic Subunit Type 3 (Fragment)	K7EIV6	19.9	9.54	0.274
Polymeric Immunoglobulin Receptor	P01833	83.2	5.74	2.549
Probable Non-Functional Immunoglobulin Kappa Variable 2D-24	A0A075B6R9	13.1	8.87	0.119
Progranulin	P28799	63.5	6.83	0.025
Prolactin-Inducible Protein	P12273	16.6	8.05	8.703
Prosaposin	C9JIZ6	58.4	5.17	0.027
Prostate Stem Cell Antigen	O43653	12	4.94	0.391
Protein Fam78B (Fragment)	H7C075	29.4	9.47	0.052
Protein Fam83G	A6ND36	90.8	6.39	0.240
Protein Leg1 Homolog	Q6P5S2	37.9	6.15	0.823
Protein Phosphatase Methylesterase 1	Q9Y570	42.3	5.97	0.018
Protein S100-A12	P80511	10.6	6.25	0.147
Protein S100-A7	P31151	11.5	6.77	0.069
Protein S100-A8	P05109	10.8	7.03	5.992
Protein S100-A9	P06702	13.2	6.13	6.438
Ras-Related Protein Rab-30 (Fragment)	E9PI18	8.8	5.36	0.090
Secretoglobin Family 1D Member 1	O95968	9.9	9.25	0.158
Secretoglobin Family 1D Member 2	O95969	9.9	8.25	1.731
Serine Protease Htra1	Q92743	51.3	7.83	0.030
Serine/Threonine-Protein Kinase Mak	P20794	70.5	9.66	0.011
Serpin B3	P29508	44.5	6.81	0.123

Continued...

Serpin B4	P48594	44.8	6.21	0.279
Serum Albumin	P02769	69.2	6.18	1.328
Serum Albumin	P02768	69.3	6.28	7.491
Sialic Acid-Binding Ig-Like Lectin 16	A6NMB1	53	9.03	0.029
Small Integral Membrane Protein 22	A0A4V7I672	14.6	6.52	0.053
Spindle And Centriole-Associated Protein 1	Q8N0Z3	96.2	7.44	0.008
Spliceosome Rna Helicase Ddx39B (Fragment)	H0YCC6	16.6	5.55	0.281
Suprabasin	Q6UWP8	60.5	7.01	0.052
Tetraspanin-1	O60635	26.3	5.25	0.119
Threonine Aspartase 1	Q9H6P5	44.4	7.75	0.035
Transcobalamin-1	P20061	48.2	5.03	0.211
Transthyretin	P02766	15.9	5.76	1.322
Tubulin Alpha Chain	F5H5D3	57.7	5.07	0.014
Tumor Necrosis Factor	P01375	110.1	7.12	0.092
Tyrosine Aminotransferase	P17735	50.4	6.3	0.031
Ubiquitin-40S Ribosomal Protein S27A	P62979	18	9.64	0.260
Uteroglobin	P11684	10	5.06	0.156
Vitronectin	P04004	54.3	5.8	0.043
Zinc-Alpha-2-Glycoprotein	P25311	34.2	6.05	0.296
Zymogen Granule Protein 16 Homolog B	Q96DA0	22.7	7.39	1.306

B.8 LBL 4.0 hours NP Protein Corona

Protein Name	Ascension Code	MW (kDa)	Calculated PI	Normalized Peptide spectral count
14-3-3 Protein Beta/Alpha	P31946	28.1	4.83	0.019
14-3-3 Protein Zeta/Delta	P63104	27.7	4.79	0.273
2-Phospho-D-Glycerate Hydro-Lyase	A0A2R8Y6G6	47.3	6.99	0.034
Actin, Alpha Cardiac Muscle 1	P68032	42	5.39	0.013
Actin, Cytoplasmic 1 (Fragment)	A0A2R8YFE2	8.8	9.2	2.202
Actin, Cytoplasmic 1	P60709	41.7	5.48	0.672
Actinin, Alpha 4, Isoform Cra_A	F5GXS2	104.8	5.44	0.072
Afamin	P43652	69	5.9	0.024
Aldehyde Dehydrogenase, Dimeric Nadp-Preferring	P30838	50.4	6.54	0.064

Continued...

Alpha-1-Acid Glycoprotein 1	P02763	23.5	5.02	1.146
Alpha-1-Acid Glycoprotein 2	P19652	23.6	5.11	0.022
Alpha-1-Antichymotrypsin	P01011	47.6	5.52	0.588
Alpha-1B-Glycoprotein	P04217	54.2	5.86	0.070
Alpha-2-Macroglobulin	P01023	163.2	6.46	0.191
Alpha-Amylase 1A	P0DUB6	57.7	6.93	0.486
Alpha-S1-Casein	P02662	24.5	5.02	0.218
Annexin A1	P04083	38.7	7.02	0.654
Annexin A5	P08758	35.9	5.05	0.045
Annexin	H0YMW4	41.9	8.13	0.283
Antibacterial Peptide Fall-39	J3KNB4	19.6	9.41	0.110
Antileukoproteinase	P03973	14.3	8.75	0.680
Antithrombin-Iii	P01008	52.6	6.71	0.123
Apolipoprotein A-I	P02647	30.8	5.76	1.506
Apolipoprotein A-Ii	V9GYM3	14.9	8.27	0.035
Apolipoprotein A-Iv	P06727	45.3	5.38	0.036
Apolipoprotein D (Fragment)	C9JF17	24.1	5.6	0.290
Azurocidin	P20160	26.9	9.5	0.079
Basement Membrane-Specific Heparan Sulfate Proteoglycan Core Protein	P98160	468.5	6.51	0.003
Basic Salivary Proline-Rich Protein 2	P02812	40.8	11.63	0.039
Beta-2-Microglobulin	P61769	13.7	6.52	0.236
Bpi Fold-Containing Family B Member 1	Q8TDL5	52.4	7.23	2.693
Bpi Fold-Containing Family B Member 2	Q8N4F0	49.1	8.72	0.473
Bpi Fold-Containing Family B Member 4	A0A669KBJ0	75.3	5.36	0.401
Brain Acid Soluble Protein 1	P80723	22.7	4.63	0.047
C-X-C Motif Chemokine 17	Q6UXB2	13.8	10.96	0.196
C3/C5 Convertase	B4E1Z4	140.9	7.18	0.023
C4A Anaphylatoxin	A0A0G2JPR0	192.8	7.03	0.087
Calcyphosin	Q13938	30.2	6.04	0.089
Calmodulin-3	P0DP25	16.8	4.22	0.127
Calmodulin-Like Protein 3	P27482	16.9	4.42	0.415
Calmodulin-Like Protein 5	Q9NZT1	15.9	4.44	1.560
Caspase-14	P31944	27.7	5.58	0.428
Catalase	P04040	59.7	7.39	0.045
Cathepsin B	E9PHZ5	41.3	6.58	0.026
Cathepsin G	P08311	28.8	11.19	0.354
Cd59 Glycoprotein	P13987	14.2	6.48	0.039

Continued...

Ceruloplasmin	P00450	122.1	5.72	0.190
Choline Transporter-Like Protein 4	Q53GD3	79.2	8.59	0.007
Coagulation Factor V	A0A0A0MRJ7	252.1	6.05	0.004
Complement C3	P01024	187	6.4	0.432
Complement Factor H	P08603	139	6.61	0.050
Coronin-1A	P31146	51	6.68	0.021
Cystatin-C	P01034	15.8	8.75	0.683
Cystatin-S	P01036	16.2	5.02	0.862
Deleted In Malignant Brain Tumors 1 Protein (Fragment)	A0A590UJF8	21.6	5.27	0.794
Desmocollin-1	Q08554	99.9	5.43	0.032
Desmoglein-1	Q02413	113.7	5.03	0.076
Desmoplakin	P15924	331.6	6.81	0.016
E3 Ubiquitin-Protein Ligase Trim56	Q9BRZ2	81.4	7.74	0.165
Elongation Factor 1-Alpha 1	P68104	50.1	9.01	0.022
Endoplasmic Reticulum Chaperone Bip	P11021	72.3	5.16	0.023
Eosinophil Cationic Protein	P12724	18.4	10.02	0.059
Extracellular Glycoprotein Lacritin	Q9GZZ8	14.2	5.5	1.441
Ezrin	E7EQR4	69.3	6.16	0.016
F-Box Only Protein 50	Q6ZVX7	30.8	6.62	0.070
Fatty Acid-Binding Protein 5	Q01469	15.2	7.01	0.495
Fibrinogen Beta Chain	P02675	55.9	8.27	0.608
Fibrinogen Gamma Chain (Fragment)	C9JU00	14	7.2	1.040
Fibrinogen Gamma Chain	C9JC84	52.3	5.63	0.288
Filaggrin	P20930	434.9	9.25	0.007
Filaggrin-2	Q5D862	247.9	8.31	0.024
Galectin-3	P17931	26.1	8.56	0.125
Galectin-3-Binding Protein	Q08380	65.3	5.27	0.257
Galectin-7	P47929	15.1	7.62	0.215
Gamma-Glutamylcyclotransferase	O75223	21	5.14	0.051
Gelsolin	P06396	85.6	6.28	0.196
Glutathione S-Transferase P	P09211	23.3	5.64	0.115
Glyceraldehyde-3-Phosphate Dehydrogenase	P04406	36	8.46	0.150
Haptoglobin	P00738	45.2	6.58	1.335
Heat Shock 27 Kda Protein	A0A6Q8PGK1	23.7	6.4	0.181
Heat Shock 70 Kda Protein 1B	A0A0G2JIW1	70.1	5.66	0.054
Heat Shock Cognate 71 Kda Protein	P11142	70.9	5.52	0.015
Hemoglobin Subunit Alpha	P69905	15.2	8.68	1.840
Hemoglobin Subunit Beta	P68871	16	7.28	1.720
Hemoglobin Subunit Delta	P02042	16	8.05	0.807

Continued...

Hemopexin	P02790	51.6	7.02	0.136
Histidine-Rich Glycoprotein	P04196	59.5	7.5	0.064
Histone H2A	A0A0U1RRH7	18.5	11.52	0.292
Histone H2B	U3KQK0	18.8	10.54	0.114
Histone H3.3 (Fragment)	K7ES00	16.6	11.84	0.099
Histone H4	P62805	11.4	11.36	1.889
Hornerin	Q86YZ3	282.2	10.04	0.015
Iggfc-Binding Protein	Q9Y6R7	571.6	5.34	0.202
Immunoglobulin Heavy Constant Alpha 1	P01876	37.6	6.51	5.201
Immunoglobulin Heavy Constant Alpha 2 (Fragment)	A0A0G2JMB2	36.5	6.1	1.255
Immunoglobulin Heavy Constant Gamma 1 (Fragment)	A0A0A0MS08	43.9	6.96	0.516
Immunoglobulin Heavy Constant Gamma 2 (Fragment)	A0A286YEY4	43.8	6.52	0.381
Immunoglobulin Heavy Constant Gamma 3 (Fragment)	A0A286YES1	49.1	6.87	0.044
Immunoglobulin Heavy Variable 1-18	A0A0C4DH31	12.8	8.84	0.084
Immunoglobulin Heavy Variable 1-2	P23083	13.1	9.13	0.081
Immunoglobulin Heavy Variable 1-69D	A0A0B4J2H0	12.7	8.47	0.255
Immunoglobulin Heavy Variable 3-49	A0A0A0MS15	13	8.62	0.125
Immunoglobulin Heavy Variable 3-72	A0A4W8ZXM2	11.2	7.97	1.781
Immunoglobulin Heavy Variable 3-74	A0A0B4J1X5	12.8	8.66	0.338
Immunoglobulin Heavy Variable 3/Or16-12 (Non-Functional) (Fragment)	A0A075B7B8	12.9	6.51	0.210
Immunoglobulin Heavy Variable 5-51	A0A0C4DH38	12.7	8.27	0.085
Immunoglobulin Heavy Variable 6-1	A0A0B4J1U7	13.5	9.2	0.200
Immunoglobulin J Chain	P01591	18.1	5.24	5.506
Immunoglobulin Kappa Constant (Fragment)	A0A5H1ZRQ3	11.7	5.87	0.231
Immunoglobulin Kappa Constant	P01834	11.8	6.52	8.721
Immunoglobulin Kappa Variable 1-17	P01599	12.8	8.68	0.127
Immunoglobulin Kappa Variable 1-33	A0A2Q2TTZ9	11.8	5.34	1.510
Immunoglobulin Kappa Variable 1-6	A0A0C4DH72	12.7	8.29	0.127
Immunoglobulin Kappa Variable 1/Or2-108 (Non-Functional) (Fragment)	A0A075B7D4	12.5	6.48	0.044
Immunoglobulin Kappa Variable 2-40	A0A087WW87	13.3	4.61	0.609

Continued...

Immunoglobulin Kappa Variable 2D-28	A0A5H1ZRS2	11	5.24	0.050
Immunoglobulin Kappa Variable 3-11	P04433	12.6	4.96	0.555
Immunoglobulin Kappa Variable 3-20	P01619	12.5	4.96	0.519
Immunoglobulin Kappa Variable 3D-7	A0A0C4DH55	13.1	5.94	0.741
Immunoglobulin Lambda Constant 2	P0DOY2	11.3	7.24	2.482
Immunoglobulin Lambda Variable 3-10	A0A075B6K4	12.4	4.83	0.087
Immunoglobulin Lambda Variable 3-16	A0A075B6K0	12.5	4.65	0.044
Immunoglobulin Lambda Variable 3-21	P80748	12.4	5.29	0.738
Immunoglobulin Lambda Variable 7-46	A0A075B6I9	12.5	7.2	0.044
Immunoglobulin Lambda-Like Polypeptide 5	A0A0B4J231	23.1	8.84	2.122
Intelectin-1	Q8WWA0	34.9	6.01	0.447
Intelectin-2	Q8WWU7	36.2	8.28	0.134
Inter-Alpha-Trypsin Inhibitor Heavy Chain H2	P19823	106.4	6.86	0.005
Interferon-Induced, Double-Stranded Rna-Activated Protein Kinase	P19525	62.1	8.4	0.009
Interleukin-1 Receptor Accessory Protein	Q9NPH3	65.4	8.12	0.025
Isoform 2 Of 6-Phosphogluconate Dehydrogenase, Decarboxylating	P52209	51.8	7.44	0.094
Isoform 2 Of Alpha-1-Antitrypsin	P01009	40.2	5.47	0.859
Isoform 2 Of Bpi Fold-Containing Family A Member 1	Q9NP55	25.2	6.06	1.390
Isoform 2 Of Calcium And Integrin-Binding Protein 1	Q99828	26	4.86	0.021
Isoform 2 Of Calnexin	P27824	71.5	4.7	0.008
Isoform 2 Of Carboxypeptidase A4	Q9UI42	43.5	8.34	0.025
Isoform 2 Of Carcinoembryonic Antigen-Related Cell Adhesion Molecule 5	P06731	76.7	5.92	0.070
Isoform 2 Of Diencephalon/Mesencephalon Homeobox Protein 1	Q8NFW5	40.6	8.7	0.027
Isoform 2 Of Egf-Containing Fibulin-Like Extracellular Matrix Protein 1	Q12805	53.7	5.02	0.010
Isoform 2 Of Fibrinogen Alpha Chain	P02671	69.7	8.06	0.070
Isoform 2 Of Fructose-Bisphosphate Aldolase A	P04075	45.2	8.25	0.023

Continued...

Isoform 2 Of Immunoglobulin Heavy Constant Mu	P01871	51.9	6.15	1.185
Isoform 2 Of Kallikrein-1	P06870	23.8	4.65	0.022
Isoform 2 Of Keratin, Type Ii Cytoskeletal 78	Q8N1N4	45	5.2	0.083
Isoform 2 Of Myosin-14	Q7Z406	231.9	5.6	0.002
Isoform 2 Of Neutral Alpha-Glucosidase Ab	Q14697	109.4	6.24	0.010
Isoform 2 Of Nucleobindin-2	P80303	50.2	5.12	0.203
Isoform 2 Of Peroxiredoxin-2	P32119	15.8	9.06	0.035
Isoform 2 Of Plastin-2	P13796	21.8	5.44	0.520
Isoform 2 Of Thioredoxin	P10599	9.4	6.04	0.517
Isoform 2 Of Transketolase	P29401	68.8	7.52	0.008
Isoform 2 Of Vitamin D-Binding Protein	P02774	39.5	5.2	0.287
Isoform 3 Of Keratin, Type I Cytoskeletal 13	P13646	45.8	4.88	0.683
Isoform 3 Of Keratin, Type Ii Cytoskeletal 80	Q6KB66	54.1	5.39	0.010
Isoform 3 Of Mesothelin	Q13421	71.4	7.36	0.030
Isoform 3 Of Phospholipid Transfer Protein	P55058	44.1	6.55	0.208
Isoform 3 Of Pyruvate Kinase Pkm	P14618	56.2	8.44	0.010
Isoform 3 Of Triosephosphate Isomerase	P60174	17.9	5.58	0.060
Isoform 3 Of Tripartite Motif-Containing Protein 46	Q7Z4K8	57.4	8.69	0.444
Isoform 3 Of Vitelline Membrane Outer Layer Protein 1 Homolog	Q7Z5L0	10.8	5.83	1.196
Isoform 3 Of Wap Four-Disulfide Core Domain Protein 2	Q14508	8.1	7.83	1.790
Isoform 4 Of Extracellular Matrix Protein 1	Q16610	63.5	6.89	0.009
Isoform 4 Of Leukotriene A-4 Hydrolase	P09960	66.8	6.7	0.024
Isoform 5 Of Clusterin	P10909	53.6	6.27	0.764
Isoform 5 Of Complement Decay-Accelerating Factor	P08174	48.5	7.88	0.011
Isoform 5 Of Deleted In Malignant Brain Tumors 1 Protein	Q9UGM3	258.3	5.43	1.415
Isoform 5 Of L-Lactate Dehydrogenase A Chain	P00338	26.7	8.15	0.162
Isoform 8 Of Fibronectin	P02751	252.7	5.94	0.147

Continued...

Isoform Alpha Of Pancreatic Secretory Granule Membrane Major Glycoprotein Gp2	P55259	59.1	5.17	0.018
Isoform Deltalf Of Lactotransferrin	P02788	73.1	7.85	6.793
Isoform F Of Mucin-1	P15941	21.5	8.66	0.025
Isoform Lmw Of Kininogen-1	P01042	47.9	6.65	0.011
Isoform N3 Of Camp-Specific 3',5'-Cyclic Phosphodiesterase 4D	Q08499	23.8	9.72	0.069
Itih4 Protein	B7ZKJ8	103.8	6.89	0.005
Junction Plakoglobin	P14923	81.7	6.14	0.086
Keratin, Type I Cuticular Ha3-I	O76009	45.9	4.82	0.023
Keratin, Type I Cytoskeletal 10 (Fragment)	A0A1B0GVI3	10	8.44	0.161
Keratin, Type I Cytoskeletal 10	P13645	58.8	5.21	4.637
Keratin, Type I Cytoskeletal 12	Q99456	53.5	4.78	0.060
Keratin, Type I Cytoskeletal 14	P02533	51.5	5.16	2.196
Keratin, Type I Cytoskeletal 16	P08779	51.2	5.05	0.558
Keratin, Type I Cytoskeletal 17	Q04695	48.1	5.02	0.123
Keratin, Type I Cytoskeletal 19	P08727	44.1	5.14	0.439
Keratin, Type I Cytoskeletal 9	P35527	62	5.24	1.946
Keratin, Type Ii Cytoskeletal 1	P04264	66	8.12	3.495
Keratin, Type Ii Cytoskeletal 1B	Q7Z794	61.9	5.99	0.349
Keratin, Type Ii Cytoskeletal 2 Epidermal	P35908	65.4	8	3.515
Keratin, Type Ii Cytoskeletal 4	P19013	56.1	6.61	0.077
Keratin, Type Ii Cytoskeletal 5	P13647	62.3	7.74	0.865
Keratin, Type Ii Cytoskeletal 6A	P02538	60	8	0.485
Keratin, Type Ii Cytoskeletal 6B	P04259	60	8	0.657
Keratin, Type Ii Cytoskeletal 6C	P48668	60	8	0.009
Keratin, Type Ii Cytoskeletal 7	P08729	51.4	5.48	0.357
Keratin, Type Ii Cytoskeletal 71	Q3SY84	57.3	6.61	0.113
Keratin, Type Ii Cytoskeletal 8	P05787	53.7	5.59	0.040
Keratinocyte Proline-Rich Protein	Q5T749	64.1	8.27	0.252
Lactoperoxidase	P22079	80.2	8.62	0.054
Late Cornified Envelope Protein 1C	Q5T751	11.5	8.37	0.092
Late Cornified Envelope Protein 2A	Q5TA79	10.8	7.91	0.049
Late Cornified Envelope Protein 2B	O14633	11.2	8.09	0.143
Leukocyte Elastase Inhibitor	P30740	42.7	6.28	0.164
Lipocalin-1	P31025	19.2	5.58	3.477
Lipocalin-15	Q6UWW0	20.4	4.94	0.686
Loricrin	P23490	25.7	8.09	0.021

Continued...

Lysozyme C	P00698	16.2	9.07	0.067
Lysozyme C	P61626	16.5	9.16	1.829
Mammaglobin-B	O75556	10.9	5.78	2.024
Matrix Metalloproteinase-9	P14780	78.4	6.06	0.076
Melanoma-Derived Growth Regulatory Protein	Q16674	14.5	8.79	0.036
Metalloproteinase Inhibitor 1	P01033	23.2	8.1	0.023
Midkine	E9PLM6	16.9	9.91	0.031
Moesin	P26038	67.8	6.4	0.071
Monocyte Differentiation Antigen Cd14	P08571	40.1	6.23	0.041
Mucin-5Ac	P98088	585.2	7.02	0.179
Mucin-5B	Q9HC84	596	6.64	0.679
Mucin-7	Q8TAX7	39.1	8.78	0.083
Myeloblastin	P24158	27.8	8.35	0.059
Myeloid Cell Nuclear Differentiation Antigen	P41218	45.8	9.76	0.024
Myeloperoxidase	P05164	83.8	8.97	0.141
Myosin-9	P35579	226.4	5.6	0.010
Neutrophil Defensin 1	P59665	10.2	6.99	1.374
Neutrophil Elastase	P08246	28.5	9.35	0.038
Neutrophil Gelatinase-Associated Lipocalin	X6R8F3	22.8	8.5	0.356
Nucleobindin-1	Q02818	53.8	5.25	0.170
Opiorphin Prepropeptide	Q99935	27.2	10.42	0.159
Peroxiredoxin-1	Q06830	22.1	8.13	0.341
Peroxiredoxin-6	P30041	25	6.38	0.043
Phosphatidylinositol 3-Kinase Catalytic Subunit Type 3 (Fragment)	K7EIV6	19.9	9.54	0.514
Pi-Plc X Domain-Containing Protein 1	Q9NUJ7	36.6	6.58	0.147
Pigment Epithelium-Derived Factor	P36955	46.3	6.38	0.012
Plasma Protease C1 Inhibitor	E9PGN7	59.5	6.76	0.072
Plasminogen	P00747	90.5	7.24	0.053
Polymeric Immunoglobulin Receptor	P01833	83.2	5.74	2.584
Prelamin-A/C	A0A6Q8PFJ0	80.9	8.27	0.033
Probable Non-Functional Immunoglobulin Kappa Variable 2D-24	A0A075B6R9	13.1	8.87	0.123
Prolactin-Inducible Protein	P12273	16.6	8.05	4.513
Proline-Rich Protein 4	A0A0J9YXF8	16.9	7.52	0.286
Prominin-1	O43490	97.1	7.27	0.039
Prosaposin	C9JIZ6	58.4	5.17	0.120

Continued...

Prostate Stem Cell Antigen	O43653	12	4.94	0.271
Protein Ambp	P02760	39	6.25	0.042
Protein Disulfide-Isomerase	P07237	57.1	4.87	0.019
Protein Leg1 Homolog	Q6P5S2	37.9	6.15	0.896
Protein S100-A14	Q9HCY8	11.7	5.24	0.092
Protein S100-A4	P26447	11.7	6.11	0.045
Protein S100-A6	P06703	10.2	5.48	0.106
Protein S100-A7	P31151	11.5	6.77	0.564
Protein S100-A8	P05109	10.8	7.03	7.133
Protein S100-A9	P06702	13.2	6.13	5.878
Protein S100-P	P25815	10.4	4.88	0.154
Ras Gtpase-Activating-Like Protein Iqgap1	P46940	189.1	6.48	0.006
Ras-Related Protein Rab-10	P61026	22.5	8.38	0.024
Retinal Dehydrogenase 1	P00352	54.8	6.73	0.020
Retinoic Acid Receptor Responder Protein 1	P49788	33.3	8.51	0.082
Retinol-Binding Protein 4	P02753	23	6.07	0.048
Ribonuclease Pancreatic	P07998	17.6	8.79	0.061
Secretoglobin Family 1D Member 1	O95968	9.9	9.25	0.273
Secretoglobin Family 1D Member 2	O95969	9.9	8.25	1.140
Serine Protease Htra1	Q92743	51.3	7.83	0.115
Serpin B12	Q96P63	46.2	5.53	0.035
Serpin B3	P29508	44.5	6.81	0.377
Serpin B4	P48594	44.8	6.21	0.373
Serum Albumin	P02769	69.2	6.18	1.649
Serum Albumin	P02768	69.3	6.28	7.777
Sialic Acid-Binding Ig-Like Lectin 16	A6NMB1	53	9.03	0.143
Skin-Specific Protein 32	Q5T750	26.2	7.97	0.206
Small Integral Membrane Protein 22	A0A4V7I672	14.6	6.52	0.074
Small Proline-Rich Protein 2G	Q9BYE4	8.2	7.96	0.263
Stromelysin-2	P09238	54.1	5.8	0.010
Sulfhydryl Oxidase 1	O00391	82.5	8.92	0.111
Suprabasin	Q6UWP8	60.5	7.01	0.071
T Cell Receptor Alpha Joining 56 (Fragment)	A0A075B6Z2	2.2	10.29	2.949
Tetraspanin-1	O60635	26.3	5.25	0.082
Tgc Domain-Containing Protein	A0A494C0J7	78.8	6.27	0.082
Thrombospondin-1	P07996	129.3	4.94	0.021
Transcobalamin-1	P20061	48.2	5.03	0.615
Transmembrane Protein 198	Q66K66	39.4	9.92	0.014

Continued...

Transmembrane Protein 201	Q5SNT2	72.2	9.22	0.008
Transthyretin	P02766	15.9	5.76	1.151
Tropomyosin Alpha-3 Chain	P06753	32.9	4.72	0.296
Tubulin Alpha Chain	F5H5D3	57.7	5.07	0.009
Tubulin Beta-4B Chain	P68371	49.8	4.89	0.011
Tumor Necrosis Factor	P01375	110.1	7.12	0.426
Ubiquitin-40S Ribosomal Protein S27A	P62979	18	9.64	0.359
Uteroglobin	P11684	10	5.06	0.862
Vimentin	P08670	53.6	5.12	0.341
Vitronectin	P04004	54.3	5.8	0.099
Wap Four-Disulfide Core Domain Protein 12	Q8WWY7	12	5.5	0.090
Zinc-Alpha-2-Glycoprotein	P25311	34.2	6.05	2.460
Zymogen Granule Protein 16 Homolog B	Q96DA0	22.7	7.39	0.831

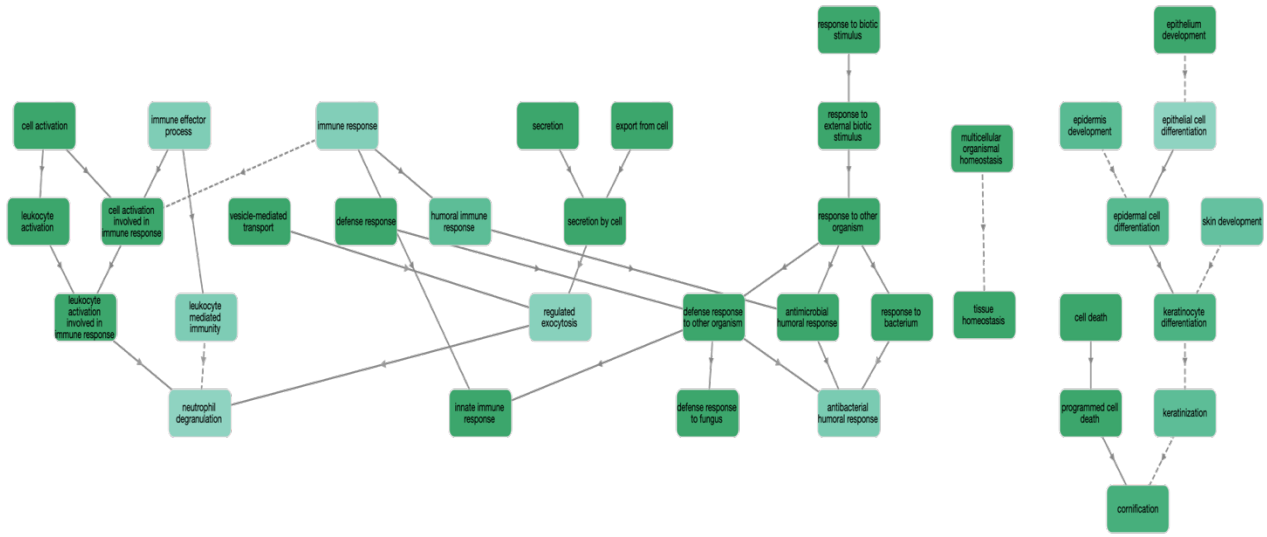

B.10 Bare OVA PNC 30 mins network

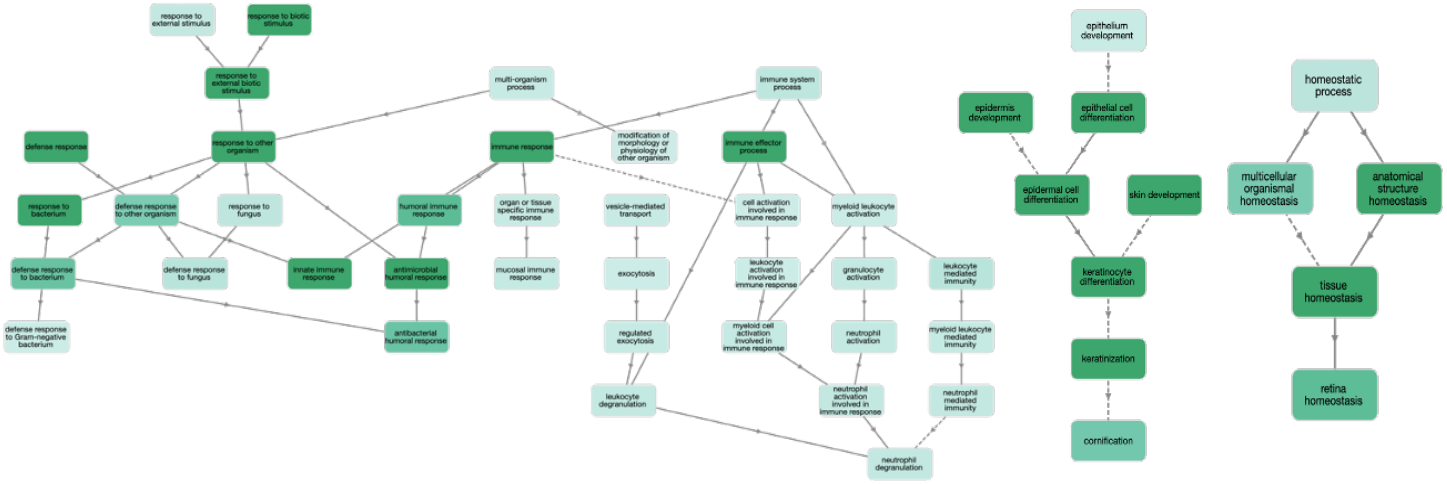

B.11 Bare OVA PNC 4 hours network

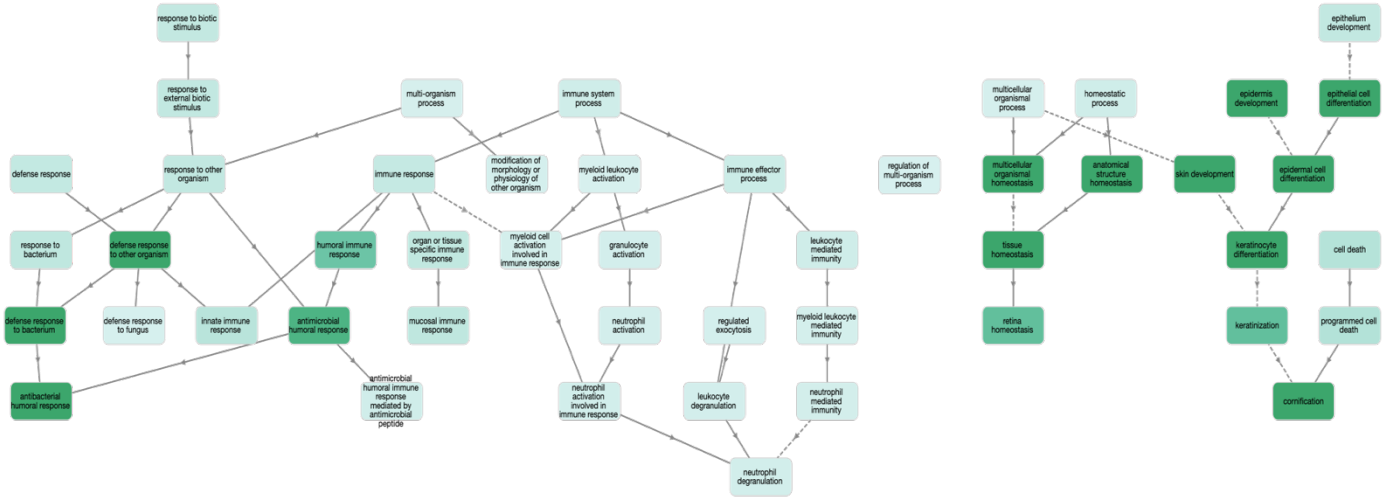

B.12 PEG PNC 30 mins network

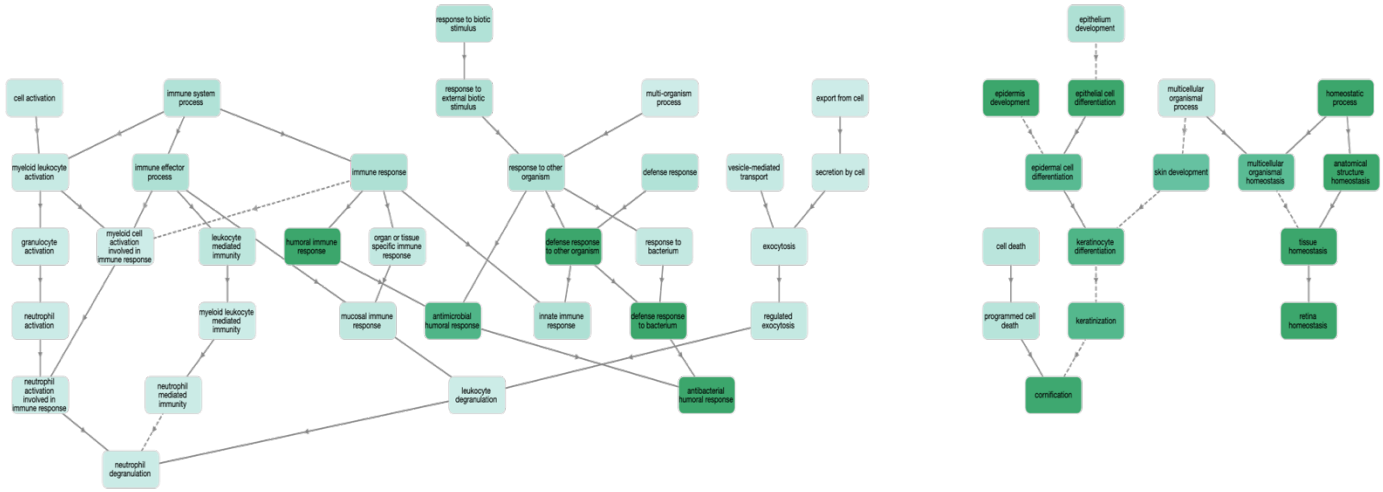

B.13 PEG PNC 4 hours network

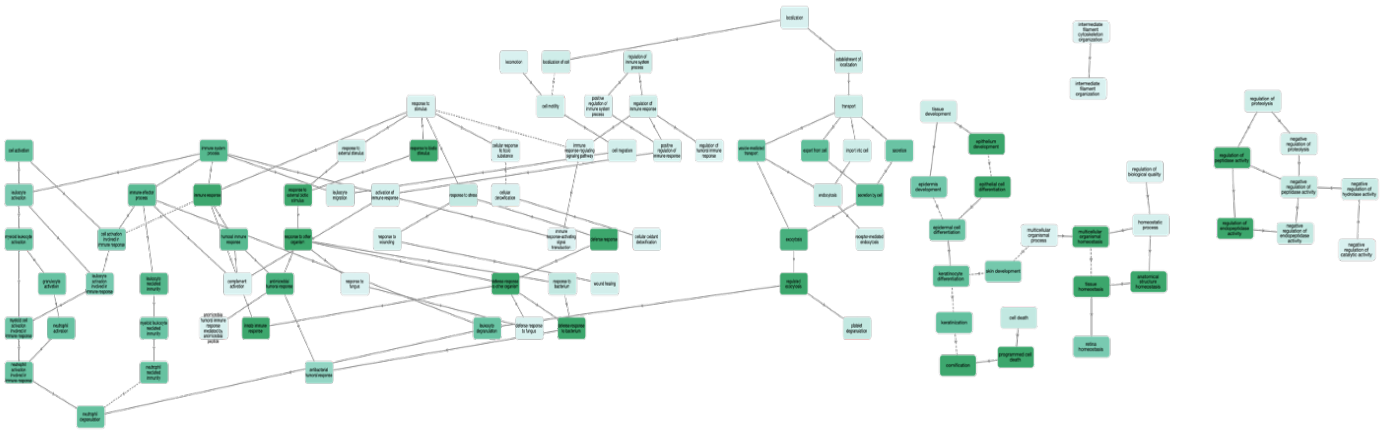

A.14 cOVA PNC 30 mins network

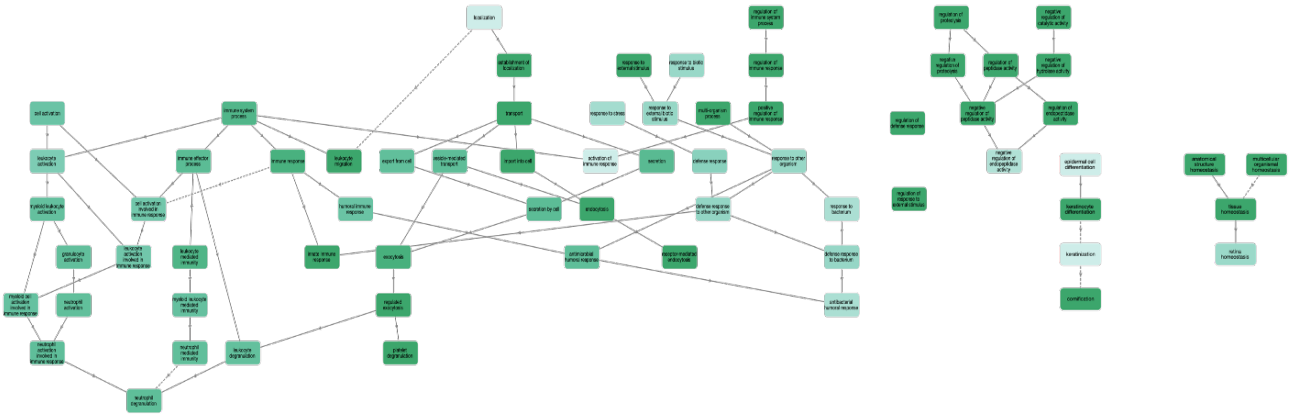

B.14 cOVA PNC 4.0 hours network

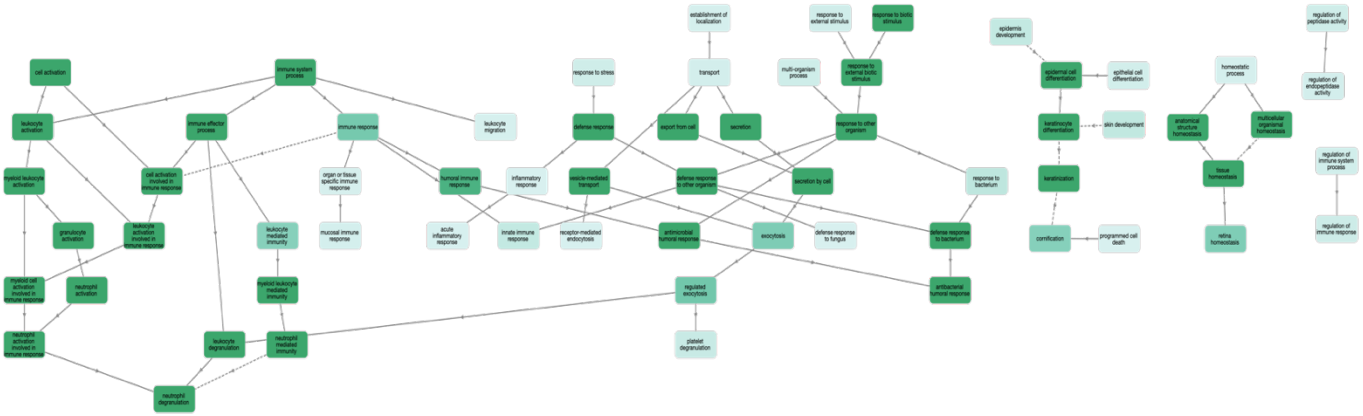

B.15 LBL PNC 30 mins network

B.16 LBL PNC 4 hours network

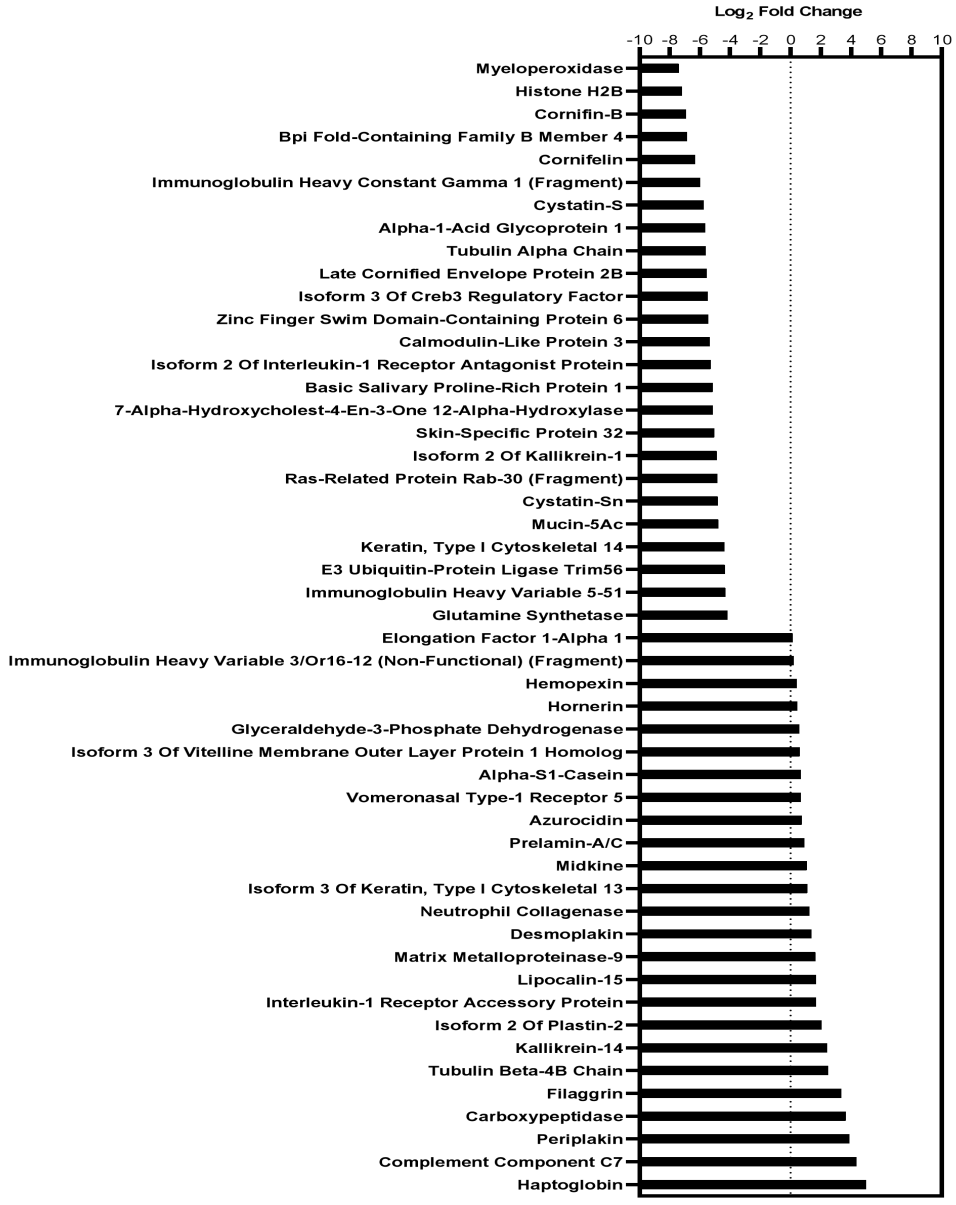

B.17 Fold change analysis 30-minute PEG PNC comparing to OVA bare PNC

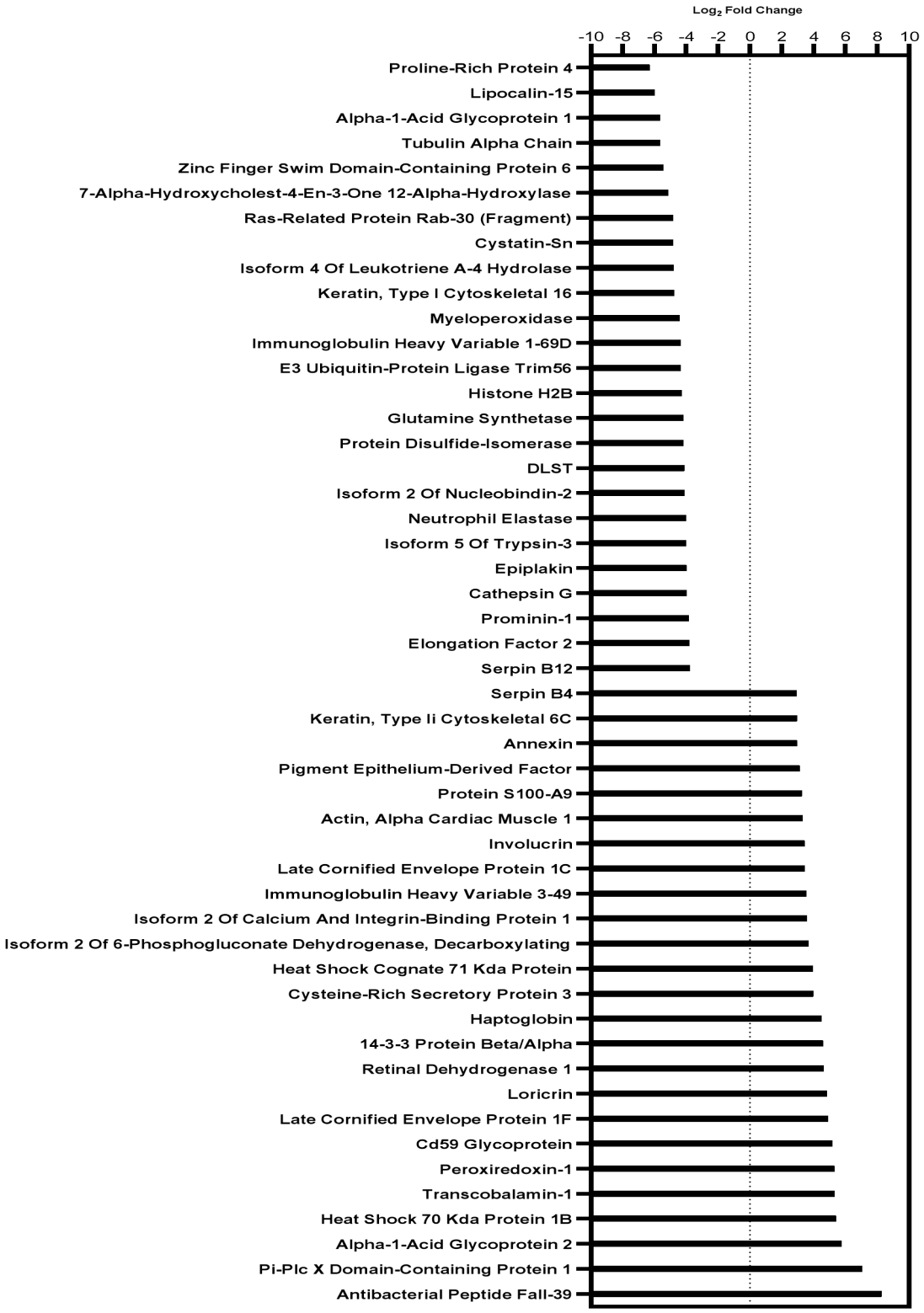

B.18 Fold change analysis 30 minute cOVA PNC comparing to OVA bare PNC

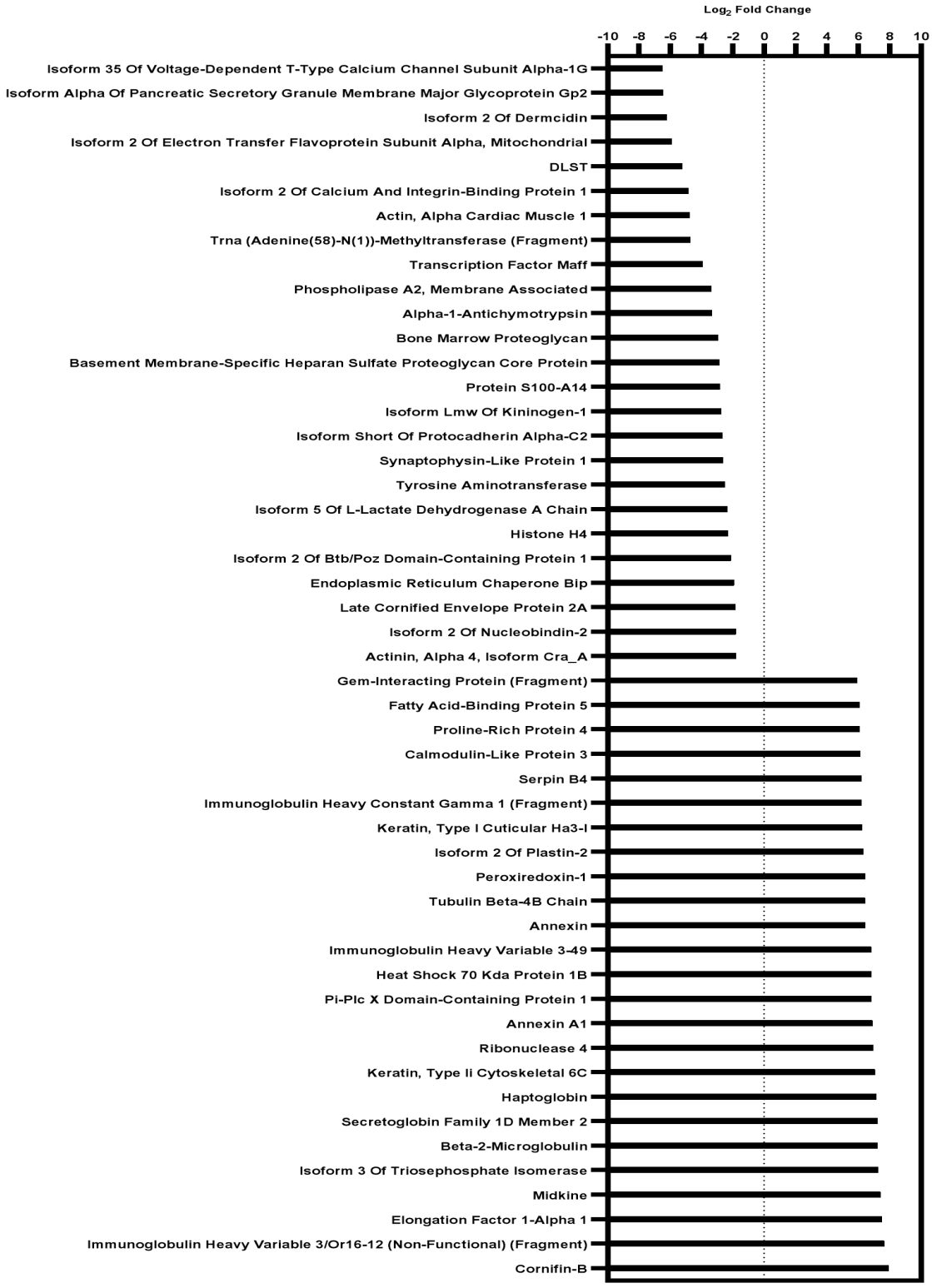

B.19 Fold change analysis 30 mins LBL PNC comparing to OVA bare PNC

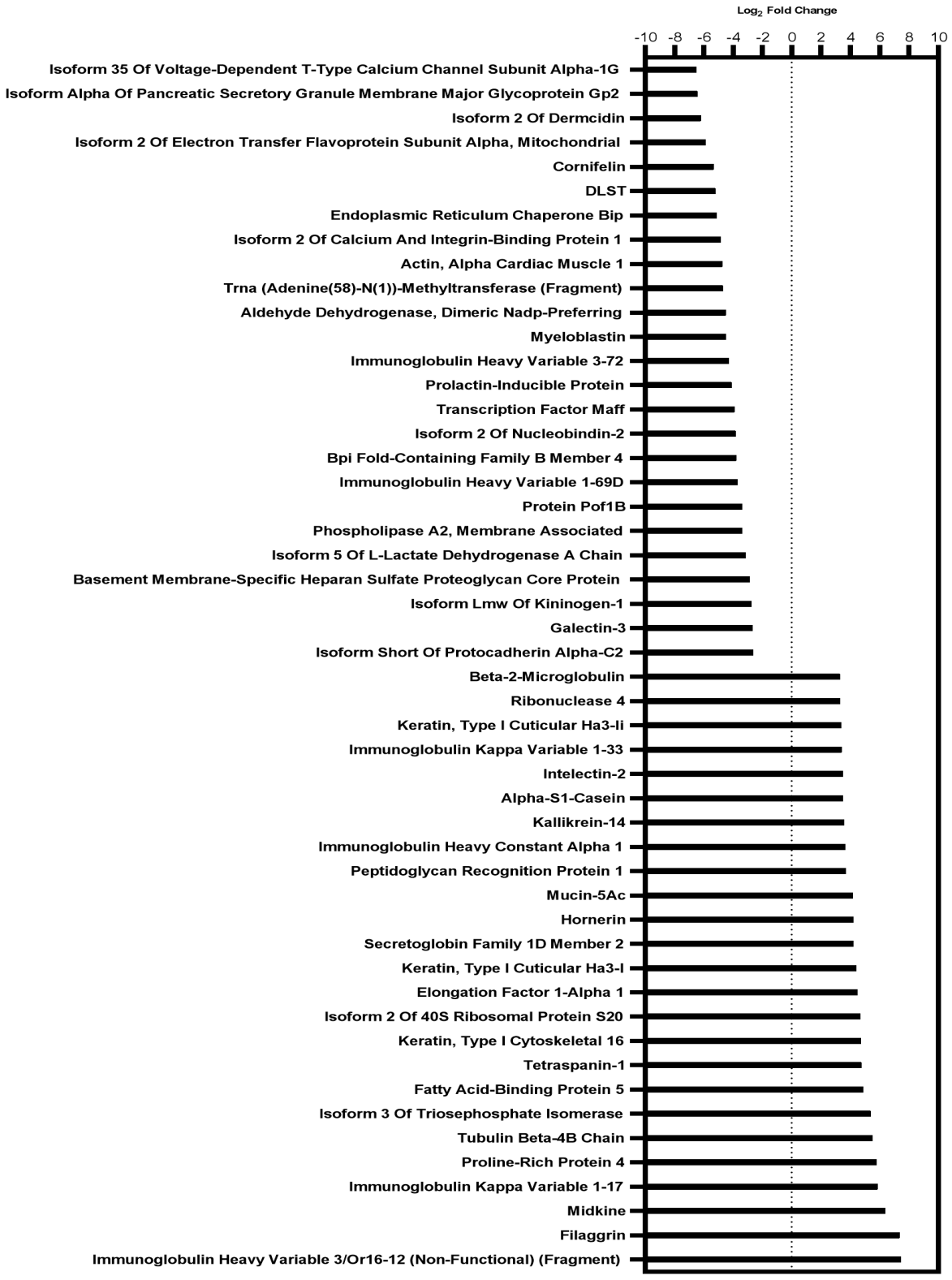

B.20 Fold change analysis 4.0 hours PEG PNC comparing to OVA bare PNC

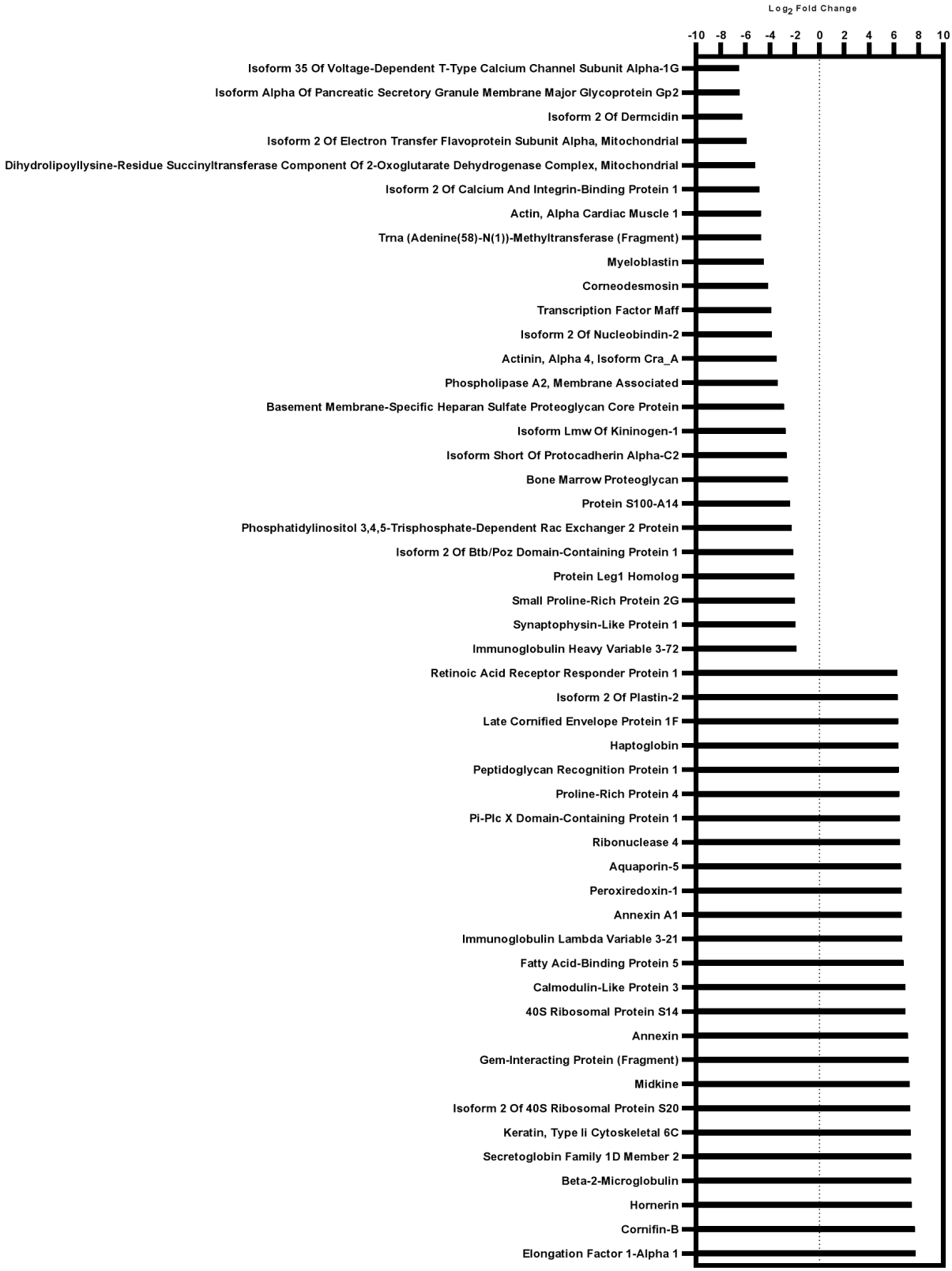

B.21 Fold change analysis 4.0 hours cOVA PNC comparing to OVA bare PNC

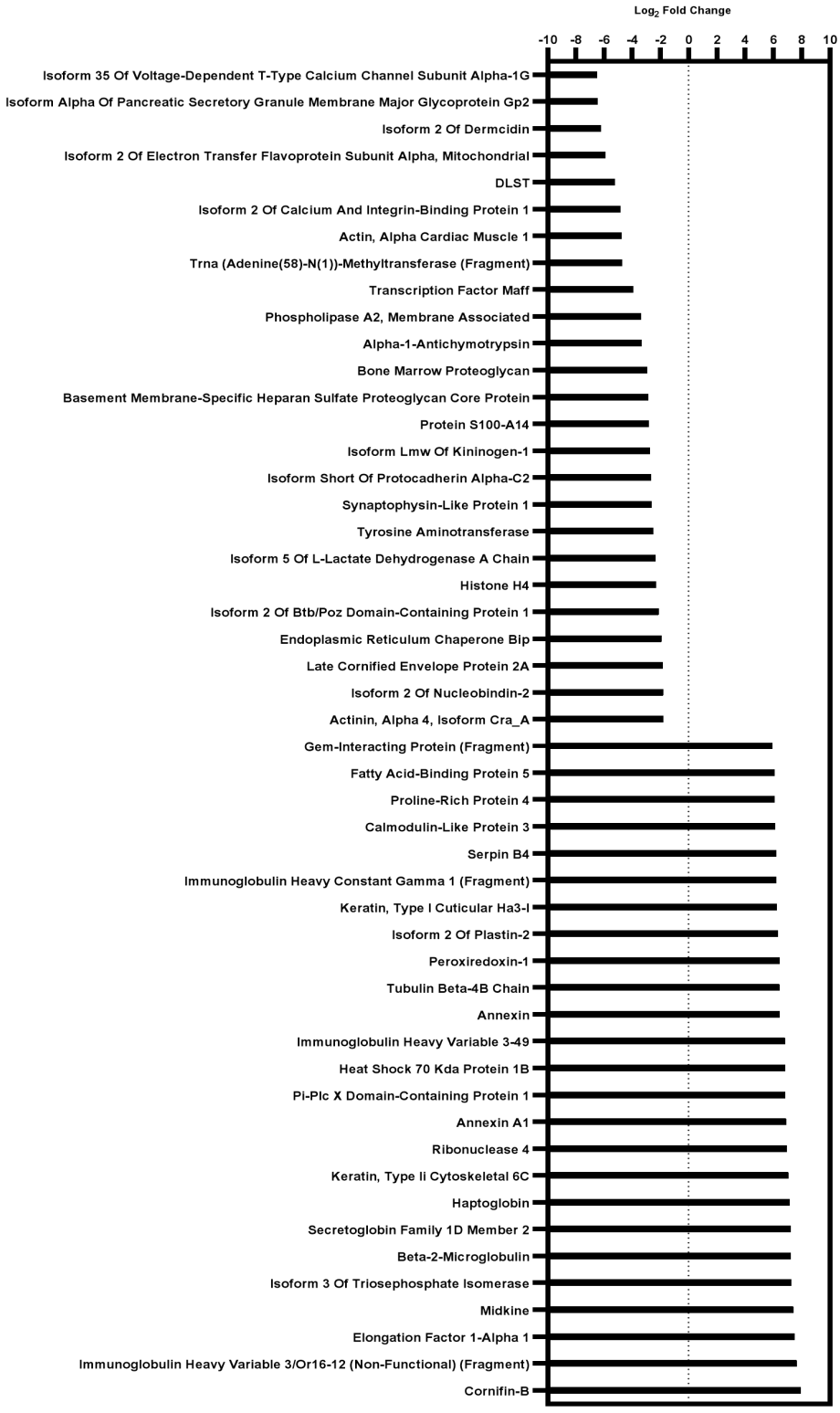

B.22 Fold change analysis 4.0 hours LBL PNC comparing to OVA bare PNC

REFERENCES

1. Telser, A. Molecular Biology of the Cell, 4th Edition. *Shock* **2002**.
2. Leal, J.; Smyth, H. D. C.; Ghosh, D. Physicochemical Properties of Mucus and Their Impact on Transmucosal Drug Delivery. *International Journal of Pharmaceutics*. 2017.
3. Evans, C. M.; Kim, K.; Tuvim, M. J.; Dickey, B. F. Mucus Hypersecretion in Asthma: Causes and Effects. *Current Opinion in Pulmonary Medicine*. 2009.
4. Pinzón Martín, S.; Seeberger, P. H.; Varón Silva, D. Mucins and Pathogenic Mucin-Like Molecules Are Immunomodulators During Infection and Targets for Diagnostics and Vaccines. *Frontiers in Chemistry*. 2019.
5. Verdugo, P. Mucin Exocytosis. In *American Review of Respiratory Disease*; 1991.
6. Leal, J.; Smyth, H. D. C.; Ghosh, D. Physicochemical Properties of Mucus and Their Impact on Transmucosal Drug Delivery. *International Journal of Pharmaceutics*. 2017.
7. Peppas, N. A.; Huang, Y. Nanoscale Technology of Mucoadhesive Interactions. *Advanced Drug Delivery Reviews*. 2004.
8. Lai, S. K.; Wang, Y. Y.; Cone, R.; Wirtz, D.; Hanes, J. Altering Mucus Rheology to "Solidify" Human Mucus at the Nanoscale. *PLoS One* **2009**.
9. Boegh, M.; Nielsen, H. M. Mucus as a Barrier to Drug Delivery - Understanding and Mimicking the Barrier Properties. *Basic and Clinical Pharmacology and Toxicology* 2015
10. Khutoryanskiy, V. V. Beyond PEGylation: Alternative Surface-Modification of Nanoparticles with Mucus-Inert Biomaterials. *Advanced Drug Delivery Reviews*. 2018.
11. Berg, J.; Tymoczko, J.; Stryer, L. *Biochemistry, 5th Edition*; 2002.
12. Thornton, D. J.; Sheehan, J. K. From Mucins to Mucus: Toward a More Coherent Understanding of This Essential Barrier. *Proceedings of the American Thoracic Society*. 2004.
13. Dekker, J.; Rossen, J. W. A.; Büller, H. A.; Einerhand, A. W. C. The MUC Family: An Obituary. *Trends in Biochemical Sciences*. 2002.
14. Bansil, R.; Turner, B. S. Mucin Structure, Aggregation, Physiological Functions and Biomedical Applications. *Current Opinion in Colloid and Interface Science*. 2006.
15. Thornton, D. J.; Rousseau, K.; McGuckin, M. A. Structure and Function of the Polymeric Mucins in Airways Mucus. *Annual Review of Physiology*. 2008.
16. Ambort, D.; Johansson, M. E. V.; Gustafsson, J. K.; Ermund, A.; Hansson, G. C. Perspectives on Mucus Properties and Formation-Lessons from the Biochemical World. *Cold Spring Harb. Perspect. Med.* **2012**.
17. Johansson, M. E. V.; Phillipson, M.; Petersson, J.; Velcich, A.; Holm, L.; Hansson, G. C. The Inner of the Two Muc2 Mucin-Dependent Mucus Layers in Colon Is Devoid of Bacteria. *Proc. Natl. Acad. Sci. U. S. A.* **2008**.
18. Knowles, M. R.; Boucher, R. C. Mucus Clearance as a Primary Innate Defense Mechanism for Mammalian Airways. *Journal of Clinical Investigation*. 2002.
19. Hattrup, C. L.; Gendler, S. J. Structure and Function of the Cell Surface (Tethered) Mucins. *Annual Review of Physiology*. 2008.
20. Phillipson, M.; Johansson, M. E. V.; Henriksnäs, J.; Petersson, J.; Gendler, S. J.; Sandler, S.; Persson, A. E. G.; Hansson, G. C.; Holm, L. The Gastric Mucus Layers: Constituents and Regulation of Accumulation. *Am. J. Physiol. - Gastrointest. Liver Physiol.* **2008**.

21. Wagner, C. E.; Turner, B. S.; Rubinstein, M.; McKinley, G. H.; Ribbeck, K. A Rheological Study of the Association and Dynamics of MUC5AC Gels. *Biomacromolecules* **2017**.
22. Hodges, R. R.; Dartt, D. A. Tear Film Mucins: Front Line Defenders of the Ocular Surface; Comparison with Airway and Gastrointestinal Tract Mucins. *Experimental Eye Research*. 2013.
23. Celli, J. P.; Turner, B. S.; Afdhal, N. H.; Ewoldt, R. H.; McKinley, G. H.; Bansil, R.; Erramilli, S. Rheology of Gastric Mucin Exhibits a PH-Dependent Sol-Gel Transition. *Biomacromolecules* **2007**.
24. Lai, S. K.; Wang, Y. Y.; Wirtz, D.; Hanes, J. Micro- and Macrorheology of Mucus. *Advanced Drug Delivery Reviews*. 2009.
25. Ainai, A.; Tamura, S. I.; Suzuki, T.; Van Riet, E.; Ito, R.; Odagiri, T.; Tashiro, M.; Kurata, T.; Hasegawa, H. Intranasal Vaccination with an Inactivated Whole Influenza Virus Vaccine Induces Strong Antibody Responses in Serum and Nasal Mucus of Healthy Adults. *Hum. Vaccines Immunother.* **2013**.
26. Jeon, Y. J.; Gil, C. H.; Won, J.; Jo, A.; Kim, H. J. Symbiotic Microbiome Staphylococcus Aureus from Human Nasal Mucus Modulates IL-33-Mediated Type 2 Immune Responses in Allergic Nasal Mucosa. *BMC Microbiol.* **2020**.
27. Khutoryanskiy, V. V. Advances in Mucoadhesion and Mucoadhesive Polymers. *Macromol. Biosci.* **2011**.
28. Li, H.; Yu, Y.; Faraji Dana, S.; Li, B.; Lee, C. Y.; Kang, L. Novel Engineered Systems for Oral, Mucosal and Transdermal Drug Delivery. *Journal of Drug Targeting*. 2013.
29. Garg, U.; Chauhan, S.; Nagaich, U.; Jain, N. Current Advances in Chitosan Nanoparticles Based Drug Delivery and Targeting. *Advanced Pharmaceutical Bulletin*. 2019.
30. Asane, G. S.; Nirmal, S. A.; Rasal, K. B.; Naik, A. A.; Mahadik, M. S.; Rao, Y. M. Polymers for Mucoadhesive Drug Delivery System: A Current Status. *Drug Development and Industrial Pharmacy*. 2008.
31. Chowdary, K. P. R.; Rao, Y. S. Mucoadhesive Microspheres for Controlled Drug Delivery. *Biological and Pharmaceutical Bulletin*. 2004.
32. Shaikh, R.; Raj Singh, T.; Garland, M.; Woolfson, A.; Donnelly, R. Mucoadhesive Drug Delivery Systems. *Journal of Pharmacy and Bioallied Sciences*. 2011.
33. Krishna Moorthy, B.; Muthukumaran, M. Recent Advances in Mucoadhesive/ Bioadhesive Drug Delivery System: A Review. *Int. J. Pharm. Med. Bio. Sc. Phanindra B al* **2013**.
34. Singh, I.; Rana, V. Techniques for the Assessment of Mucoadhesion in Drug Delivery Systems: An Overview. *J. Adhes. Sci. Technol.* **2012**.
35. Yang, R.; Wei, T.; Goldberg, H.; Wang, W.; Cullion, K.; Kohane, D. S. Getting Drugs Across Biological Barriers. *Advanced Materials*. 2017.
36. Anantrao, J. H.; Nath, P. A.; Nivrutti, P. R. Drug Penetration Enhancement Techniques in Drug Delivery System: A Review. *J. Pharm. Res. Int.* **2021**.
37. Madhav, N. V. S.; Shakya, A. K.; Shakya, P.; Singh, K. Orotransmucosal Drug Delivery Systems: A Review. *Journal of Controlled Release*. 2009.
38. Gibaldi, M.; Boyes, R. N.; Feldman, S. Influence of First-pass Effect on Availability of Drugs on Oral Administration. *J. Pharm. Sci.* **1971**.
39. Laffleur, F. Mucoadhesive Polymers for Buccal Drug Delivery. *Drug Development and Industrial Pharmacy*. 2014.

40. Khutoryanskiy, V. V. Advances in Mucoadhesion and Mucoadhesive Polymers. *Macromol. Biosci.* **2011**.
41. Mythri, G.; Kavitha, K.; Kumar, M. R.; Jagadeesh Singh, S. D. Novel Mucoadhesive Polymers- A Review. *Journal of Applied Pharmaceutical Science*. 2011.
42. Bomsel, M.; Alfsen, A. Entry of Viruses through the Epithelial Barrier: Pathogenic Trickery. *Nature Reviews Molecular Cell Biology*. 2003.
43. Dubald, M.; Bourgeois, S.; Andrieu, V.; Fessi, H. Ophthalmic Drug Delivery Systems for Antibiotherapy- A Review. *Pharmaceutics*. 2018.
44. Mohammed, N.; Sanoj Rejinold, N.; Mangalathillam, S.; Biswas, R.; Nair, S. V.; Jayakumar, R. Fluconazole Loaded Chitin Nanogels as a Topical Ocular Drug Delivery Agent for Corneal Fungal Infections. *J. Biomed. Nanotechnol.* **2013**.
45. Sah, A. K.; Suresh, P. K.; Verma, V. K. PLGA Nanoparticles for Ocular Delivery of Loteprednol Etabonate: A Corneal Penetration Study. *Artif. Cells, Nanomedicine Biotechnol.* **2017**.
46. Liu, Z.; Anderson, J. D.; Deng, L.; Mackay, S.; Bailey, J.; Kersh, L.; Rowe, S. M.; Guimbellot, J. S. Human Nasal Epithelial Organoids for Therapeutic Development in Cystic Fibrosis. *Genes (Basel).* **2020**.
47. Siti Sarah, C. O.; Shukri, N. M.; Mohd Ashari, N. S.; Wong, K. K. Zonula Occludens and Nasal Epithelial Barrier Integrity in Allergic Rhinitis. *PeerJ* **2020**.
48. Shin, S. H.; Ye, M. K.; Lee, D. W.; Chae, M. H.; Han, B. Da. Nasal Epithelial Cells Activated with Alternaria and House Dust Mite Induce Not Only Th2 but Also Th1 Immune Responses. *Int. J. Mol. Sci.* **2020**.
49. Bernocchi, B.; Carpentier, R.; Betbeder, D. Nasal Nanovaccines. *International Journal of Pharmaceutics*. 2017.
50. Yu, X. C.; Yang, J. J.; Jin, B. H.; Xu, H. L.; Zhang, H. Y.; Xiao, J.; Lu, C. T.; Zhao, Y. Z.; Yang, W. A Strategy for Bypassing the Blood-Brain Barrier: Facial Intradermal Brain-Targeted Delivery via the Trigeminal Nerve. *J. Control. Release* **2017**.
51. Ross, T. M.; Martinez, P. M.; Renner, J. C.; Thorne, R. G.; Hanson, L. R.; Frey, W. H. Intranasal Administration of Interferon Beta Bypasses the Blood-Brain Barrier to Target the Central Nervous System and Cervical Lymph Nodes: A Non-Invasive Treatment Strategy for Multiple Sclerosis. *J. Neuroimmunol.* **2004**.
52. Bonaccorso, A.; Musumeci, T.; Serapide, M. F.; Pellitteri, R.; Uchegbu, I. F.; Puglisi, G. Nose to Brain Delivery in Rats: Effect of Surface Charge of Rhodamine B Labeled Nanocarriers on Brain Subregion Localization. *Colloids Surfaces B Biointerfaces* **2017**.
53. Dhakal, S.; Renu, S.; Ghimire, S.; Lakshmanappa, Y. S.; Hogshead, B. T.; Feliciano-Ruiz, N.; Lu, F.; HogenEsch, H.; Krakowka, S.; Lee, C. W.; et al. Mucosal Immunity and Protective Efficacy of Intranasal Inactivated Influenza Vaccine Is Improved by Chitosan Nanoparticle Delivery in Pigs. *Front. Immunol.* **2018**.
54. Wang, Y.; Deng, L.; Kang, S. M.; Wang, B. Z. Universal Influenza Vaccines: From Viruses to Nanoparticles. *Expert Review of Vaccines*. 2018.
55. Subramanian, P. Mucoadhesive Delivery System: A Smart Way to Improve Bioavailability of Nutraceuticals. *Foods*. 2021.
56. Mei, L.; Chen, J.; Yu, S.; Huang, Y.; Xie, Y.; Wang, H.; Pan, X.; Wu, C. Expansible Thermal Gelling Foam Aerosol for Vaginal Drug Delivery. *Drug Deliv.* **2017**.
57. Shaikh, R.; Raj Singh, T.; Garland, M.; Woolfson, A.; Donnelly, R. Mucoadhesive Drug Delivery Systems. *Journal of Pharmacy and Bioallied Sciences*. 2011.

58. Liu, M.; Zhang, J.; Shan, W.; Huang, Y. Developments of Mucus Penetrating Nanoparticles. *Asian Journal of Pharmaceutical Sciences*. 2014.
59. Porsio, B.; Craparo, E. F.; Mauro, N.; Giammona, G.; Cavallaro, G. Mucus and Cell-Penetrating Nanoparticles Embedded in Nano-into-Micro Formulations for Pulmonary Delivery of Ivacaftor in Patients with Cystic Fibrosis. *ACS Appl. Mater. Interfaces* **2018**.
60. Popov, A.; Enlow, E.; Bourassa, J.; Chen, H. Mucus-Penetrating Nanoparticles Made with "Mucoadhesive" Poly(Vinyl Alcohol). *Nanomedicine Nanotechnology, Biol. Med.* **2016**.
61. Mahlert, L.; Anderski, J.; Mulac, D.; Langer, K. The Impact of Gastrointestinal Mucus on Nanoparticle Penetration – in Vitro Evaluation of Mucus-Penetrating Nanoparticles for Photodynamic Therapy. *Eur. J. Pharm. Sci.* **2019**.
62. Lai, S. K.; Wang, Y. Y.; Hanes, J. Mucus-Penetrating Nanoparticles for Drug and Gene Delivery to Mucosal Tissues. *Advanced Drug Delivery Reviews*. 2009.
63. Ensign, L. M.; Tang, B. C.; Wang, Y. Y.; Tse, T. A.; Hoen, T.; Cone, R.; Hanes, J. Mucus-Penetrating Nanoparticles for Vaginal Drug Delivery Protect against Herpes Simplex Virus. *Sci. Transl. Med.* **2012**.
64. Rossi, S.; Vigani, B.; Sandri, G.; Bonferoni, M. C.; Caramella, C. M.; Ferrari, F. Recent Advances in the Mucus-Interacting Approach for Vaginal Drug Delivery: From Mucoadhesive to Mucus-Penetrating Nanoparticles. *Expert Opinion on Drug Delivery*. 2019.
65. Alp, G.; Aydogan, N. Lipid-Based Mucus Penetrating Nanoparticles and Their Biophysical Interactions with Pulmonary Mucus Layer. *Eur. J. Pharm. Biopharm.* **2020**.
66. Craparo, E. F.; Porsio, B.; Sardo, C.; Giammona, G.; Cavallaro, G. Pegylated Polyaspartamide-Polylactide-Based Nanoparticles Penetrating Cystic Fibrosis Artificial Mucus. *Biomacromolecules* **2016**.
67. Popov, A.; Schopf, L.; Bourassa, J.; Chen, H. Enhanced Pulmonary Delivery of Fluticasone Propionate in Rodents by Mucus-Penetrating Nanoparticles. *Int. J. Pharm.* **2016**.
68. Nafee, N.; Forier, K.; Braeckmans, K.; Schneider, M. Mucus-Penetrating Solid Lipid Nanoparticles for the Treatment of Cystic Fibrosis: Proof of Concept, Challenges and Pitfalls. *Eur. J. Pharm. Biopharm.* **2018**.
69. Anderski, J.; Mahlert, L.; Mulac, D.; Langer, K. Mucus-Penetrating Nanoparticles: Promising Drug Delivery Systems for the Photodynamic Therapy of Intestinal Cancer. *Eur. J. Pharm. Biopharm.* **2018**.
70. Blanco, E.; Shen, H.; Ferrari, M. Principles of Nanoparticle Design for Overcoming Biological Barriers to Drug Delivery. *Nature Biotechnology*. 2015.
71. Leal, J.; Smyth, H. D. C.; Ghosh, D. Physicochemical Properties of Mucus and Their Impact on Transmucosal Drug Delivery. *International Journal of Pharmaceutics*. 2017.
72. Ways, T. M. M.; Ng, K. W.; Lau, W. M.; Khutoryanskiy, V. V. Silica Nanoparticles in Transmucosal Drug Delivery. *Pharmaceutics*. 2020.
73. Ways, T. M. M.; Ng, K. W.; Lau, W. M.; Khutoryanskiy, V. V. Silica Nanoparticles in Transmucosal Drug Delivery. Pharmaceutics. 2020.
74. Agibayeva, L. E.; Kaldybekov, D. B.; Porfiryeva, N. N.; Garipova, V. R.; Mangazbayeva, R. A.; Moustafine, R. I.; Semina, I. I.; Mun, G. A.; Kudaibergenov, S. E.; Khutoryanskiy, V. V. Gellan Gum and Its Methacrylated Derivatives as in Situ Gelling Mucoadhesive Formulations of Pilocarpine: In Vitro and in Vivo Studies. *Int. J. Pharm.* **2020**.

75. Mansfield, E. D. H.; De La Rosa, V. R.; Kowalczyk, R. M.; Grillo, I.; Hoogenboom, R.; Sillence, K.; Hole, P.; Williams, A. C.; Khutoryanskiy, V. V. Side Chain Variations Radically Alter the Diffusion of Poly(2-Alkyl-2-Oxazoline) Functionalised Nanoparticles through a Mucosal Barrier. *Biomater. Sci.* **2016**.
76. Akbari, A.; Lavasanifar, A.; Wu, J. Interaction of Cruciferin-Based Nanoparticles with Caco-2 Cells and Caco-2/HT29-MTX Co-Cultures. *Acta Biomater.* **2017**.
77. Dykman, L. A. Gold Nanoparticles for Preparation of Antibodies and Vaccines against Infectious Diseases. *Expert Review of Vaccines*. 2020. (1) Ouellette, M.; Masse, F.; Lefebvre-Demers, M.; Maestracci, Q.; Grenier, P.; Millar, R.; Bertrand, N.; Prieto, M.; Boisselier, É. Insights into Gold Nanoparticles as a Mucoadhesive System. *Sci. Rep.* **2018**.
78. Akbarzadeh, A.; Rezaei-Sadabady, R.; Davaran, S.; Joo, S. W.; Zarghami, N.; Hanifehpour, Y.; Samiei, M.; Kouhi, M.; Nejati-Koshki, K. Liposome: Classification, Preparation, and Applications. *Nanoscale Res. Lett.* **2013**.
79. Darley, E.; Singh, J. K. D.; Surace, N. A.; Wickham, S. F. J.; Baker, M. A. B. The Fusion of Lipid and DNA Nanotechnology. *Genes*. 2019.
80. Xing, H.; Hwang, K.; Lu, Y. Recent Developments of Liposomes as Nanocarriers for Theranostic Applications. *Theranostics*. 2016.
81. Godino, E.; López, J. N.; Foschepoth, D.; Cleij, C.; Doerr, A.; Castellà, C. F.; Danelon, C. De Novo Synthesized Min Proteins Drive Oscillatory Liposome Deformation and Regulate FtsA-FtsZ Cytoskeletal Patterns. *Nat. Commun.* **2019**.
82. Schwendener, R. A. Liposomes as Vaccine Delivery Systems: A Review of the Recent Advances. *Therapeutic Advances in Vaccines*. 2014.
83. Alp, G.; Aydogan, N. Lipid-Based Mucus Penetrating Nanoparticles and Their Biophysical Interactions with Pulmonary Mucus Layer. *Eur. J. Pharm. Biopharm.* **2020**.
84. Mert, O.; Lai, S. K.; Ensign, L.; Yang, M.; Wang, Y. Y.; Wood, J.; Hanes, J. A Poly(Ethylene Glycol)-Based Surfactant for Formulation of Drug-Loaded Mucus Penetrating Particles. *J. Control. Release* **2012**.
85. Le-Vinh, B.; Steinbring, C.; Wibel, R.; Friedl, J. D.; Bernkop-Schnürch, A. Size Shifting of Solid Lipid Nanoparticle System Triggered by Alkaline Phosphatase for Site Specific Mucosal Drug Delivery. *Eur. J. Pharm. Biopharm.* **2021**.
86. Newby, J. M.; Seim, I.; Lysy, M.; Ling, Y.; Huckaby, J.; Lai, S. K.; Forest, M. G. Technological Strategies to Estimate and Control Diffusive Passage Times through the Mucus Barrier in Mucosal Drug Delivery. *Advanced Drug Delivery Reviews*. 2018.
87. Dawson, M.; Krauland, E.; Wirtz, D.; Hanes, J. Transport of Polymeric Nanoparticle Gene Carriers in Gastric Mucus. *Biotechnol. Prog.* **2004**.
88. Suk, J. S.; Xu, Q.; Kim, N.; Hanes, J.; Ensign, L. M. PEGylation as a Strategy for Improving Nanoparticle-Based Drug and Gene Delivery. *Advanced Drug Delivery Reviews*. 2016.
89. Zhang, X.; Zhang, S.; Kang, Y.; Huang, K.; Gu, Z.; Wu, J. Advances in Long-Circulating Drug Delivery Strategy. *Curr. Drug Metab.* **2018**.
90. Hong, S.; Choi, D. W.; Kim, H. N.; Park, C. G.; Lee, W.; Park, H. H. Protein-Based Nanoparticles as Drug Delivery Systems. *Pharmaceutics*. 2020.
91. Khot, S.; Rawal, S. U.; Patel, M. M. Dissolvable-Soluble or Biodegradable Polymers. In *Drug Delivery Devices and Therapeutic Systems*; 2021.
92. Voci, S.; Gagliardi, A.; Fresta, M.; Cosco, D. Antitumor Features of Vegetal Protein-Based Nanotherapeutics. *Pharmaceutics*. 2020.

93. Lai, J. C. C.; Karunarathna, H. M. T. K.; Wong, H. H.; Peiris, J. S. M.; Nicholls, J. M. Neuraminidase Activity and Specificity of Influenza A Virus Are Influenced by Haemagglutinin-Receptor Binding. *Emerg. Microbes Infect.* **2019**.
94. Yameen, B.; Choi, W. Il; Vilos, C.; Swami, A.; Shi, J.; Farokhzad, O. C. Insight into Nanoparticle Cellular Uptake and Intracellular Targeting. *Journal of Controlled Release*. 2014.
95. Bochicchio, S.; Lamberti, G.; Barba, A. A. Polymer–Lipid Pharmaceutical Nanocarriers: Innovations by New Formulations and Production Technologies. *Pharmaceutics*. 2021.
96. Verma, D.; Gulati, N.; Kaul, S.; Mukherjee, S.; Nagaich, U. Protein Based Nanostructures for Drug Delivery. *J. Pharm.* **2018**.
97. Balmelli, C.; Roden, R.; Potts, A.; Schiller, J.; De Grandi, P.; Nardelli-Haefliger, D. Nasal Immunization of Mice with Human Papillomavirus Type 16 Virus-Like Particles Elicits Neutralizing Antibodies in Mucosal Secretions. *J. Virol.* **1998**.
98. Witten, J.; Samad, T.; Ribbeck, K. Selective Permeability of Mucus Barriers. *Current Opinion in Biotechnology*. 2018.
99. Suk, J. S.; Xu, Q.; Kim, N.; Hanes, J.; Ensign, L. M. PEGylation as a Strategy for Improving Nanoparticle-Based Drug and Gene Delivery. *Advanced Drug Delivery Reviews*. 2016.
100. Cu, Y.; Saltzman, W. M. Controlled Surface Modification with Poly(Ethylene)Glycol Enhances Diffusion of PLGA Nanoparticles in Human Cervical Mucus. *Mol. Pharm.* **2009**
101. Busch, R. T.; Karim, F.; Weis, J.; Sun, Y.; Zhao, C.; Vasquez, E. S. Optimization and Structural Stability of Gold Nanoparticle-Antibody Bioconjugates. *ACS Omega* **2019**.
102. Khan, K. H. DNA Vaccines: Roles against Diseases. *GERMS*. 2013.
103. Bruinsmann, F. A.; Vaz, G. R.; De Cristo Soares Alves, A.; Aguirre, T.; Pohlmann, A. R.; Guterres, S. S.; Sonvico, F. Nasal Drug Delivery of Anticancer Drugs for the Treatment of Glioblastoma: Preclinical and Clinical Trials. *Molecules*. 2019.
104. Costa, C. P.; Barreiro, S.; Moreira, J. N.; Silva, R.; Almeida, H.; Sousa Lobo, J. M.; Silva, A. C. In Vitro Studies on Nasal Formulations of Nanostructured Lipid Carriers (NLC) and Solid Lipid Nanoparticles (SLN). *Pharmaceuticals*. 2021.
105. Sun, B.; Xia, T. Nanomaterial-Based Vaccine Adjuvants. *Journal of Materials Chemistry B*. 2016.
106. Bode, C.; Zhao, G.; Steinhagen, F.; Kinjo, T.; Klinman, D. M. CpG DNA as a Vaccine Adjuvant. *Expert Review of Vaccines*. 2011.
107. Klinman, D. M. CpG DNA as a Vaccine Adjuvant. *Expert Review of Vaccines*. 2003.
108. Sanina, N. Vaccine Adjuvants Derived from Marine Organisms. *Biomolecules*. 2019.
109. Seferian, P. G.; Martinez, M. L. Immune Stimulating Activity of Two New Chitosan Containing Adjuvant Formulations. *Vaccine* **2000**.
110. Bellettato, C. M.; Scarpa, M. Possible Strategies to Cross the Blood–Brain Barrier. *Ital. J. Pediatr.* **2018**.
111. Si, X. A.; Xi, J. Modeling and Simulations of Olfactory Drug Delivery with Passive and Active Controls of Nasally Inhaled Pharmaceutical Aerosols. *J. Vis. Exp.* **2016**.
112. Wang, Y.; Deng, L.; Gonzalez, G. X.; Luthra, L.; Dong, C.; Ma, Y.; Zou, J.; Kang, S. M.; Wang, B. Z. Double-Layered M2e-NA Protein Nanoparticle Immunization Induces Broad Cross-Protection against Different Influenza Viruses in Mice. *Adv. Healthc. Mater.* **2020**.

113. Deng, L.; Mohan, T.; Chang, T. Z.; Gonzalez, G. X.; Wang, Y.; Kwon, Y. M.; Kang, S. M.; Compans, R. W.; Champion, J. A.; Wang, B. Z. Double-Layered Protein Nanoparticles Induce Broad Protection against Divergent Influenza A Viruses. *Nat. Commun.* **2018**.
114. Champion, J. A.; Pustulka, S. M.; Ling, K.; Pish, S. L. Protein Nanoparticle Charge and Hydrophobicity Govern Protein Corona and Macrophage Uptake. *ACS Appl. Mater. Interfaces* **2020**.
115. He, P.; Davis, S. S.; Illum, L. In Vitro Evaluation of the Mucoadhesive Properties of Chitosan Microspheres. *Int. J. Pharm.* **1998**.
116. Ouellette, M.; Masse, F.; Lefebvre-Demers, M.; Maestracci, Q.; Grenier, P.; Millar, R.; Bertrand, N.; Prieto, M.; Boisselier, É. Insights into Gold Nanoparticles as a Mucoadhesive System. *Sci. Rep.* **2018**.
117. I. F. Sbalzarini and P. Koumoutsakos. Feature Point Tracking and Trajectory Analysis for Video Imaging in Cell Biology, Journal of Structural Biology 151(2):182-195, 2005.
118. J. A. Helmuth, C. J. Burckhardt, U. F. Greber, and I. F. Sbalzarini. Shape reconstruction of subcellular structures from live cell fluorescence microscopy images. Journal of Structural Biology, 167:1–10, 2009.
119. Vilekar, P.; Awasthi, S.; Natarajan, A.; Anant, S.; Awasthi, V. EF24 Suppresses Maturation and Inflammatory Response in Dendritic Cells. *Int. Immunol.* **2012**.
120. Amici, A.; Caracciolo, G.; Digiacomo, L.; Gambini, V.; Marchini, C.; Tilio, M.; Capriotti, A. L.; Colapicchioni, V.; Matassa, R.; Familiari, G.; et al. In Vivo Protein Corona Patterns of Lipid Nanoparticles. *RSC Adv.* **2017**.
121. Duttagupta, P. A.; Boesteanu, A. C.; Katsikis, P. D. Costimulation Signals for Memory CD8+ T Cells during Viral Infections. *Critical Reviews in Immunology*. 2009.
122. Van Gisbergen, K. P. J. M.; Klarenbeek, P. L.; Kragten, N. A. M.; Unger, P. P. A.; Nieuwenhuis, M. B. B.; Wensveen, F. M.; ten Brinke, A.; Tak, P. P.; Eldering, E.; Nolte, M. A.; et al. The Costimulatory Molecule CD27 Maintains Clonally Diverse CD8+ T Cell Responses of Low Antigen Affinity to Protect against Viral Variants. *Immunity* **2011**.
123. Wang, X.; Liu, L. H.; Ramström, O.; Yan, M. Engineering Nanomaterial Surfaces for Biomedical Applications. *Experimental Biology and Medicine*. 2009.
124. Auría-Soro, C.; Nesma, T.; Juanes-Velasco, P.; Landeira-Viñuela, A.; Fidalgo-Gomez, H.; Acebes-Fernandez, V.; Gongora, R.; Parra, M. J. A.; Manzano-Roman, R.; Fuentes, M. Interactions of Nanoparticles and Biosystems: Microenvironment of Nanoparticles and Biomolecules in Nanomedicine. *Nanomaterials*. 2019.
125. Mitchell, M. J.; Billingsley, M. M.; Haley, R. M.; Wechsler, M. E.; Peppas, N. A.; Langer, R. Engineering Precision Nanoparticles for Drug Delivery. *Nature Reviews Drug Discovery*. 2021.
126. Nguyen, V. H.; Lee, B. J. Protein Corona: A New Approach for Nanomedicine Design. *International Journal of Nanomedicine*. 2017.
127. Saptarshi, S. R.; Duschl, A.; Lopata, A. L. Interaction of Nanoparticles with Proteins: Relation to Bio-Reactivity of the Nanoparticle. *J. Nanobiotechnology* **2013**.
128. Mohammad-Beigi, H.; Hayashi, Y.; Zeuthen, C. M.; Eskandari, H.; Scavenius, C.; Juul-Madsen, K.; Vorup-Jensen, T.; Enghild, J. J.; Sutherland, D. S. Mapping and Identification of Soft Corona Proteins at Nanoparticles and Their Impact on Cellular Association. *Nat. Commun.* **2020**.
129. Nguyen, V. H.; Lee, B. J. Protein Corona: A New Approach for Nanomedicine Design. *International Journal of Nanomedicine*. 2017.

130. Papini, E.; Tavano, R.; Mancin, F. Opsonins and Dysopsonins of Nanoparticles: Facts, Concepts, and Methodological Guidelines. *Frontiers in Immunology*. 2020.
131. Rampado, R.; Crotti, S.; Caliceti, P.; Pucciarelli, S.; Agostini, M. Recent Advances in Understanding the Protein Corona of Nanoparticles and in the Formulation of "Stealthy" Nanomaterials. *Frontiers in Bioengineering and Biotechnology*. 2020.
132. Abbina, S.; Takeuchi, L. E.; Anilkumar, P.; Yu, K.; Rogalski, J. C.; Shenoi, R. A.; Constantinescu, I.; Kizhakkedathu, J. N. Blood Circulation of Soft Nanomaterials Is Governed by Dynamic Remodeling of Protein Opsonins at Nano-Biointerface. *Nat. Commun.* **2020**.
133. Longmire, M.; Choyke, P. L.; Kobayashi, H. Clearance Properties of Nano-Sized Particles and Molecules as Imaging Agents: Considerations and Caveats. *Nanomedicine*. 2008.
134. Blanco, E.; Shen, H.; Ferrari, M. Principles of Nanoparticle Design for Overcoming Biological Barriers to Drug Delivery. *Nature Biotechnology*. 2015.
135. Mitchell, M. J.; Billingsley, M. M.; Haley, R. M.; Wechsler, M. E.; Peppas, N. A.; Langer, R. Engineering Precision Nanoparticles for Drug Delivery. *Nature Reviews Drug Discovery*. 2021.
136. Ghanem, R.; Laurent, V.; Roquefort, P.; Haute, T.; Ramel, S.; Gall, T. Le; Aubry, T.; Montier, T. Optimizations of in Vitro Mucus and Cell Culture Models to Better Predict in Vivo Gene Transfer in Pathological Lung Respiratory Airways: Cystic Fibrosis as an Example. *Pharmaceutics*. 2021.
137. Ali, N.; Mattsson, K.; Rissler, J.; Karlsson, H. M.; Svensson, C. R.; Gudmundsson, A.; Lindh, C. H.; Jönsson, B. A. G.; Cedervall, T.; Kåredal, M. Analysis of Nanoparticle-Protein Coronas Formed in Vitro between Nanosized Welding Particles and Nasal Lavage Proteins. *Nanotoxicology* **2016**.
138. Walkey, C. D.; Olsen, J. B.; Song, F.; Liu, R.; Guo, H.; Olsen, D. W. H.; Cohen, Y.; Emili, A.; Chan, W. C. W. Protein Corona Fingerprinting Predicts the Cellular Interaction of Gold and Silver Nanoparticles. *ACS Nano* **2014**.
139. Miotto, G.; Magro, M.; Terzo, M.; Zaccarin, M.; Da Dalt, L.; Bonaiuto, E.; Baratella, D.; Gabai, G.; Vianello, F. Protein Corona as a Proteome Fingerprint: The Example of Hidden Biomarkers for Cow Mastitis. *Colloids Surfaces B Biointerfaces* **2016**.
140. Wisniewski, J.R., et al., Universal sample preparation method for proteome analysis. Nat Methods, 2009. 6(5): p. 359-62.
141. Rinker, T.E., et al., Microparticle-mediated sequestration of cell-secreted proteins to modulate chondrocytic differentiation. Acta Biomaterialia, 2017.
142. Mi, H.; Muruganujan, A.; Casagrande, J. T.; Thomas, P. D. Large-Scale Gene Function Analysis with the Panther Classification System. *Nat. Protoc.* **2013**.
143. Mi, H.; Muruganujan, A.; Huang, X.; Ebert, D.; Mills, C.; Guo, X.; Thomas, P. D. Protocol Update for Large-Scale Genome and Gene Function Analysis with the PANTHER Classification System (v.14.0). *Nat. Protoc.* **2019**.
144. Tziastoudi, M.; Tsezou, A.; Stefanidis, I. Cadherin and Wnt Signaling Pathways as Key Regulators in Diabetic Nephropathy. *PLoS One* **2021**.
145. Nogoy, F. M.; Jung, Y. J.; Kang, K. K.; Cho, Y. G. Physico-Chemical Characterization and Transcriptome Analysis of 5-Methyltryptophan Resistant Lines in Rice. *PLoS One* **2019**.

146. Pomaznoy, M.; Ha, B.; Peters, B. GOnet: A Tool for Interactive Gene Ontology Analysis. *BMC Bioinformatics* **2018**.
147. Aguilan, J. T.; Kulej, K.; Sidoli, S. Guide for Protein Fold Change and: P-Value Calculation for Non-Experts in Proteomics. *Mol. Omi.* **2020**.
148. Raudvere, U.; Kolberg, L.; Kuzmin, I.; Arak, T.; Adler, P.; Peterson, H.; Vilo, J. G:Profiler: A Web Server for Functional Enrichment Analysis and Conversions of Gene Lists (2019 Update). *Nucleic Acids Res.* **2019**.
149. Peterson, H.; Kolberg, L.; Raudvere, U.; Kuzmin, I.; Vilo, J. Gprofiler2 -- an R Package for Gene List Functional Enrichment Analysis and Namespace Conversion Toolset g: Profiler. *F1000Research* **2020**.
150. Müller, A. C.; Giambruno, R.; Weißer, J.; Májek, P.; Hofer, A.; Bigenzahn, J. W.; Superti-Furga, G.; Jessen, H. J.; Bennett, K. L.; Matsushima, Y.; et al. Pathway Enrichment Analysis and Visualization of Omics Data Using g:Profiler, GSEA, Cytoscape and EnrichmentMap. *Nat. Protoc.* **2019**.
151. Weiss, A.C.G., H.M. Herold, S. Lentz, M. Faria, Q.A. Besford, C.-S. Ang, F. Caruso, and T. Scheibel, *Surface Modification of Spider Silk Particles to Direct Biomolecular Corona Formation.* ACS Applied Materials & Interfaces, 2020. **12**(22): p. 24635-24643.
152. Niknejad, H.; Mahmoudzadeh, R. Comparison of Different Crosslinking Methods for Preparation of Docetaxel-Loaded Albumin Nanoparticles. *Iran. J. Pharm. Res.* **2015**.
153. Goor, O. J. G. M.; Brouns, J. E. P.; Dankers, P. Y. W. Introduction of Anti-Fouling Coatings at the Surface of Supramolecular Elastomeric Materials: Via Post-Modification of Reactive Supramolecular Additives. *Polym. Chem.* **2017**.
154. Yu, K.; Andruschak, P.; Yeh, H. H.; Grecov, D.; Kizhakkedathu, J. N. Influence of Dynamic Flow Conditions on Adsorbed Plasma Protein Corona and Surface-Induced Thrombus Generation on Antifouling Brushes. *Biomaterials* **2018**.
155. Liu, Z. G. Molecular Mechanism of TNF Signaling and Beyond. *Cell Research*. 2005.
156. Yasumura, J.; Shimizu, M.; Toma, T.; Yashiro, M.; Yachie, A.; Okada, S. Clinical Significance of Serum Soluble TNF Receptor I/II Ratio for the Differential Diagnosis of Tumor Necrosis Factor Receptor-Associated Periodic Syndrome From Other Autoinflammatory Diseases. *Front. Immunol.* **2020**.
157. Wang, X.; Lin, Y. Tumor Necrosis Factor and Cancer, Buddies or Foes? *Acta Pharmacologica Sinica*. 2008.
158. Telser, A. Molecular Biology of the Cell, 4th Edition. *Shock* **2002**.
159. Hirayama, T.; Yagi, T. The Role and Expression of the Protocadherin-Alpha Clusters in the CNS. *Current Opinion in Neurobiology*. 2006.
160. Katafiasz, B. J.; Nieman, M. T.; Wheelock, M. J.; Johnson, K. R. Characterization of Cadherin-24, a Novel Alternatively Spliced Type II Cadherin. *J. Biol. Chem.* **2003**.
161. Kelley, W. J.; Fromen, C. A.; Lopez-Cazares, G.; Eniola-Adefeso, O. PEGylation of Model Drug Carriers Enhances Phagocytosis by Primary Human Neutrophils. *Acta Biomater.* **2018**.
162. Snelgrove, R. J. Leukotriene A4 Hydrolase: An Anti-Inflammatory Role for a Proinflammatory Enzyme. *Thorax* **2011**.
163. Lominadze, G.; Powell, D. W.; Luerman, G. C.; Link, A. J.; Ward, R. A.; McLeish, K. R. Proteomic Analysis of Human Neutrophil Granules. *Mol. Cell. Proteomics* **2005**.
164. Hou, J. C.; Min, L.; Pessin, J. E. Chapter 16 Insulin Granule Biogenesis, Trafficking and Exocytosis. *Vitamins and Hormones*. 2009.

165. Termini, C. M.; Gillette, J. M. Tetraspanins Function as Regulators of Cellular Signaling. *Frontiers in Cell and Developmental Biology*. 2017.
166. Rus, H.; Cudrici, C.; Niculescu, F. The Role of the Complement System in Innate Immunity. *Immunologic Research*. 2005.
167. Elkington, P. T. G.; O'Kane, C. M.; Friedland, J. S. The Paradox of Matrix Metalloproteinases in Infectious Disease. *Clin. Exp. Immunol.* **2005**.
168. Watanabe, R.; Maeda, T.; Zhang, H.; Berry, G. J.; Zeisbrich, M.; Brockett, R.; Greenstein, A. E.; Tian, L.; Goronzy, J. J.; Weyand, C. M. MMP (Matrix Metalloprotease)-9-Producing Monocytes Enable T Cells to Invade the Vessel Wall and Cause Vasculitis. *Circ. Res.* **2018**.
169. Ulluwishewa, D.; Anderson, R. C.; McNabb, W. C.; Moughan, P. J.; Wells, J. M.; Roy, N. C. Regulation of Tight Junction Permeability by Intestinal Bacteria and Dietary Components. *Journal of Nutrition*. 2011.
170. Brunner, J.; Ragupathy, S.; Borchard, G. Target Specific Tight Junction Modulators. *Advanced Drug Delivery Reviews*. 2021.
171. Huang, M.; Ma, Z.; Khor, E.; Lim, L. Y. Uptake of FITC-Chitosan Nanoparticles by A549 Cells. *Pharm. Res.* **2002**.
172. Grewal, T.; Hoque, M.; Conway, J. R. W.; Reverter, M.; Wahba, M.; Beevi, S. S.; Timpson, P.; Enrich, C.; Rentero, C. Annexin A6—A Multifunctional Scaffold in Cell Motility. *Cell Adhesion and Migration*. 2017.
173. Yameen, B.; Choi, W. Il; Vilos, C.; Swami, A.; Shi, J.; Farokhzad, O. C. Insight into Nanoparticle Cellular Uptake and Intracellular Targeting. *Journal of Controlled Release*. 2014.
174. Suk, J. S.; Xu, Q.; Kim, N.; Hanes, J.; Ensign, L. M. PEGylation as a Strategy for Improving Nanoparticle-Based Drug and Gene Delivery. *Advanced Drug Delivery Reviews*. 2016.
175. Vianello, F.; Cecconello, A.; Magro, M. Toward the Specificity of Bare Nanomaterial Surfaces for Protein Corona Formation. *International Journal of Molecular Sciences*. 2021.
176. Judge, E. P.; Hughes, J. M. L.; Egan, J. J.; Maguire, M.; Molloy, E. L.; O'Dea, S. Anatomy and Bronchoscopy of the Porcine Lung: A Model for Translational Respiratory Medicine. *American Journal of Respiratory Cell and Molecular Biology*. 2014.